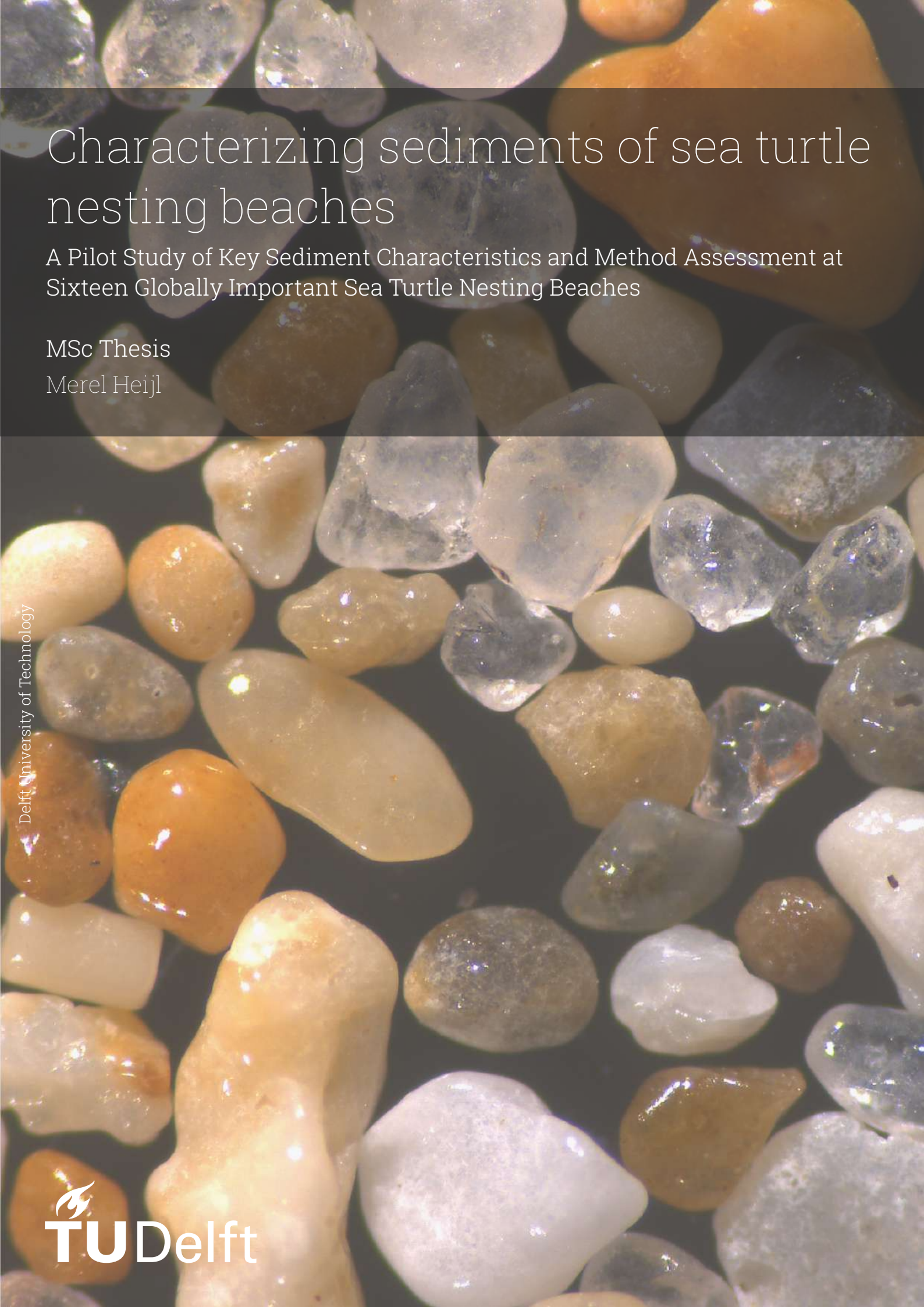

Characterizing sediments of sea turtle nesting beaches

A Pilot Study of Key Sediment Characteristics and Method Assessment at Sixteen Globally Important Sea Turtle Nesting Beaches

MSc Thesis

Merel Heijl

Delft University of Technology

TU Delft

Characterizing sediments of sea turtle nesting beaches

A Pilot Study of Key Sediment Characteristics and Method Assessment at Sixteen Globally Important Sea Turtle Nesting Beaches

by

Merel Heijl

MSc Thesis of Civil Engineering
Hydraulic Engineering - Coastal Engineering

Student number:	4831969
Supervisors:	Dr.ing. José A. Á. Antolínez
	Dr. A. Kirichek
	Ir. J.C. Christiaanse
Project duration:	September, 2024 - April, 2025
Faculty:	Civil Engineering, Delft

TU Delft

Preface

This thesis marks the completion of my Master's degree in Coastal Engineering at the Tu Delft, bringing my journey in studying Civil Engineering to a close. Throughout this thesis, I have gained significant knowledge about how climate change affects sea turtle beaches, the importance of sediment characteristics of sea turtle beaches, the methods to analyze all sediment characteristics and how to conserve the sea turtle nesting beaches.

When analyzing different sediment characteristics, I encountered various research methods. Instead of learning about these methods in a lecture, I had the opportunity to experience them firsthand, gaining a better understanding of how they work in practice. Many of these methods are widely used in professional applications. The methods I employed were conducted in different labs, including TU Delft, Boskalis and Deltares. Working in multiple labs allowed me to experience different work environments, each with its own strengths. In every lab, the people were incredibly helpful and supportive.

The research process was both challenging and rewarding. From planning experiments and analyzing samples to interpreting results, I faced various obstacles, particularly with time management. However, the guidance and support from my supervisors and people working in the lab where I conducted my research played a significant role in overcoming these challenges.

I hope this research provides valuable insights into sea turtle conservations and its connection to sediment characteristics.

Merel Heijl
Delft, April 2025

Acknowledgements

We express our gratitude and acknowledgements to the individuals and organisations who have collected and provided the sediment samples analysed as part of this study. They are listed below for each study site. Additionally, we thank Dr. Zara Botterell and Prof. Brendan Godley from the University of Exeter, who organized and stored the samples, hosted us on campus, and helped arrange the transport of the samples to Delft University of Technology. Without the efforts of Zara, Brendan, and the contributors listed below this study would not have been possible. North East Bay, Ascension Island: Sam Weber and Andy Richardson from the Ascension Island Government Conservation & Fisheries Department and University of Exeter, UK. Dirk Hartog Island, Australia: Corrine Douglas and Tony Tucker from the Department of Biodiversity, Conservation and Attractions (DBCA), Australia. Delambre Island, Australia: Corrine Douglas, Ryan Douglas, and Katherine Bennett from the Department of Biodiversity, Conservation and Attractions (DBCA), Australia. Needhams, Barbados: Julia Horrocks and Ivon Vassileva from the Barbados Sea Turtle Project, University of West Indies Cave Hill. Busca Vida, Brazil: Denise Santos de Mora and Manuela Regina Borja Bosquirolli from Projecto Tamar base Praia do Forte - BA. Joao Barrosa, Cabo Verde: Samir Martins from Bios Cabo Verde. Diego Garcia, Chagos: Nicole Esteban from Swansea University, UK. Ostional, Costa Rica: Vanessa Bézy from Wildlife Conservation Association in collaboration with Jairo Quiros from Ostional National Wildlife Refuge. Corozalito, Costa Rica: Daniela Rojas-Cañizales from CREMA, Rescue Center for Endangered Marine Species. Awala-Yalimapo, French Guiana: Nicolas Paranthoën from ONCFS. Mayumba, Gabon: Angela Formia from the Wildlife Conservation Society. Poilao Island, Guinnea-Bissau: Ana R. Patrício from Faculdade de Ciências da Universidade de Lisboa, Lisbon, Portugal. Masirah Island, Oman: Craig Turley from The Environment Society of Oman (ESO). Aldabra Atoll, Seychelles: Nancy Bunbury from SIF. Archie Carr, USA: Tiffany Dawson from the University of Central Florida. Padre Island, USA: Jessica Clark, Martha Villalba, and Dimitra Guerrero from Padre Island National Seashore.

I would like to personally express my gratitude to my supervisors for dedicating their time to me. Dr.ing. J.A. Antolínez provided essential guidance in establishing the foundation of my master's thesis and introduced me to all the people who assisted me in finding the right research methods for this study. Ir. J.C. Christiaanse supported me in structuring my thesis and provided valuable feedback and insights on how to improve my work. Dr. A. Kiricheck guided me throughout the process and gave feedback during progress meetings.

I would also like to express my gratitude to Susana Costas for assisting me with the qualitative analyses of my samples before I conducted the quantitative research. The experiments I conducted for my thesis began at the Waterlab at the TU Delft. Here, I would like to express my gratitude to Chantal and Pieter for their support with guidance on methodologies at TU Delft. After completing my experiments at the TU Delft, I continued my research at Boskalis. I am grateful to Annouk Rey for facilitating my access to Boskalis laboratory and for connecting me with Joey Boganen, who guided me through the laboratory work and engaged in insightful discussions that introduced new ideas for my master's thesis. I also wish to thank Jurre van der Werf for helping me understand the significance of sediment characteristics. At

the end of November, I began my research at Deltares, where I had the privilege of receiving guidance from Dr. Miguel de Lucas Pardo. I am grateful for his guidance, expertise and willingness to share his knowledge throughout my research. His insightful advice not only helped me determine the most relevant experiments for my thesis but also significantly improved my understanding of sediment analysis. Beyond his technical support, his encouragement made my time at Delatres productive. I also want to express my gratitude to Saskia Huisman, who supported me in the Deltares lab and made our lunch breaks especially enjoyable. Additionally, I would like to thank John Langstraat, Ir. Cihan Cengiz and Marcel for their assistance in setting up various methods for analyzing sediment characteristics in my samples. Furthermore, I extend my gratitude to the GEO department at Deltares for introducing me to the company and for the enjoyable lunch and coffee breaks that made my experience even more memorable.

Summary

With increasing threats from climate change, the vulnerability of coastal areas is heightened. One major challenge is the degradation of beaches due to flooding and erosion. Tropical and subtropical beaches are crucial nesting sites of sea turtles who are essential to marine ecosystems by supporting the preservation of coral reef and transporting nutrients from the ocean to coastal environments. Developing engineering maintenance or designing nature-based solutions can help mitigate the effects of flooding and erosion, preserving or expanding sea turtle nesting beaches. To effectively develop nature-based solutions that enhance sea turtle beaches by improving nesting suitability and reducing flooding and erosion, an understanding of the natural processes on small-scale environmental variables, such as sediment characteristics, are essential. The sediment characteristics are important for the survival of sea turtles because they influence the nesting behavior, egg survival and hatching success. Unfortunately, current data on sediment characteristics are scarce, especially at a global scale, which makes it difficult to identify global patterns of these characteristics across sea turtle nesting beaches.

The aim of this study was to analyze key sediment characteristics of sixteen globally significant sea turtle nesting beaches and to evaluate different experimental methods to investigate these sediment characteristics as a pilot study. The key sediment characteristics in this pilot study included color, particle size, particle grading, particle shape, bulk density, solid particle density, angle of repose, thermal retention, and porosity. This research served as a pilot study for a more extensive analysis that will be applied to approximately 2000 sediment samples from 209 sea turtle nesting beaches worldwide. To achieve this, 32 sediment samples were examined from sixteen beaches, with one sample taken from the nesting line and one from the shoreline at each location. The nesting line was identified by visible nests and body pits, while the shoreline was defined as the highest point of debris left by the retreating tide. The sediment samples were analyzed using both qualitative and quantitative methods in different laboratories (TU Delft, Boskalis and Deltares). Qualitative methods included the Munsell color chart, Power scale, classification of sorting (well-sorted vs. poorly sorted), sand ruler and LEICA digital microscope. Quantitative methods included dry sieving, Dynamic Image Analysis (DIA), Static Light Scattering (SLS), free-fall & vibration table, volume of water displacement, helium gas displacement pycnometer, image-based angle of repose analysis and thermal retention analysis.

The results showed that all sixteen nesting beaches in this study were composed of well-sorted, medium-sized sand. These beaches may also be characterized by particles with moderate roundness and high circularity. Variations in bulk density and solid particle density suggested that sea turtles nest in diverse beach conditions, without a clear preference for specific density values. Results for angle of repose and thermal retention did not yield meaningful patterns related to sea turtle nesting preferences. Porosity values were consistent with those typically found in sandy environments. However, definitive conclusions about sea turtle nesting preferences can not be drawn at this stage, given the limited sample size and the lack of comparative data from non-nesting beaches. The findings should be considered suggestive rather than conclusive, and their main purpose is to guide future research directions.

This study also identified differences between key sediment characteristics at the nesting- and shoreline. While some variation was observed, no general statically significant differences were found between these two environments. Based on these findings, future large-scale studies may consider initially focusing on the sediment samples at the nesting line. No clear relationships were observed between sediment characteristics and latitude, and sea turtle species did not show distinct preferences for specific sediment characteristics. However, these findings should be further investigated with a large number of sampling sites.

For large-scale sediment analysis, DIA would be the most efficient alternative to analyze particle size and it also provides information on particle shape. Although dry sieving remained the most reliable method, it might be time-consuming for analyzing a large number of sediment samples. Regarding solid particle density analysis, the helium gas pycnometer seemed to be the most accurate option. However, it required professional expertise. Nevertheless, no significant differences were revealed between results obtained from the gas pycnometer and the volume of water displacement. The reliability of the water displacement method remained uncertain, and further testing was necessary to validate its accuracy or consider alternative methods.

Based on the outcomes of this pilot study, future research is recommended to pursue a more comprehensive and globally representative understanding of sediment characteristics at sea turtle nesting beaches. This will involve analyzing sediment samples from 209 beaches, focusing on the nesting line. The extended study will asses key characteristics, including color, particle size, particle shape, bulk density, solid particle density and porosity. The resulting dataset will provide essential information for researchers, ecologists and coastal engineers, and may contribute to the development of nature-based solutions, such as beach nourishment, to protect sea turtle nesting areas.

Contents

List of Figures

List of Tables

Nomenclature

Abbreviations

Abbreviation	Definition
CC	Caretta Caretta (Loggerhead turtle)
CM	Chelonia Mydas (Green turtle)
CPA	Computerized Particle Analyzer
DC	Dermochelys Coriacea (Leatherback turtle)
DIA	Dynamic image analysis
EI	Eretmochelys Imbricata (Hawksbill turtle)
IUCN	International Union for Conservation of Nature
LK	Lepidochelys Kempii (Kemp's Ridley turtle)
LO	Lepidochelys Olivacea (Olive Ridley turtle)
LOI	Loss On Ignition
ND	Natator Depressus (Flatback turtle)
NL	Nesting Line
PSD	Particle Size Distribution
RI	Refractive Index
SEM	Scanning Electron Microscopy
SL	Shoreline
SLR	Sea Level Rise
SLS	Static Light Scattering
TGA	Thermogravimetric Analysis
TKI	Topconsortium voor Kennis en Innovatie
TU	Technische Universiteit
XRF	X-Ray Fluorescence

1

Introduction

1.1. Background

Sea turtles have existed far longer than humans. They have been navigating the world's oceans for more than 100 million years (Oceana 2010). There are seven sea turtle species, including Loggerhead turtle (CC), Green turtle (CM), Hawksbill turtle (EI), Leatherback turtle (DC), Olive Ridley turtle (LO), Kemp's Ridley turtle (LK) and Flatback turtle (ND). In the absence of these sea turtles, most of the marine ecosystems would suffer greatly. Every specie plays a vital role in the world's oceans. Green sea turtles are essential to seagrass ecosystems because few species consume seagrass. Their grazing encourages new growth and prevents the seagrass from becoming too long and dense (WWF 2025). They also digest seagrass quickly, and their waste returns nutrients to the ecosystem, supporting other plants and animals (WWF 2025). Hawksbill sea turtles are important to coral reef ecosystems because they are significant predators of sea sponges (Łukowiak et al. 2018). By regulating sponge populations, they contribute to the reef's healthy balance. Leatherback sea turtles play a crucial role in maintaining jellyfish populations across the world's oceans, as jellyfish are their primary food source (Mrosovsky et al. 2009). Yet today, sea turtles face severe challenges, not only from human activities, but particularly from climate change (Mancino et al. 2023). According to the International Union for Conservation of Nature, six out of the seven sea turtle species are classified as endangered (IUCN Red List Of Threatened Species n.d.). Climate change intensifies rising sea levels and increased storm activities, accelerating coastal erosion and flooding, which threaten sea turtle nesting beaches. The degradation of these beaches is a major challenge to sea turtle nesting success. This challenge is further intensified by the geographical distribution of nesting sites. Many are located in the tropics, regions prone to tropical cyclone activity and within developing countries, making them particularly vulnerable (Vitousek et al. 2017).

To protect the sea turtle nesting beaches, it is essential to develop engineering solutions or designing nature-based strategies to mitigate the impacts of flooding and erosion. Nature-based solutions are innovative conservation approaches that aim to protect, manage, and restore natural ecosystems while delivering long-term benefits to human societies (IUCN 2020). In addition, these solutions can offer protection to coastal communities facing similar climate risks.

1.2. Knowledge gap

To develop effective nature-based solutions, an understanding of the natural processes within the coastal ecosystem is essential. This includes not only large-scale hydrodynamic processes, such as wave action and sediment transport, but also small-scale environmental variables at the nesting site level, such as sediment characteristics.

The sediment characteristics are important for the survival of sea turtles because they influence the nesting behavior, egg survival and hatching success (J. Mortimer 1990 & T. Zhang et al. 2025). Despite their ecological importance, detailed data on sediment characteristics at sea turtle nesting beaches remain limited, particularly in remote areas with limited access to scientific resources. For example, access to scientific equipment, standardized sampling methods, and long-term monitoring is often lacking. Furthermore, while most studies have focused on specific nesting sites, there is no comprehensive, standardized analysis that integrates findings at a global level (Campbell 2019, Cisneros et al. 2017, Fadini et al. 2011 & Siqueira-Silva et al. 2020). As result, a global understanding of which sediment characteristics are important for sea turtle nesting success remains unclear.

This lack of large-scale data makes it difficult to identify global patterns in sediment characteristics across sea turtle nesting beaches. Therefore, there is a need for research that both evaluates sediment characteristics at a global scale and explores consistent, feasible methods for sediment analysis.

1.3. Research objective

The aim of this study was to analyze key sediment characteristics of sixteen globally significant sea turtle nesting beaches and to evaluate different experimental methods to investigate these sediment characteristics as a pilot study. By doing so, the research serves as a foundation for a more extensive analysis that will eventually be applied to all available sediment samples. Understanding both the relevant sediment characteristics and the most effective methods for their investigation will enhance the accuracy and efficiency of the large-scale study. This understanding will contribute to broader knowledge of future nature-based coastal interventions that protect both sea turtle populations and coastal communities.

The research focused on analyzing sediment samples from sixteen important nesting beaches, which are among the most frequently visited by sea turtles worldwide. These samples, provided by the University of Exeter, include sediments collected from both the nesting- and the shorelines at these sites. The nesting line was identified by visible nests and body pits, while the shoreline was defined as the highest point of debris left by the retreating tide. The study focused on key sediment characteristics identified in previous literature as influencing the nesting success of sea turtles, including color, particle size, particle grading, particle shape, bulk density, solid particle density, angle of repose, thermal retention, and porosity. Additionally, this study covered all seven sea turtle species.

1.4. Research questions

In order to achieve the main objectives of this study, the following research questions have been formulated. The central research question was: *What global patterns in key sediment characteristics can be identified across sixteen globally important sea turtle nesting beaches, and how can these characteristics be efficiently analyzed?*

The key sediment characteristics in this pilot study included color, particle size, particle grading, particle shape, bulk density, solid particle density, angle of repose, thermal retention, and porosity. To comprehensively address this question, several sub-research questions have been defined:

1. Which methods can be applied and are available at TU Delft, Boskalis and Deltares to assess the key sediment characteristics?
2. How do key sediment characteristics vary across the sixteen selected nesting beaches, specifically at the nesting line?
3. How do key sediment characteristics differ between the nesting line and the shoreline?
4. How are the key sediment characteristics of sea turtle nesting beaches associated with latitude?
5. Do specific sea turtle species show preferences for particular key sediment characteristics?
6. What are the most feasible methods for analyzing particle size and solid particle density in sediment samples from sea turtle nesting beaches?

1.5. Thesis outline

The literature review in Chapter 2 provides an overview of existing research on coastal environments, sea turtle nesting habitats, and methodological approaches to sediment analysis. The chapter identifies the impacts of climate change on coastal areas and highlights key sediment characteristics (color, particle size, particle grading, particle shape, bulk density, solid particle density, angle of repose, thermal retention, and porosity) that influence the nesting success of sea turtles. Based on findings in literature, the first sub question is partly answered; *which methods can be applied to assess the sediment characteristics?*

The second part of the first sub question is answered in Chapter 3. This chapter consists of three parts: qualitative analyses (Section 3.3), quantitative analyses (Section 3.4), and comparative testing of existing datasets (Section 3.5). Section 3.3 focus on how to assess the sediment characteristics: color, particle shape, grading, and size. Based on the results of these qualitative analyses, certain quantitative analyses will be performed. Section 3.4 shows the quantitative analyses which assess particle size, grading, shape, bulk density, solid particle density, angle of repose, thermal retention, and porosity. Section 3.5 reveals how all findings are analyzed.

The results (Chapter 4) presents the key findings from the three analyses. With both qualitative and quantitative analyses, the second sub question is answered: *How do key sediment characteristics vary across the sixteen selected nesting beaches, specifically at the nesting line?*. With the comparative analyses the remaining four sub questions are answered: *how do key sediment characteristics differ between the nesting line and the shoreline?, how are the key sediment characteristics of sea turtle nesting beaches associated with latitude?, how are the key sediment characteristics of sea turtle nesting beaches associated with latitude?, do specific sea turtle species show preferences for particular key sediment characteristics? and what are the most feasible methods for analyzing particle size and solid particle density in sediment samples from sea turtle nesting beaches?*

In the discussion (Chapter 5) the findings of this study are interpreted in the context of existing literature. Potential coastal management solutions are discussed and the limitations of this pilot study are addressed. In Chapter 6 conclusions are drawn. Based on these conclusions a plan for future research

has been developed.

2

Literature review

2.1. Sea turtles

Sea turtles help keep ocean ecosystems healthy. They play a significant role in their environment and influence the species around them, which is why they are considered keystone species. There are seven sea turtle species globally: the Loggerhead turtle (Caretta caretta, CC), the Green turtle (Chelonia mydas, CM), the Hawksbill turtle (Eretmochelys imbricata, EI), the Leatherback turtle (Dermochelys coriacea, DC), the Olive Ridley turtle (Lepidochelys olivacea, LO), the Kemp's Ridley turtle (Lepidochelys kempii, LK), and the Flatback turtle (Natator depressus, ND). They breed every one to three years and usually hatch at the same beaches where they were born.

Marine ecosystems benefit from the presence of Loggerhead turtles, as their shells provide habitat for organisms such as barnacles, crabs, and algae (National Geographic n.d.(d)). Loggerhead turtles prefer coastal habitats in subtropical and temperate regions of the Mediterranean Sea, and the Pacific, Indian, and Atlantic Oceans (IUCN Red List Of Threatened Species n.d.). They can travel long distances to their breeding sites. They navigate at sea using the Earth's magnetic field, where each shoreline has a unique magnetic signature. Hatching occurs throughout the year, but primarily in the summer, during which females can lay two to five clutches with different mates (National Geographic n.d.(d)). The nesting beaches of Loggerhead turtles are generally sandy, wide, open beaches bordered by low dunes and a flat sandy shore face (Miller et al. 2003). Christiaanse et al. found that Loggerhead turtles prefer nesting regions with low tidal ranges and minimal surge levels (Christiaanse et al. 2024). Furthermore, Loggerhead turtle nesting regions show slight negative correlations with the distance to the nearest seagrass habitat and median surge levels (Christiaanse et al. 2024).

Green sea turtles are essential to seagrass ecosystems because few species consume seagrass. Their grazing encourages new growth and prevents the seagrass from becoming too long and dense (WWF 2025). They also digest seagrass quickly, and their waste returns nutrients to the ecosystem, supporting other plants and animals (WWF 2025). Green turtles are found in tropical and subtropical coastal waters globally. There are two varieties of Green turtles, and scientists are still debating whether they are distinct species or subspecies. The Atlantic Green turtle typically inhabits the coasts of Europe

and North America, while the Eastern Pacific Green turtle is found along coastal seas from Alaska to Chile (National Geographic n.d.(a)). Similar to Loggerheads, Green turtles migrate long distances from their feeding sites to their sandy hatching beaches. Mating occurs every two to four years, usually in shallow waters along the shore. Females often choose to nest at the same beach where their mothers laid their eggs. Christiaanse et al. indicated that nesting regions for Green turtles have weak negative correlations with tidal range and strong negative correlations with extreme surge levels and distance to the closest coral habitat (Christiaanse et al. 2024). Weak positive correlations were noted with median wind velocity at nesting regions. Furthermore, significant positive relationships were observed with sea surface temperature (Christiaanse et al. 2024).

Hawksbill sea turtles are important to coral reef ecosystems because they are significant predators of sea sponges (Łukowiak et al. 2018). By removing prey such as sponges from the reef's surface, they facilitate access for reef fish to feeding areas. Hawksbill turtles inhabit the tropical waters of the Atlantic, Pacific, and Indian Oceans, preferring shallow waters. Female Hawksbill turtles hatch at beaches where they were born every two to five years (National Geographic n.d.(b)). Nesting regions for Hawksbill turtles show a significant positive correlation with sea surface temperature and a weak positive correlation with median surge levels. There is a strong negative correlation of the Hawksbill's nesting regions with extreme surge levels and distance to the nearest coral habitat, along with a weaker negative correlation with distance to the nearest seagrass habitat (Christiaanse et al. 2024).

Leatherback sea turtles play a crucial role in maintaining jellyfish populations across the world's oceans, as jellyfish are their primary food source (Mrosovsky et al. 2009). Leatherback turtles are globally distributed across the tropical and temperate waters of the Atlantic, Pacific, and Indian Oceans, and the Mediterranean Sea. They can adapt their body temperature to cold waters by retaining body heat. Male Leatherbacks spend their entire lives at sea, but female Leatherbacks return to the same beaches from which they hatched (National Geographic n.d.(c)). According to Christiaanse et al., nesting regions for Leatherback turtles are significantly negatively correlated with extreme surge levels and weakly negatively correlated with the tidal range (Christiaanse et al. 2024). Strong positive correlations are observed with sea surface temperature, and weak positive correlations are found with median surge levels (Christiaanse et al. 2024).

Olive Ridley turtles help maintaining the health of coral reefs and sea grass beds. They prefer open oceans worldwide. Their nesting beaches are globally spread in tropical and subtropical areas and are active from June to December (National Geographic n.d.(e)). Nesting regions for Olive Ridley turtles exhibit slight negative relations with the distance to the nearest coral habitat. There is a notable positive correlation with sea surface temperature and mild positive correlations with median wave period, distance to ocean currents above 0.3 m/s, and distance to the nearest seagrass habitat (Christiaanse et al. 2024).

Kemp's Ridley turtles are primarily found in the Gulf of Mexico. This species is the most endangered sea turtle species. Their nesting period is typically between May and July (Oceana n.d.(b)).

The Flatback turtle inhabits the coastal waters of Australia and Papua New Guinea. Unlike most sea turtle species, the Flatback turtle does not undertake long migrations. Flatback turtles only nest on beaches in Australia and lay fewer eggs than other sea turtles. As previously mentioned, there is limited data on these turtles, and therefore their extinction status is unknown. However, the Australian

government considers the Flatback turtle to be vulnerable, as their situation is likely similar to that of other sea turtle species (Oceana n.d.(a)).

Despite their long evolutionary history, sea turtles face severe challenges. In addition to human-induced pressures such as fisheries, coastal development and pollution, climate change has emerged as a particularly critical challenge for sea turtle populations worldwide (Mancino et al. 2023). As keystone species, the disappearance of sea turtles from its habitat, the natural balance can be disrupted, leading to various impacts on both flora and fauna. According to the International Union for Conservation of Nature (IUCN), six of these species are globally threatened. The IUCN Red List categorizes species into nine levels of conservation status: Not Evaluated, Data Deficient, Least Concern, Near Threatened, Vulnerable, Endangered, Critically Endangered, Extinct in the Wild, and Extinct. The Hawksbill and Kemp's Ridley turtles are listed as Critically Endangered, the Green turtle as Endangered, and the Loggerhead, Olive Ridley, and Leatherback turtles as Vulnerable. The Flatback turtle, due to insufficient data, is listed as Data Deficient (IUCN Red List Of Threatened Species n.d.). Given the endangered status of sea turtle species and the increasingly severe effects of climate change on coastal environments, it is essential to understand how these climate changes impact coastal systems and, in particular, how they affect sea turtles.

2.2. Effects of climate Change

Global ecosystems are undergoing significant changes due to climate change, with serious consequences for biodiversity (Mancino et al. 2023). Marine ecosystems are particularly affected, not only by climate change but also by anthropogenic pressure such as global overfishing, which has resulted in a 39% decline in marine species and a 50% reduction in coral reefs worldwide (Mancino et al. 2023). Despite these pressures, climate change remains the greatest threat, with 14% of all ocean species already heavily impacted (Mancino et al. 2023). Sea turtles are essential for understanding the broader impacts of global changes in ecosystems. They serve as important indicators due to their survival and behavior are closely tied to their surroundings, making them valuable species for studying the effects of climate change on marine biodiversity (Mancino et al. 2023).

2.2.1. Climate change impacts on sea turtles

Climate change induced several threats, including high incubation temperature, increased sea surface temperature, SLR and higher storm activities (Patrício et al. 2021). These changes impact sea turtle populations in various ways, such as altering sex ratios, hatching success, breeding patterns and nesting site availability (Patrício et al. 2021).

Sea turtles have temperature-dependent-sex-determination (TSD). With increasing temperature due to climate change, some sea turtle populations may become predominantly female (Patrício et al. 2021). Even minor fluctuations in nest temperatures during incubation can critically influence hatching success. Additionally, the breeding capabilities of sea turtles are determined by their physical condition and therefore they are dependent on environmental conditions which will be altered by climate change (Patrício et al. 2021).

SLR will likely reduce the availability of nesting beaches, especially in developed regions where natural sediment transport is restricted due to coastal developments (Patrício et al. 2021). The rising sea levels

can lead to increased saltwater inundation, altering the salinity of nesting environments and negatively affecting hatching success (Patrício et al. 2021). Additionally, enhanced storm activities associated with climate change are likely to exacerbate beach erosion, wash away nests, alter sediment supply, change beach profiles and flood nests, increasing egg mortality and reducing reproductive success (Fuentes et al. 2010). Storms can change beach morphology, causing significant beach face lowering and retreat within hours or days, while recovery under calmer conditions may take weeks to months. This intensification of beach erosion is expected to lead to a decline in available nesting areas for sea turtles (Chevallier et al. 2023).

Sea turtles have the potential to adapt to environmental changes by altering their spatial and temporal distribution or adjusting their nesting and feeding behavior. However, their unique reproductive physiology makes them vulnerable to climate conditions, especially when in the incubation time and development of their eggs (Mancino et al. 2023). Nevertheless some sea turtle species are beginning to adapt to climate change, but their responses are often not rapid enough to cope with the accelerating pace of environmental changes (Patrício et al. 2021). This situation highlights the urgent need for innovative conservation strategies.

2.2.2. Climate change impacts on coastal areas

There is growing awareness within coastal engineering of the urgent need to develop long-term conservation strategies that enhance the resilience of coastal areas to the impacts of climate change. Due to climate change, the global mean sea level has risen at an accelerating pace over the past 25 years and is projected to continue rising (Nerem et al. 2018). Sea level rise (SLR) is closely linked to greenhouse gas emission, the primary drivers of climate change. These gasses trap heat in the atmosphere, leading to accelerating SLR, the melting of ice caps and disruptions in local climates. However, the rise in mean sea level is not uniform across the globe, as various factors create region-specific differences, complicating the implementation of universal solutions. In addition to SLR, climate change will modify wave patterns and storm surges, both of which play crucial roles in shaping coastal regions (Slott et al. 2006). Unfortunately, the understanding and projections of these factors are less advanced compared to SLR, and as a result, they have not been fully incorporated into risk assessments, overlooking critical drivers of coastal impacts (Toimil et al. 2019). Climate change also leads to rising temperatures and shifts in large-scale atmospheric circulation patterns, which can affect the frequency and intensity of tropical cyclones and extra-tropical storms. However, projecting the response of storms to a warming climate remains challenging due to complexity of thermodynamic processes. Although the overall number of tropical cyclones is expected to decline or remain stable, their intensity is likely to increase as sea surface temperature rises. Projections indicate that the percentage of the more powerful storms will increase, along with a rise in maximum wind speed (Muis et al. 2023). As a result of SLR and changes in storm activity, coastal flooding and erosion are expected to become more frequent. Vousdoukas et al. provided a comprehensive global analysis of sandy shoreline changes over the 21st century, revealing a general trend of intensifying erosion on sandy beaches, worsened by higher greenhouse gas emissions (Vousdoukas et al. 2020).

This growing risk of flooding and erosion has promoted coastal zones to adapt. Historically, most adaptations relied on rigid structural solutions designed for cost-effectiveness over their lifetimes (Kraus 1996). However, nowadays coastal engineering defense work on sandy shorelines is shifting towards

soft and hybrid systems, which allow beaches to remain more dynamic and resilient by utilizing natural buffers and sedimentation processes (Hanson et al. 2002). This evolving approach to coastal management reflects increasing awareness of climate change and its long-term impacts. Coastal engineering must now incorporate climate change into both mid- and long-term planning decisions. Interventions should be viewed as part of the broader coastal system rather than in isolation (Hall et al. 2003 & Nicholls, Townend, et al. 2013). Furthermore, coastal engineering strategies must adopt flexible approaches due to the long timescale of SLR (Clark et al. 2016 & Nicholls, Brown, et al. 2018).

Recently, the importance of ecosystems in coastal protection has received special attention, in so called nature-based solutions. While there is no definitive proof that nature-based solutions are more effective than conventional coastal protections, they offer advantages by being more adaptable to the uncertainties of climate change (Toimil et al. 2019). For instance, projects like the Sand Engine in the Netherlands demonstrate the potential of nature-based solutions to evolve with changing climate conditions. However, the scientific knowledge and design criteria for many nature-based solutions are still underdeveloped, necessitating further research (Toimil et al. 2019).

2.3. Nesting habitat of sea turtles

To develop effective nature-based solutions requires a thorough understanding of the natural processes within the coastal ecosystem. Sediments play a central role in these processes, as they are closely linked to the morphology and dynamics of the coastal processes. Changes in sediments can alter the physical characteristics of beach ecosystems (a.o. slope, width, tidal range) (Cisneros et al. 2017). These physical characteristics not only shape the beach itself but also influence, for example, which organisms inhabit it and how species like sea turtles nest and survive. Previous studies indicate that the characterization of sediments influence the survival of sea turtles, because they affect the nesting behavior, egg survival and hatching success of sea turtles (J. Mortimer 1990, Cisneros et al. 2017, Siqueira-Silva et al. 2020, Fadini et al. 2011 & T. Zhang et al. 2025).

2.3.1. Nesting site selection

Sea turtles nest on sandy beaches. A potential nesting beach must require several characteristics for successful nesting: (1) nesting beaches must be easily accessible from the ocean, (2) high enough to avoid frequent submersion by tides, (3) have sufficient sand cohesion to permit nest construction and (4) maintain temperatures favorable for egg development (Miller et al. 2003). Despite consistent trends in nesting site selection, the precise environmental factors influencing sea turtle nesting behavior remain not fully understood (Miller et al. 2003, Siqueira-Silva et al. 2020 & Fadini et al. 2011). Siqueira-Silva et al. revealed that anthropization and slope of the beach were important factors that reduce the number of sea turtle nests at a beach (Siqueira-Silva et al. 2020). Human activities, such as tourism and settlement, and a very flat beach reduced the nesting density (Siqueira-Silva et al. 2020).

The place where sea turtles lay their eggs has serious consequences for hatchling survival. The embryos are sensitive to extreme environmental conditions in three key aspects: (1) moisture level (substrate humidity and salinity) (2) gas diffusion, and (3) thermal conditions (Miller et al. 2003). Changes in moisture level, gas diffusion and thermal conditions can influence how the others affect the embryo. Moisture affects water uptake and gas flow. Gas exchange is critical for oxygen supply and temperature controls development rate and sex ratio (Miller et al. 2003). These three aspects could be influenced

due to several sediment characteristics, including particle size and particle shape (J. Mortimer 1990), indicating the importance of sediment characteristics

The factors driving nesting site selection and the impacts of beach characteristics on hatching success are not yet fully understood (Fadini et al. 2011). Nevertheless, several factors have been identified to be relevant: particle size (J. Mortimer 1990), mineral composition of the sand, nest inundation, height above sea level, and distance from the sea (Fadini et al. 2011).

2.3.2. Sediment characteristics

Some studies investigated the influence of sediment characteristics of sea turtle nesting beaches on the survival of sea turtles in various ways, including nesting behavior, egg survival and hatching success.

Particle size is the most analyzed sediment characteristic across different studies at sea turtle nesting beaches (Cisneros et al. 2017, Siqueira-Silva et al. 2020, J. Mortimer 1990, Miller et al. 2003, Fadini et al. 2011, Campbell 2019). These studies found that sea turtles prefer to nest in sand-sized particles. However, how coarse or fine the particles are differ per study. Cisneros et al. evaluated sediment characteristics at green, leatherback, and loggerhead nesting beaches in Palm Beach County in Florida. The study found that beaches with larger particle sizes had lower nesting and hatching success (Cisneros et al. 2017). However, Mortimer revealed that green turtle nesting beaches differ greatly in particle size, but the majority of green turtle beaches are characterized by moderately sorted sand with mean particle diameters ranging from 0.2-1.0 mm (J. Mortimer 1990). Nevertheless, Mortimer found no correlation between particle size and green turtle population density, suggesting that particle size is not a primary factor in nesting site selection (J. Mortimer 1990).

Mortimer also revealed that that females of the green turtle have difficulty constructing egg chambers in coarse, dry sand (J. Mortimer 1990). In these conditions, females often dig multiple trial chambers and return to the beach multiple times before successfully nesting, unlike in fine sand where they typically dig only one chamber (J. Mortimer 1990). A study of 300 Loggerhead nesting sites in Japan found that sand softness was the most significant characteristics influencing nesting beach selection (Kikukawa et al. 1999). These studies indicate that density could be an important sediment characteristic affecting the nesting behavior of sea turtles.

As previous mentioned moisture level, gas diffusion and thermal conditions are really important for the survival of sea turtle embryos (Subsection 2.3.1 *Nesting site selection*). Sediment characteristics, like particle size, grading and shape, play a critical role in these aspects (Miller et al. 2003 & J. Mortimer 1990). For example, larger particle sizes create more porosity, providing larger, more interconnected void spaces that enhance gas exchange (J. Mortimer 1990). This allows gases like oxygen to diffuse into the nest and carbon dioxide to escape. However, excessive air-filled voids, could be due to too large particles or poorly graded, can lead to egg dehydration (J. Mortimer 1990). J. Mortimer 1990 showed that higher hatching successes was associated with sand that had low air-filled pore space, meaning the driest substrates were linked to lower clutch survival of the green turtle (J. Mortimer 1990). McGehee demonstrated that the most successful nesting sites in Florida of the CC turtle has a moisture content of 25% (McGehee 1990) and Miller et al. revealed that loggerhead turtle eggs incubate in high humidity and well-ventilated substrates (Miller et al. 2003). However, although the moisture content of nesting beaches play a vital role in the development of sea turtle embryos, it is not a reliable long-term

indicator of nesting success, since moisture content varies daily and seasonally (Wood and Bjorndal 2000).

In a study conducted in Brazil, Fadini et al. examined the effects of bioclast volume, albedo and particle size on Loggerhead turtle hatching success and incubation duration (Fadini et al. 2011). Bioclasts are skeletal fragments incorporated into sedimentary deposits (Encyclopedia Britannica n.d.). Albedo, the percentage of solar radiation reflected by a surface, plays a crucial role in beach temperature. Darker sands absorb more radiation and result in higher temperatures, while lighter sands reflect more light, resulting in lower temperatures. This means that darker sands have a low albedo and lighter sands have a high albedo (Fadini et al. 2011). The study found that albedo had the greatest influence on the incubation duration of sea turtle embryos compared to bioclast volume and particle size. Incubation was shorter in nests on sediments with lower albedo (darker sand). However, at one beach, incubation duration was longer in lower albedo sediments due to the presence of biogenic materials that conduct less heat, extending incubation time. This research show that carbonate content (and therefore the overall mineral composition) and color might play an important role in the survival of sea turtles. According to Cisneros et al., beaches with higher carbonate content revealed reduced nesting and hatching success for green, Leatherback, and Loggerhead turtles and Mortimer found that green turtle nesting beaches differ greatly in color and mineral composition (Cisneros et al. 2017 & J. Mortimer 1990).

Studies demonstrated that salinity of the beach greatly influence the nesting selections and survival rates (Wood and Bjorndal 2000, Miller et al. 2003 & J. Mortimer 1990). Nesting beaches of the green turtle in Australia have a lower salt content in surface sand compared to beaches where turtles do not nest (Wood and Bjorndal 2000). Additionally, clutch survival rates of the green turtles were negatively correlated with high salinity levels (J. Mortimer 1990) and according to Miller et al. loggerhead turtle eggs incubate in low salinity substrates (Miller et al. 2003). Like moisture, however, salinity varies with weather and seasons, making it an unreliable long-term indicator (Wood and Bjorndal 2000).

2.4. Methodological approaches to sediment analysis

To enhance the understanding of global patterns in key sediment characteristics, these properties must be analyzed. A review of the literature on methodological approaches to sediment analysis is essential for identifying reliable techniques and data collection.

Sediment characteristics can be categorized into two main groups: physical properties and chemical properties. Each property offers valuable insights into the composition, behavior and function of sediments from both environmental and engineering perspectives. Physical properties refers to characteristics of samples that can be observed and measured without altering the sample's chemical composition. The physical properties described in this section include particle size, grading, density, porosity, and permeability. In contrast, chemical properties describe characteristics of the sample that can be observed in a chemical reaction. The chemical properties discussed in this section include zeta potential, flocculation rate, organic matter content, calcium carbonate content, and mineral composition. Various methodological approaches are used to analyze different sediment characteristics and the most commonly utilized techniques are described in this section (Table 2.1).

Properties	Methodological approaches	Sediment characteristics	Sediment type
Physical	Sieve analysis	Particle size and grading	Coarse & medium
	Sedimentation column	Settling velocity & Particle size and grading	Medium
	Hydrometer tests	Particle size and grading	Medium & fine
	Sedigraph method	Particle size and grading	Fine
	SLS	Particle size and grading	Fine
	CPA	Particle size, grading and shape	Medium & fine
	Pycnometer	Density & Porosity	Coarse & medium
	Volumetric flask	Density & Porosity	Coarse & medium
	Gravimetric	Density & Porosity	Coarse & medium
	Gas pycnometer	Density & Porosity	Medium & fine
	Mercury porosimetry	Porosity	Medium & fine
	Constant head test	Permeability	Coarse & medium
	Falling head test	Permeability	Fine
	Triaxial method	Permeability	All three
	Using Empirical equations from PSD	Permeability	
	ZetaSizer	Zeta potential	Fine
	ZetaNano	Zeta potential	Fine
	FLOCCAM	Flocculation	Fine
Chemical	Microscope	Organic matter & Mineral composition	All three
	LOI	Organic matter	All three
	TGA	Organic matter & Calcium carbonate content	All three
	Hydrogen peroxide	Organic matter & Calcium carbonate content	All three
	Hydrochloric acid with volumetric determination	Calcium carbonate content	All three
	Hydrochloric acid with mass loss	Calcium carbonate content	All three
	SEM	Mineral composition	Medium & fine
	XRF	Mineral composition	Medium & fine
	Wet chemistry	Mineral composition	Medium & fine

Table 2.1: Overview of methodological approaches from the literature review. This overview categorizes sediment types as coarse, medium, or fine based on the grain size typically analyzed by each method. Coarse sediments include coarse sand, gravel, and larger particles. Medium sediments include medium sand and fine sand. Fine sediments include very fine sand, silt, clay, and smaller particles. The methods highlighted in gray were used in this study.

2.4.1. Particle size and grading

Particle size is one of the primary variables used to analyze sediments. This sediment characteristic is commonly expressed using the median particle diameter (D_{50}). D_{50} represent a central reference point in the sediment particle size distribution and is therefore a reliable indicator of the overall grain size. The 'D' represents the particle size diameter and '50' indicates that 50$\%$ of the sample's total weight consists of finer particles. Particle size classification can range from large boulders to very fine particles such as clay. Geologists often use the Wentworth classification for this purpose, as illustrated in Figure 2.1 (Bosboom and Stive 2023). Sand, a non-cohesive material, is classified by a particle size diameter between 63 μm and 2 mm, primarily consisting of quartz and carbonate. This material is abundant worldwide, especially in subtropics and lower mid-latitudes regions. Sediments finer than a particle size diameter of 63 μm are defined as silt or clay. Clay particles have a large surface area relative to their volume, making them chemically active and tend to have cohesive properties (Bosboom and Stive 2023).

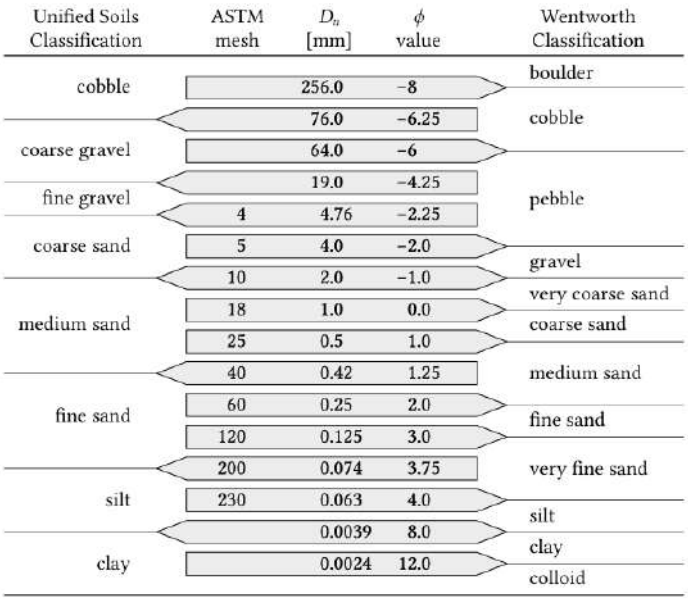

Figure 2.1: Wentworth classification (Wentworth 1922 & Bosboom and Stive 2023).

Another way to describe sediment texture is through grading, which refers to the uniformity of particle sizes (P. Webb 2020). Sediments can be described as well-sorted if the ratio D_{90}/D_{10} is small (< 1.5), indicating uniform particle sizes. A large ratio (> 3) indicates poorly sorted or well-graded samples with a wide variety of particle sizes (Bosboom and Stive 2023).

Particle size distribution (PSD) describes the range and proportion of particle sizes present in a sample. This can be measured using several methods: (1) sieving, (2) sedimentation column, (3) hydrometer tests, (4) the sedigraph method, (5) Static Light Scattering (SLS), and (6) Computerized Particle Analyzer (CPA). Currently, the two most commonly used methods are sieving and laser diffraction (K. Zhang et al. 2015).

Sieve analysis is commonly used for samples samples containing sand or gravel-sized particles (TU Delft n.d.). A sieve analysis separate particles by size using a stack of sieves with increasingly smaller openings. Each sieve collects particles that are larger than their openings, but smaller than the openings of the sieves above it. The sieves are weighed to determine the percentage of the total sample mass retained by each sieve. The procedure can be done by wet or dry sieving, according to British standards (BS 1377-1/2:1990).

Sedimentation column is an alternative method for sand and gravel size particles. This method measures the settling velocity of particles in a water column and the appropriate settling velocity equation is used to calculate PSD (TU Delft n.d.). A weighed sample is poured into a tall, transparent column filled with water. The particles will settle according to their size and weight, with larger particles settling faster. Due to the small sample size, the effect of sediment concentration in the settling cloud on particle velocity is negligible. However, the disadvantages of this method is that the length of the column is too short to accurately measure very coarse particles, as they settle too quickly and reach the bottom before sufficient data can be collected (TU Delft n.d.).

Hydrometer tests are used to measure PSD of particles finer than 0.075 mm, which are too fine

for sieving (TU Delft n.d.). The test is based on Stokes' Law, which states that the settling velocity of particles in a fluid is proportional to their particle size. Smaller particles settle more slowly due to their terminal velocity. The terminal velocity is a constant speed that a falling object reaches when the gravitational force equals the drag and buoyancy forces. A hydrometer is a device that measures the density of the suspension by at a given depth over time. As sedimentation occurs, the density of the suspension decreases causing the hydrometer to float lower in the liquid. The procedure involves dispersing a dry sample in distilled water or another dispersing agent to prevent flocculation. The mixture is poured into a cylinder, which is then agitated to ensure even particle distribution throughout the column. At specific time intervals, the hydrometer is used to measure the suspension density.The depth at which the hydrometer floats corresponds to the concentration of particles still in suspension. The effective depth and time are used with Stokes' Law to calculate the size of particles in suspension (Sanz 2018). From these readings, the PSD curve is constructed, showing the percentage of particles finer than each size.

The **sedigraph method**, like hydrometer tests, is based on Stokes' Law but employs X-rays to track particle sedimentation and calculate settling velocities (Sanz 2018). A parallel X-ray beam is used to measure changes in the concentration of suspended particles during settling at different depths and time intervals. The settling velocity is determined by dividing the distance traveled by the time taken (Sanz 2018). The sedigraph processes the sedimentation data and calculates the particle size distribution (PSD), providing a detailed analysis of particle sizes.

Static Light Scattering, also known as laser diffraction, measures particle size by analyzing the scattering patterns of light as a laser beam passes through a dispersed sample. The technique determines the angular variation of scattered light: large particles scatter light at small angles, while small particles scatter light at large angles. The observed scattering pattern is analyzed using the Mie theory of light scattering, which quantifies the scattering and absorption of light by particles (Malvern Panalytical n.d.).

Image-based particle characterization provides information about particle size distribution (PSD) and other sediment characteristics. Static image analysis and dynamic image analysis (DIA) are the most commonly used methods for 2D image-based particle characterization (Iskander and Li 2024). A Computerized Particle Analyzer (CPA) is a device that employs DIA to capture the size and shape of particles as fine as 10 microns. In this method, particles are dropped past a camera on a moving tray, and their shadows are detected using LED backlighting. The captured data is processed to determine particle size and shape (Clyde 2019).

Each of these methods produces slightly different PSD results, particularly in the fine particles (< 10 μm) (Sanz 2018). Some studies combine methods: sieving for coarse particles and sedimentation (hydrometer and sedigraph) for fine particles. However, using both methods is time consuming and a large amount of sample is needed (Sanz 2018). SLS is less time consuming and can measure a full particle size spectrum, including very fine particles (2 nm to 2 μm), which cannot be analyzed by traditional methods because the do not settle (hydrometer and sedigraph). Nevertheless, traditional methods (sieving, hydrometer, sedigraph) remain the most widely used in industry, making it crucial to evaluate whether their results are comparable to those from SLS. Studies have shown that SLS tends to underestimates the amount of fines particles (Sanz 2018).

Sanz studied the PSD of various sediment samples using sieving, hydrometer test, SLS and the sedi-

graph test (Sanz 2018). The results confirmed that laser diffraction techniques underestimate fine particle content, as noted in previous studies. To address this, Sanz proposed a new protocol for SLS analysis, aligning its PSD results more closely with traditional methods (Sanz 2018). However, some discrepancies between the different PSDs remain due to measurement errors and the mathematical adjustments made by equipment software (Sanz 2018). Sanz also recommended sieving for sand-sized particles, as it provides better results compared to SLS (Sanz 2018).

Zhang et al. also investigated differences between PSD results from sieving and SLS (using a wet dispersion unit) (K. Zhang et al. 2015). They found that dry sieving measures the second-smallest particle dimension, as particles orient themselves to pass through the sieve opening, given sufficient time. SLS techniques, on the other hand, measure various particle dimensions randomly as particles pass through the light beam. SLS then calculates the equivalent spherical diameter of the particles, assuming all particles are spherical. Therefore, with perfectly spherical particles, dry-sieving and SLS should produce identical PSD results. However, the PSDs of nonspherical particles can differ based on the degree of asphericity (K. Zhang et al. 2015).

Zhang et al. proposed a methodology to determine the most accurate PSD, starting with visually observe the sediment sample under the microscope (K. Zhang et al. 2015). This step helps assess particle size, shape and mineralogy, which provides information about whether dry sieving or SLS analysis is a feasible technique for PSD analysis. Zhang et al. stated that dry sieving should be the preferred technique if the sediment sample consists mainly of sand-sized particles, unless there insufficient sample available (K. Zhang et al. 2015). If highly aspherical particles are observed under the microscope, CPA should be used to determine particle shape. If dry sieving is not feasible, SLS techniques could be utilized as an alternative (K. Zhang et al. 2015).

2.4.2. Density and Porosity

The density and porosity of sediment samples are widely measured sediment properties. The density of solids is independent of temperature and pressure and is defined as mass per unit volume (TU Delft n.d.). Sediment density can be categorized depending on which aspect of the sediment is being studied. The most common densities are bulk density and solid particle density:

- *Bulk density* (ρ_b = m_s / V_t) refers to the mass of oven-dried solids (m_s) per unit bulk volume (V_t) of the sediment, which includes both the volume of solids and the pore space. It is a dynamic soil property that strongly depends on the quantity and size of the pore spaces, as well as the composition of the sediment (Carter and Gregorich 2008). More compact sediments have higher bulk densities than loose, porous sediments. Sandy sediments typically have a higher bulk density because they contain relatively little pore space and are usually low in organic matter (Carter and Gregorich 2008). The bulk density of surface mineral soil typically ranges from 1.0 to 1.6 g/cm^3 (Walters 2021).
- *Solid particle density* (ρ_s = m_s / V_s) is the ratio of the mass of oven-dried solids (m_s) to the volume of solid particles (V_s), excluding the pore spaces. This density determines several interrelationships between porosity, bulk density, air space, and sedimentation rates in fluids (Carter and Gregorich 2008). Solid particle density is independent of porosity and is generally a stable characteristic. In sand fractions it typically ranges from 2.60 to 2.75 g/cm^3 (Santos et al. 2022). The most commonly used reference value for quartz-based sand is 2.65 g/cm^3 (Bosboom and

Stive 2023). Feldspar is the second most common mineral found on sandy beaches, while other minerals, often classified as heavy minerals, typically have densities exceeding 2.7 g/cm^3.

Porosity refers to the percentage of void space within a material, which is influenced by various factors such as the material type. It is defined as the ratio of the volume of pore space to the total volume of the material. Porosity typically ranges from 0.25 (25$\%$) to 0.5 (50$\%$) for natural sands, with 0.4 being a commonly used value (Bosboom and Stive 2023).

The most common methods for determining the solid particle density are the pycnometer and volumetric flask methods due to their accuracy and affordability (Santos et al. 2022). Although the pycnometer method is more precise, it is time-consuming and requires specialized glassware, including a vacuum pump. The volumetric flask method is less expensive but also requires a significant amount of time to perform. Both methods are widely used in soil analysis to determine the density of the solid particles within a soil sample, excluding the pore spaces (Santos et al. 2022).

There are different approaches to determine soil particle density and while they share common foundations with widely used techniques, slight procedural variations exist depending on the laboratory setup and available equipment. In this literature review, the methodologies described by Santos er al. are discussed (Santos et al. 2022).

In the pycnometer method, the process begins by weighing the pycnometer filled with air-free water. Then, the dry soil sample is weighed and added to the pycnometer. The pycnometer is then half-filled with distilled water and boiled to remove air from the soil. This boiling processes differs from Santos et al., where they use a vacuum for air extraction, but boiling is the original methodology. After boiling, the mass of the pycnometer, soil, and water is measured (Santos et al. 2022). Soil particle density is then calculated using the formula below (Santos et al. 2022):

$$d_{PM} = \frac{Ma}{a - b} \tag{2.1}$$

Where, *Ma* is mass of dry soil, *a* is the mass of the pycnometer filled with water and dry soil and *b* is the mass of the pycnometer, soil and distilled water (Santos et al. 2022).

The volumetric flask method, on the other hand, relies on the change in volume. A pre-weighed dry soil sample is added to a volumetric flask containing a known volume of alcohol. The flask is shaken to allow the alcohol to penetrate the soil capillaries, and then the mixture is left to rest for a set time. The flask is subsequently filled with alcohol to a specific volume (Santos et al. 2022). The soil particle density is then calculated using formula 2.2 (Santos et al. 2022). Unfortunately, alcohol will alter the chemical composition of a soil sediment sample.

$$d_{VFM} = \frac{Ma}{VT - Vu} \tag{2.2}$$

Where, *Ma* is mass of dry soil, *VT* is the volume of the volumetric flask and *Vu* is the alcohol volume used to complete the volumetric flask containing the soil sample (Santos et al. 2022).

Santos et al. aimed to develop a methodology that determine the particle density using only a precision scale, so that the method is entirely gravimetric (Santos et al. 2022). They compared the particle

densities of a purely gravimetric method with the two traditional methods and concluded the new method showed consistent values and advances. Santos et al. proposed an entirely gravimetric method to simplify the process of determining particle density (Santos et al. 2022). This method requires only a precision scale and uses no calibrated glassware. The methodology has been shown to produce consistent results when compared to the traditional pycnometer and volumetric flask methods. To determine particle density with the gravimetric method, five values are needed: the weight of the dry soil, the weight of the empty flask, the weight of the flask filled with alcohol, the weight of the flask filled with both soil and alcohol, and the density of the alcohol. This simplified method minimizes errors, reduces the need for specific equipment, and provides reliable measurements with fewer steps and less time (Santos et al. 2022). The particle density using a purely gravimetric method is determined according to Equation 2.3 (Santos et al. 2022).

$$d_{PGM} = \frac{\frac{W_s}{(W_{va}-W_{ve})-W_{vsa}}}{d_a} \tag{2.3}$$

Where, W_s is the weight of the soil added to the flask,W_{va} is the volumetric flask weight filled with alcohol, W_{ve} is the empty volumetric flask weight, W_{vsa} is the weight of volumetric flask filled with both soil and alcohol, and d_a is the alcohol density (Santos et al. 2022).

Nowadays, gas pycnometers are commonly used to calculate solid particle density more precisely by utilizing a gas rather than the traditional liquid displacement method. Using a probing gas, like helium, provide more accurate results because they can penetrate the smallest pores, even those with diameters smaller than one nanometer (Microtrac n.d.(a)).

With the bulk density and solid particle density, the total porosity can be calculated using Equation 2.4 (L. E. Flint and A. L. Flint 2002).

$$Porosity(\phi) = 1 - \frac{\rho_b}{\rho_s} \tag{2.4}$$

Porosity can also be determined using mercury porosimetry, which provides information about pore size distribution, total porosity, and pore connectivity. In this method, a dried sample is placed in a chamber filled with mercury, and pressure is applied to force mercury into the pores. By measuring the amount of mercury that enters the pores at each pressure level, data on pore volume and size distribution can be obtained. Although this method is widely used, it has some disadvantages: mercury porosimetry is a destructive test and mercury is toxic (Univerzita Karlova n.d.).

The density and porosity of sediment sample can be determined using a variety of experimental techniques. However, the values obtained can vary depending on the method employed. This variation is primarily due to each technique treats volume in relation to the void spaces within the sediment sample (P.A. Webb 2001).

2.4.3. Permeability

Soil permeability, often referred to as hydraulic conductivity, measures the ability of water to flow through soil in terms of a permeability coefficient (k) (Humboldt Mfg. Co. n.d.). Water moves through the soil due to the interconnected voids and particle structure within the soil. Soils with high permeability allow

water to flow easily. Several factors affect soil permeability, including the structure of voids between the particles, hydraulic gradient, soil type, texture, PSD. Although empirical formulas exist for estimating permeability, a wide range of laboratory tests and field tests allow for direct measurement. The selected method depends on the soil type, the purpose of the test and the required level of precision (Humboldt Mfg. Co. n.d.). All test results are interpreted using Darcy's law, which describes how easily water flows through a certain medium.

To determine the permeability coefficient of a sediment sample, two main laboratory tests are commonly used: the constant head test and the falling head test. The constant head test is typically performed for cohesionless, highly permeable soils such as sands and gravels, whereas the falling head test is generally employed for cohesive or less permeable soils (Humboldt Mfg. Co. n.d.). The constant head test involves a device consisting of a cell containing the sediment sample, with reservoirs at the top and bottom. The top reservoir holds de-aired water, while the bottom reservoir collects water that has passed through the soil sample. During a falling head test, the sediment sample is saturated and placed in a container connected to a piezometric tube filled with de-aired water up to a specified level (Humboldt Mfg. Co. n.d.). According to the Australian Standards AS1289, the triaxial method is the third commonly used test for determining soil permeability. This method is performed under a constant hydraulic gradient and employs automated pressure controllers to measure the volume change (Coffey Testing 2024).

Several studies have developed correlations between soil properties and permeability. Hydraulic conductivity can be estimated from PSD using empirical equations. Hazen proposed this first empirical correlation. However, he stated that this correlation is only applicable for soils with a uniformity coefficient (D_{60}/D_{10}) of less than five and D_{10} particle size is ranged of 0.1 mm to 3.0 mm (Preene groundwater consulting 2014). Many other researchers, such as Kozeny-Carman and Terzaghi, have also studied the relationship between permeability and PSD (Odong 2008). Odong evaluated the applicability and reliability of commonly used formulas for determining the hydraulic conductivity of unconsolidated soil and rock materials (Odong 2008). They concluded that the Kozeny-Carman formula provided the best overall estimation of permeability, followed closely by Hazen's formula (Odong 2008).

2.4.4. Zeta potential and flocculation rate

Zeta potential is a measure of the surface charge at the boundary layer between a solid surface and a surrounding liquid. This parameter is obtained through electrokinetic experiments (Sanz 2018). Understanding the zeta potential is essential for interpreting the behavior of particles in suspension, making it a crucial parameter. It indicates the stability of sediment particles suspended in water. A high zeta potential signifies strongly charged particles, which repel each other, creating a stable suspension where particles do not easily flocculate. In contrast, a low zeta potential indicates particles weaker charges, meaning the particles particles can flocculate more easily, which may lead to sedimentation.

Zeta potential is an important parameter in determining particle interactions based on surface charge. However, for coarse sediments like sand measuring the zeta potential is less relevant. This is because sand particles have a smaller surface area compared to clay particles, zeta potential is influenced by the interaction between particles and their surrounding. Therefore, clay particles, which have a larger surface area, are more prone to flocculation. The ZetaSizer and ZetaNano are two devices that measure zeta potential. Both use laser Doppler velocimetry to evaluate the motion of particles (Sanz

2018).

A FLOCCAM device can be used to determine flocculation. This video microscopy technique records videos to analyze the size, shape, and settling velocity of flocs. However, it can only be used for particles smaller than twenty microns (Ali et al. 2022).

2.4.5. Organic matter

Organic matter in sediments usually consists of feces and remains of plants and animals. It is an essential component for understanding the ecological health of an environment. Organic matter can be visualized using a microscope. Its presence in a sample is often indicated by darker coloration compared to mineral components. Additionally, mass loss at specific temperatures is commonly used to quantify organic matter and carbonates in sediment samples (total organic carbon) (Bensharada et al. 2021). The loss on ignition (LOI) and thermogravimetric analysis (TGA) are both methods based on mass loss, although both are destructive to the sediment sample.

The LOI method is based on the principle that a sample loses weight at specific temperatures, which represents the loss of particular components. Standard LOI uses three temperatures stages: (1) at 150°C, where mass loss is associated with water evaporation, (2) at 550°C, where organic matter is consumed, leaving ash and CO_2 and (3) at 950°C, where carbonates decompose, releasing CO_2 (Bensharada et al. 2021).
LOI is widely used due to its affordability and simplicity. However, it requires a relatively large sample size (3-5g). Other fators that may influence the accuracy of the LOI method include furnace type, sample positioning, duration of exposure to each temperature, and operator errors during the weighing process (Bensharada et al. 2021).

TGA is an instrumental method that measures the sample mass as a function of temperature and time. The advantages of TGA include the speed of analysis, the small sample size required, reduced weighing errors due to automated mass determination and continuous mass monistoring during the analysis (Bensharada et al. 2021).

A study by Bensharada et al. evaluated the comparability of the LOI and TGA. The study concluded that both methods produce reliable results for measuring organic matter and carbonate content (Bensharada et al. 2021). However, TGA provides additional information about the specific temperature at which mass is lost, which can help detect other temperature-related changes in the sediment, such as mineral dehydration (Bensharada et al. 2021).

Another method for determining the organic matter content involves the use of hydrogen peroxide and evaporation. In this process, hydrogen peroxide breaks down the organic matter, and the sediment is then dried to evaporate water and oxidized organic material (Boskalis Environmental n.d.(c)). The weight loss provides an estimate of the organic matter content.

2.4.6. Calcium carbonate content

Tropical island beaches often appears white, because they contain calcium carbonate, which is derived from skeletons and shells of marine organisms, such as coral. In addition to TGA and LOI methods described in paragraph *Organic matter* of subsection 2.4.5, there are two other commonly used techniques to determine calcium carbonate content.

One method involves volumetric determination. Hydrochloric acid is added to a dry soil sample, which decomposes carbonate into water and carbon dioxide. The volume of the carbon dioxide that is formed is measured using a Scheibler device. This volume is then compared with the volume of carbon dioxide formed by pure calcium carbonate under the same conditions (Boskalis Environmental n.d.(b)). However, this method is destructive to the sediment sample.

Another method measures the loss of mass to determine the percentage of calcium in the sample. By treating the sample with hydrochloric acid, calcium-containing substances dissolve. Unfortunately, this method is also destructive to the sediment sample (Boskalis Environmental n.d.(d)).

2.4.7. Mineral composition

The mineral composition is crucial for determining both physical and chemical properties, such as color, electrical conductivity, density and hardness. Minerals often have distinct colors, but identifying different minerals can be challenging without sufficient experience (The Australian Museum n.d.). Minerals in sediments are typically derived from processes, such as weathering of rocks, volcanic gasses, oxidation, or saltwater interactions, resulting in various types of minerals (Libretexts n.d.). Understanding mineral composition can provide valuable insights into sediment's origin, transport history, and depositional environment.

A widely used method for analyzing sediment mineralogy is optical microscopy. This technique helps identify minerals in the sample by their optical properties, including color, shape, refractive index differences and cleavage (The Australian Museum n.d.). Although this approach requires expertise in mineral identification, it is effective in examining the texture and relationship between minerals in the sediment.

There are several analytical techniques used by mineralogists and petrologists to determine the mineral composition of sediments. Common methods include Scanning Electron Microscopy (SEM) and X-Ray Fluorescence (XRF). SEM uses a beam of electrons to reveal fine details of mineral particles, while XRF interacts with atoms in the sample, causing electrons to be temporarily elevated to higher energy states. When the electrons return to their original states, characteristic radiation is emitted, which helps identify different elements and minerals. Unfortunately, these machines are very expensive (Libretexts n.d.).

Before the 1960, geologists primarily relied on "wet chemistry" for analyzing rocks and minerals, including gravimetric, volumetric and colorimetric analysis. In gravimetric analysis, a solid precipitate is produced by reacting the acidic solution with reagents, and the amount of an element of in the original sample is determined by weighing the precipitate. Volumetric analysis involves titrating the sample until a specific reaction occur, with the volume of reagent used being proportional to the element of interest. Colorimetric analysis is based on a color change caused by a reaction with a reagent, with the intensity of the color indicating the concentration of the element (Libretexts n.d.).
Disadvantages of "wet-chemistry" include the large sample sizes required (which are destroyed during the process), the need for different procedures for various elements, and the time consuming nature of obtaining accurate results. Today, "wet-chemistry" is rarely used as more advanced techniques have become available (Libretexts n.d.).

3

Methodology

3.1. Sediment samples and study sites

In collaboration with the University of Exeter, roughly 2000 sediment samples were provided from 209 nesting beaches for sea turtles around the world. Figure A.1 in Appendix A shows the locations of these 209 nesting beaches. For each beach, ten sediment samples were collected: five samples along different transects of the shoreline and five along different transects of the turtle nesting line. The shoreline was defined as the highest point of debris left by the retreating tide. Since multiple shorelines could exist depending on the tide cycles, the most recent visible shoreline at the time of sampling was selected as the representative shoreline. The turtle nesting line was approximately determined by visible nests and body pits. If a sediment sample location coincided with a turtle nesting pit, the sample was taken two meters to the left or right of the nest.

The five transects were positioned at 10%, 30%, 50%, 70% and 90% of the beach section. Sediment samples were collected from the top 2 cm of sand within a 25 cm x 25 cm quadrant using a trowel, yielding a sample volume of 1.25 liters. An example of how sampling sites were selected is shown in Figure 3.1.

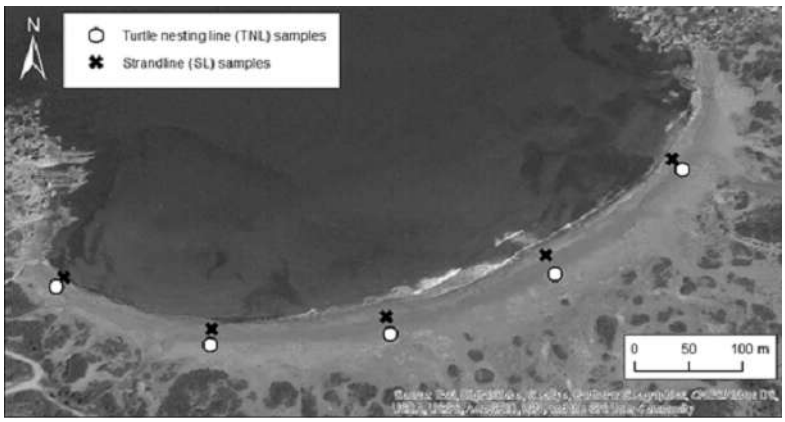

Figure 3.1: Example of sediment sampling at different transects along a beach, with samples taken at the nesting line (circles) and the shoreline (crosses).

Each sand sample was stored in plastic zip bags labeled with an identification code representing the beach and its country. If the sample was taken from the nesting line, it was marked ”NL” with the corresponding transect, whereas samples from the shoreline were labeled ”SL”. For example, the code for a sediment sample from the nesting line in the 50% transect of Ascension Island would be AI/SW/NEB NL50, while the code for the sample of the shoreline would be AI/SW/NEB SL50.

This study focused on sediment samples taken mid-transect at 50% of the beach. In addition, only the beaches with the most frequent nested were considered in this study. Figure 3.2 illustrates the global distribution of these beaches. Table 3.1 lists the associated beach locations, countries, and codes. It is important to note that the codes on the plastic zip bags may occasionally differ slightly from the sample codes used in this study. This variation arises because the bags are labeled with the sample names provided by the University of Exeter. The priority in this study was given to samples from the nesting line, as these locations were where nesting clutches were found and were less likely to vary seasonally compared to the shoreline. An overview of the nesting beaches included in this study, along with detailed information on each nesting site is presented in Appendix A Table A.1.

Figure 3.2: The sixteen sea turtle nesting beach locations included in this study, representing frequently visited nesting sites.

Site	Country	Sample code
North East Beach	Ascension Island	AI/SW/NEB
Delambre Island	Australia	AU/CD/D
Dirk Hartog Island	Australia	AU/CD/TB
Needhams	Barbados	BB/JH/DH
Busca Vida	Brazil	BR/DS/BV
Diego Garcia	Chagos	CA/NE/I
Corozalito	Costa Rica	CR/DJ/C
Playa Ostional	Costa Rica	CR/VB/PO
Joao Barrosa	Cabo Verde	CV/SM/JB
Yalimapo	French Guiana	FG/NP/Y
Mayumba	Gabon	GA/AF/MB
Poilao Island	Guinea-Bissau	GB/ED/P
Masirah Island	Oman	OM/CT/B1
Aldabra Atoll	Seychelles	SC/NB/CC
Padre Island	US	US/DG/PI
Archie Carr	US	US/TD/AC

Table 3.1: The sixteen key sea turtle nesting beaches with associated sites, countries and codes

This study included all seven sea turtle species. Table 3.2 shows which sea turtle specie were found at which beach.

Beach	CC	CM	DC	EI	LK	LO	ND
AI/SW/NEB		✓					
AU/CD/D		✓		✓			✓
AU/CD/TB	✓						
BB/JH/DH			✓				
BR/DS/BV	✓	✓		✓		✓	
CA/NE/I		✓		✓			
CR/DJ/C		✓	✓	✓		✓	
CR/VB/PO		✓				✓	
CV/SM/JB	✓						
FG/NP/Y		✓		✓		✓	
GA/AF/MB		✓	✓	✓		✓	
GB/ED/P		✓					
OM/CT/B1	✓						
SC/NB/CC		✓					
US/DG/PI					✓	✓	
US/TD/AC	✓	✓					

Table 3.2: Sea turtle species present at each nesting beach included in this study. Abbreviations: CC = Loggerhead turtle, CM = Green turtle, DC = Leatherback turtle, EI = Hawksbill turtle, LK = Kemp's ridley turtle, LO = Olive Ridley turtle, ND = Flatback turtle.

3.2. Analyses sediment characteristics

The analyses of several sediment characteristics in this study consisted of qualitative and quantitative analyses (Table 3.3).

Sediment Characteristic	Methods	Approach	Lab	Samples tested	Notes
Particle size	Sand ruler	Qualitative	TU Delft	32	
	Dry Sieving	Quantitative	TU Delft	32	
	Static Light Scattering (SLS)	Quantitative	Deltares	32	Malvern Mastersizer 2000
	Dynamic Image Analysis (DIA)	Quantitative	Boskalis	32	CPA HAVER 2-1
Particle grading	Well sorted / Poorly sorted	Qualitative	TU Delft	32	
	Dry Sieving	Quantitative	TU Delft	32	
	DIA	Quantitative	Boskalis	32	CPA HAVER 2-1
	SLS	Quantitative	Deltares	32	Malvern Mastersizer 2000
Particle shape	Power scale	Qualitative	TU Delft	32	
	Microscope	Qualitative	Deltares	32	
	DIA	Quantitative	Boskalis	32	CPA HAVER 2-1
Bulk density	Free-Fall	Quantitative	Boskalis	32	Minimum density in loose state
	Vibration Table	Quantitative	Boskalis	32	Maximum density in compact state
Solid particle density	Volume of water displacement	Quantitative	Deltares	32	
	Helium gas displacement pycnometer	Quantitative	Deltares	7*	
Color	Munsell Color Chart	Qualitative	TU Delft	32	
Angle of repose	Image-Based Angle of repose analysis	Quantitative	Deltares	32	Using ImageJ
Heat retention	Thermal retention analysis	Quantitative	Deltares	16**	
Porosity	Using bulk and solid particle density	Quantitative			

Table 3.3: Overview of the analyzed sediment characteristics and the methods used. *Seven nesting line samples analyzed using the helium gas displacement pycnometer include: AI/SW/NEB, AU/CD/D, BB/JH/DH, CR/DJ/C, GA/AF/MB, SC/NB/CC, US/TD/AC. **Sixteen nesting line samples were tested using thermal retention analysis.

3.3. Qualitative analyses

To select the appropriate quantitative analysis methods for evaluation of various sediment characteristics, it was important to have qualitative data about the sediment samples. Conducting qualitative analyses of the samples on macroscopic level, help planning quantitative experiments more effectively, saving time and reducing costs by avoiding unsuitable tests. These macroscopic analyses were used for precise visualization of **color**, **particle shape, grading** and **size** of the samples.

To classify the **color** of the sediment, a Munsell Color Chart was used. This is a standardized color system, widely used in the geology field to provide a consistent method for describing colors and is based on three dimensions: hue, value and chroma. Hue represent the type of color, such as Red (R), Yellow (YR) or Green (G). Value describes the lightness or darkness of the color on a scale from 0 (dark) to 10 (white) and lastly chroma refers to the intensity of the color, in other words how 'pure' the color is. The scale of chroma is measured from low to high, starting at 0 representing a completely neutral color (Munsell Color Company 2017).

The **particle shape** was determined by using the Power scale (Figure 3.3). Powers proposed a six-class roundness scale, ranging from "very angular" to "well-rounded" (Powers 1953). To develop this classification system, models of particles with varying degrees of sphericity (low and high) and roundness were used. Roundness refers to how sharp the edges and corners of sediment particles are and it is unrelated to the overall shape or size of the particles (Powers 1953). Sediment samples can be compared to this classification to quickly estimate their roundness. This characteristic is important because it helps determine the transport history of the sediment. For example, sediments with higher roundness are often associated with longer transport distances, while angular sediments are typically from nearby sources and have undergone less movement.

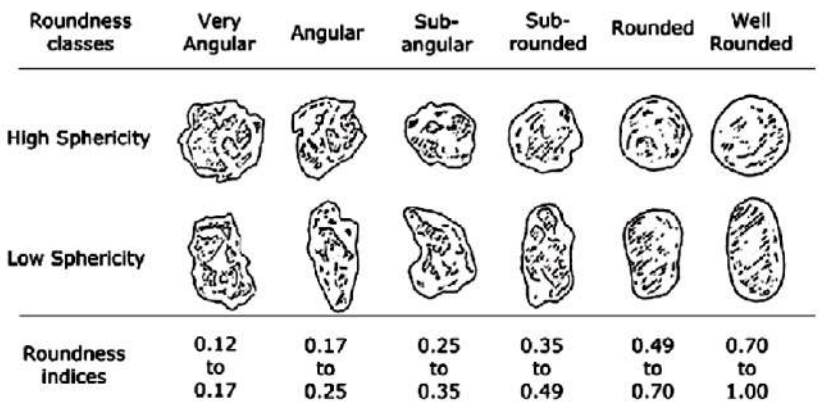

Figure 3.3: Particle angularity according to the Power scale (Chu et al. 2009).

Particle grading describes how fine to coarse particle sizes are distributed in the sample. It was classified as well-sorted (poorly graded) or poorly-sorted (well graded), as shown in Figure 3.4.

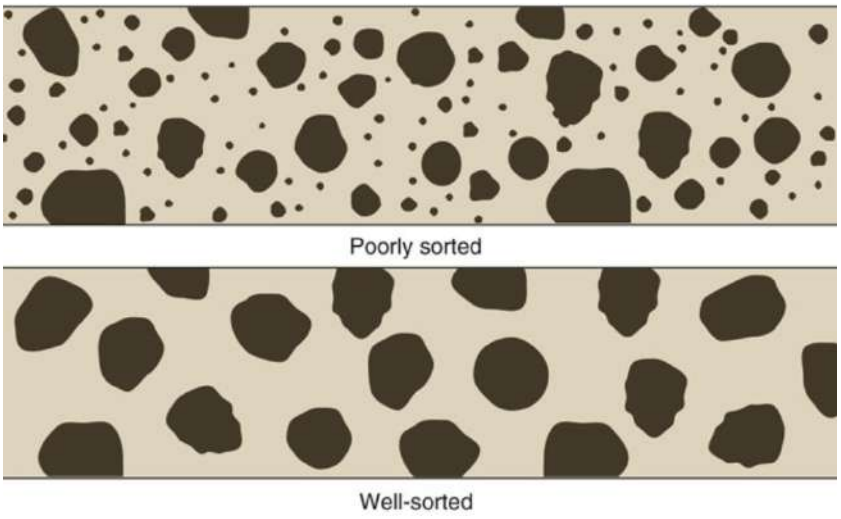

Figure 3.4: Sediment grading used for qualitative analysis (U.S National Park Service n.d.).

The **median particle size** of all sediment samples was determined by utilizing a sand ruler. The median is the diameter at which half of the sample's particles are larger and half are smaller. The sand ruler estimates particle size in μm, with common intervals of: 63, 90, 125 ,180, 250, 355, 500, 710, 1000, 1400, 2000 (Eijkelkamp Soil Water n.d.). Table 3.4 presents the classification of the sand fraction.

Median particle size (μm)	Characterization
63-105	Extreme fine
105-150	Very fine
150-210	Medium fine
210-300	Medium coarse
300-420	Very coarse
420-2000	Extreme coarse

Table 3.4: Classification of the sand fraction using a sand ruler (acc, NEN 5104) (Eijkelkamp Soil Water n.d.).

In addition to the macroscopic qualitative analysis, all sediment characteristics were also studied on microscopic level, using the LEICA digital microscope. This microscope provided clear images of all the samples.

Prior to utilizing the LEICA digital microscope, the samples were dried completely in a furnace at 105 to 110 °C for 24 hours. Thereafter, a small amount of the sample was transferred into a Petri dish to ensure a clear view with the microscope. Care was taken to obtain a representative portion of the sample, especially as a small sample was required.

The LEICA microscope was connected to a computer containing the LEICA software. Images were captured at three different magnification levels (1x, 2x, and 4x) to observe various sediment characteristics at different levels of detail. A measurement scale of 500 μm was added to each image.

3.4. Quantitative analyses

Different sediment characteristics were analyzed by similar methods. For example, both particle size and particle shape were determined by DIA, see Table 3.3.

3.4.1. Dry Sieving

Dry sieving is primarily used to determine the **PSD** and **grading**. This method is applicable to sediment samples consisting predominantly of sand, with minimal amounts of silt and clay. The procedure corresponds to the British standards for soils for civil engineering purposes, BS1377-2:1990.

Apparatus:

- Test sieves with the following aperture sizes: 2 mm, 1.18 mm, 0.85 mm, 600 μm, 425 μm, 300 μm, 212 μm, 150 μm and 63 μm;
- A balance readable to 1.0 g;
- A balance readable to 0.1 g;
- A drying oven capable of maintaining a temperature of 105 to 110°C;
- A mechanical sieve shaker;
- A sieve pan;
- A sieve lid;
- A scoop;
- Disposable aluminum trays;
- Waterproof marker.

The sample preparation followed sections 7.3 and 7.4.5 of BS 1377-1:1990, which specify that a minimum of 130 grams of sample had to be at 105 to 110°C for 24 hours. The sample was considered ready for testing when the oven-dried sample weight stabilized within 0.1% of its total mass. Disposable aluminum trays were used for oven drying, and to ensure proper identification, the sample code was written on the trays using a waterproof marker.

Each sieve, the aluminum tray, and the aluminum tray containing the oven-dried sample were weighed prior to sieving. This method utilized test sieves with apertures of 2 mm or smaller, deviating slightly from

BS1377-2, due to the absence of particles larger than 2 mm as identified during qualitative analysis (excluding shells, rocks, or small twigs). Additionally, a test sieve with apertures of 0.85 mm was included to achieve finer gradation of particle sizes.

The sieves were stacked in descending order, with the largest aperture sieve on top and the smallest at the bottom, ending with a sieve pan. The tower of sieves was placed on the mechanical sieve shaker. After placing the sample into the sieve tower, the tower was sealed with a sieve lid, and the shaking process started. According to BS1377-2:1990, the minimum shaking period is ten minutes. In this study, the sample was shaken for 15 minutes to ensure thorough separation. After shaking, each sieve was carefully weighed to determine the distribution of particle sizes.

The outcomes of the dry sieving experiment were the masses of the remaining sample in each sieve. Using these values, the passing percentages of the sample through each sieve were calculated to construct a cumulative particle size distribution (PSD) curve.

3.4.2. Dynamic Image Analysis

DIA is primarily used to determine the **PSD** and **grading**. During DIA, a high-resolution digital line scan camera records and analyzes a stream of particles against the background of an LED light source (Labmate n.d.). The camera detects shadow projections of the particles in real time from one side and, using the system's software, measures each particle's size and shape (Microtrac n.d.(b)).

This study utilized the HAVER CPA 2-1, which is specifically designed for fine bulk materials with a particle size range of 20 μm to 30 mm. The HAVER CPA 2-1 laboratory unit is integrated with the HAVER CpaServ software, which operates on Windows-based systems (Haver and Boecker n.d.). This device employs DIA in accordance with ISO 13322-2, to analyze particle size and shape for dry materials (Microtrac n.d.(b)).

Apparatus:

- HAVER CPA 2-1;
- Computer containing HAVER CpaServ software;
- A drying oven capable of maintaining a temperature of 105 to 110°C.

The sample had to be oven-dried at 105 to 110 $^\circ$C for 24 hours before analysis. According to Boskalis, a coffee cup's worth of sand was generally sufficient for analysis. However, for samples with a significant amount of gravel, a larger quantity of material was recommended to ensure accurate results. Before starting the measurement, the preferred sieve apertures had to be pre-defined in the software. The apertures used in the Dry Sieving method (2 mm, 1.18 mm, 0.85 mm, 600 μm, 425 μm, 300 μm, 212 μm, 150 μm and 63 μm) were also entered into the CPA software. This ensured direct comparability between the CPA results and traditional sieving methods. At the computer connected to the CPA device, the measurement is initiated via the HAVER CpaServ software. Once the measurement began, the sample was introduced into the funnel of the CPA. After adding the sample, the operator had to indicate in the software that the sample had been introduced, and the system will start the measurement process. The duration of the measurement depended on the sample size, with larger sediment samples requiring more time to analyze.

The CPA generated a text file (TXT format) containing the results. This file included the percent passing

on specific sieve apertures, D_{10}, D_{50}, D_{90}, roundness, circularity, sphericity and the uniformity index.

3.4.3. Static Light Scattering

The **PSD** and **grading** of samples can be measured using SLS with a Malvern Mastersizer. This study employed the Malvern Mastersizer 2000, available at Deltares. The Mastersizer operates using the Malvern particle analysis software, which employs Mie theory to analyze particle-light interactions. Mie theory quantifies the scattering and absorption of light by particles (Malvern Panalytical n.d.). The theory requires the refractive index (RI) of the material as an input parameter. For this study, the RI was set to 1.52, which is a recommended value for sand.

Apparatus:

- Malvern Mastersizer 2000;
- A drying oven capable of maintaining a temperature of 105 to 110 °C;
- Disposable aluminum trays;
- Waterproof marker;
- Three 1000 mL beakers;
- Peristaltic pump;
- Two small hoses;
- Two clothespins;
- A magnetic stirrer;
- Absorbent cloth (to clean spills)

The sample was oven-dried at 105 to 110 °C prior to analysis to ensure consistent conditions across all samples. The sample was considered suitable for testing when its oven-dried weight stabilized within 0.1% of its total mass. Disposable aluminum trays were used for oven drying, and to ensure proper identification, the sample code was written on the trays using a waterproof marker.

Prior to measurement, the Mastersizer was prepared and calibrated following Deltares' standard operating instructions. A blank measurement was performed to verify the absence of residual particles, and calibration standards were applied if necessary. The RI was set to 1.52, the particle absorption index to 0.1 (suitable for sand), and the dispersant refractive index to 1.33, corresponding to water.

Hoses connecting the beaker containing the dispersant (water) to the Mastersizer were installed, with a peristaltic pump placed on one of the hoses to circulate the water. The dispersant used in this study is water. Clothespins were used to stabilize the hoses and prevent movement during operation. The dispersant was maintained at room temperature or slightly warm to avoid potential issues with the Mastersizer system. A magnetic stirrer was used to maintain a consistent flow in the beaker, ensuring even dispersion of sand particles in the water.

A small amount of sample (one or two teaspoons) was introduced into the beaker while the magnetic stirrer was active. The sample concentration was adjusted until the laser obscuration displayed on the Mastersizer software reached the recommended range (typically above 4%). The Mastersizer software was then turned on to begin the measurement process, which consisted of eight measurement cycles.

The software automatically notified the operator upon completion of the eight cycles, at which point the magnetic stirrer was turned off.

After the measurement, the system was cleaned by placing the suction hose into a beaker of clean water, allowing the system to flush thoroughly. The outlet hose was directed into an empty beaker to collect the wastewater. Once the system was flushed and no residual particles remained, the system was prepared for the next sample to be tested.

The Mastersizer 2000 generated an excel file containing the results of the volume percentages of each particle size ranging from $1.1 \cdot 10^{-5}$ mm to 10 mm.

3.4.4. Free-Fall & Vibration Table

The **bulk density** was determined using the Free-Fall and Vibration Table method, in which the Free-Fall method determined the minimum density where the sample was in loose state and the Vibration Table method determined the maximum density where the sample was in compact state.

These method are not suitable for materials containing particles larger than 6.3 mm (Boskalis Environmental n.d.(a)). The minimal density method followed the standards outlined in BS1377-4:1990: *Methods of test for soils for civil engineering purposes: Compaction-related tests*. However, the procedure for determining the maximum density in this study deviated from BS1377-4:1990. Unlike the standard method, water and a vibrating hammer were not used to avoid potential crushing of the particles in the sample.

Instead, the maximum density was determined using the method employed by Boskalis, as they confirmed that this method produced reliable results.

Apparatus:

- A glass measuring cylinder of 250 ml;
- A drying oven capable of maintaining a temperature of 105 to 110 °C;
- A funnel;
- A mechanical sieve shaker;
- A rubber bung;
- A balance readable to 0.01 g;
- Disposable aluminum trays;
- Waterproof marker;
- A distribution device.

According to BS1377-1:1990 the sample had to be oven-dried at 105 to 110 °C for 24 hours. The sample was considered suitable for testing when its oven-dried weight stabilized within 0.1% of its total mass. Disposable aluminum trays were used for oven drying, and to ensure proper identification, the sample code was written on the trays using a waterproof marker.

For determining the *minimum density*, a 250 mL measuring cylinder was weighed. Then, using a funnel, the sample was poured into the cylinder and weighed again. The amount of sample in the cylinder was not required to be specific, but it was ensured that the material could move freely inside

the cylinder during shaking. After the sample was added, a rubber bung was placed securely on top of the cylinder to prevent spillage. The cylinder was shaken to loosen the material, turned upside down, and then carefully returned to an upright position once the sand had settled. The volume was recorded by measuring the mean surface level of the sand, calculated as the midpoint between the highest and lowest points. To avoid jolting, the cylinder was not placed on the table during this procedure. This procedure was repeated ten times to ensure accuracy and consistency.

The *maximum density* was determined by placing the 250 mL measuring cylinder on a mechanical sieve shaker, where it was shaken for at least two minutes or until no further reduction in the level of the surface of the sand was observed. Between repeated measurements of the maximum density, the material was loosened to reset its condition before compaction. This process was also repeated ten times to obtain reliable results.

The parameters obtained from the Free-Fall and Vibration Table method included the weight of the sample, the midpoint volume of the sample measured ten times after the Free-Fall method, and the volume of the sample measured ten times after the Vibration Table method. Using Equation 3.1, the mass of each sample and the mean volumes from both the Free-Fall and Vibration Table methods were used to calculate the minimum and maximum densities.

$$\rho = \frac{m_{sample}}{V} \tag{3.1}$$

In which, m_{sample} represented the weight of the sediment sample, and V denoted the mean volume obtained from either the Free-Fall or Vibration Table method.

3.4.5. Helium gas displacement pycnometer

A helium gas displacement pycnometer allows to precise determination of **solid particle density**. This study utilized the AccuPyc 1330 Pycnometer at Deltares.

Apparatus:

- The AccuPyc 1330 Pycnometer;
- A drying oven capable of maintaining a temperature of 105 to 110 °C;
- Disposable aluminum trays;
- A Waterproof marker;
- A balance readable to 0.01 g;
- A balance readable to 0.001 g.

The sample (approximately 20 g) was oven-dried at 105 to 110 °C prior to analysis to ensure consistent conditions across all samples and to eliminate any moisture that could affect the results. The sample was considered suitable for testing when its oven-dried weight stabilized within 0.1% of its total mass. Disposable aluminum trays were used for oven drying, and to ensure proper identification, the sample code was written on the trays using a waterproof marker.

Next, the dried sample was introduced into the chamber of the AccuPyc 1330 Pycnometer. Before filling, the empty chamber was weighed, and after the sample was added, the filled chamber was weighed

again to determine the mass of the sample. Then, the chamber was placed in the AccyPyc 1330 and sealed. The pycnometer operated by filling the chamber with helium gas, which penetrated even the tiniest pores in the material. The displacement of helium gas was measured by the device to calculate the exact volume of the solid particles, excluding any pores or voids.

The output of the AccuPyc 1330 Pycnometer was the solid particle density.

3.4.6. Volume of water displacement

Besides the helium gas pycnometer, determination of **solid particle density** can be performed using various methods, including: the Volumetric Flask Method, Pycnometer Method, and Purely Gravimetric Method, as outlined in paragraph *Density and Porosity* of subsection 2.4.2. This study employed a slightly modified method designed to minimize sediment sample usage, based on professional experience at the Deltares laboratory.

Apparatus:

- A glass measuring cylinder of 10 mL;
- A drying oven capable of maintaining a temperature of 105 to 110 °C;
- A small funnel;
- A balance readable to 0.01 g;
- A vacuum chamber;
- A small measuring scoop;
- A Waterproof marker.

Two 10 mL measuring cylinders were used. Both cylinders were marked and weighed to identify which sample was contained in each cylinder. Sediment samples were then added to the cylinders, and the cylinders were weighed again. Distilled water was introduced to each cylinder, and the cylinders were weighed once more, with the water volume being recorded.

Next, the cylinders were placed in a vacuum chamber for more than 30 minutes to release trapped air between the solid particles. After this process, the water volume was recorded again. This procedure was repeated for all 32 sediment samples.

To calculate the solid particle density, Equation 3.2 was applied:

$$\rho_s = \frac{m_s}{V_s} = \frac{m_{c+s} - m_c}{V_{aftervacuum} - V_w} \tag{3.2}$$

Here, m_s represents the weight of the sediment sample, V_s denotes the solid particle volume, $m_c + s$ is the combined weight of the sediment sample and the measuring cylinder, m_c is the weight of the measuring cylinder alone, $V_{aftervacuum}$ represents the volume of water and the sediment sample after vacuuming, and V_w denotes the volume of water initially added.

3.4.7. Image-Based Angle of Repose Analysis

To determine the **angle of repose**, a slope analysis was performed using photographic documentation and ImageJ software. This method is based on expertise developed at the Deltares laboratory.

Apparatus:

- Digital camera with a stand;
- ImageJ software;
- Large funnel;
- Tray;
- Horizontal platform;
- Brush;
- Drying oven capable of maintaining a temperature of 105 to 110 °C.

Before conducting the slope analysis, the sample had to be completely dry. If the sample was not already dry, it had to be oven-dried at 105 to 110 °C prior to analysis.

A horizontal platform was placed on top of a tray. The funnel was positioned above the platform and filled with the sample. Once the funnel was filled, it was slowly lifted to allow the sand to pour out freely into the tray, forming a natural sand pile shape. After the pile was formed, a photograph of the sand pile was taken with a digital camera. The camera was positioned at the side to ensure the profile of the sand pile was clearly visible.

Using the photograph of the sand pile, the slope was analyzed in ImageJ software. The slope of the sand pile was traced to measure the angles between the surface of the sand and the horizontal plateau. The mean of these angles represents the angle of repose. Figure 3.5 shows how the angle of repose was determined by using α_1 and α_2.

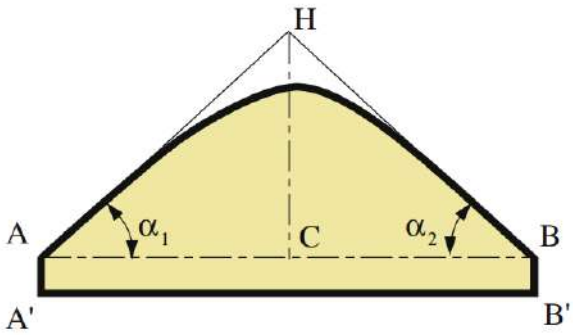

Figure 3.5: Definition of angle of repose in experiments (Nakashima et al. 2010).

3.4.8. Thermal Retention Analysis

With the Thermal Retention Analysis, the **heat retention** of sediment samples can be determined. This test was developed based on professional experience at the Deltares laboratory. Analyzing heat retention is particularly relevant for sea turtles, as incubation temperature influences hatching success and sex ratios.

Apparatus:

- Drying oven capable of maintaining a temperature of 105 to 110 °C;
- Disposable aluminum trays;

- Waterproof marker;
- A balance readable to 0.01 g;
- Temperature probe with a stand;
- Insulated cup;
- Signal conditioning device;
- Analog input module;
- Power supply unit;
- Computer containing the Delft Measure software.

To ensure a uniform starting temperature, sediment samples were placed in disposable aluminum trays labeled with a waterproof marker for identification. These trays were then heated in an oven to approximately 100°C. After heating, the samples were carefully transferred to pre-weighed insulated cups to minimize heat exchange with the surrounding environment.

Before inserting the temperature probe in the sample, it was pre-heated in hot water to minimize temperature differences between the probe and the sample, reducing initial fluctuations.

The probe was calibrated such that a voltage output of 2–10 V corresponded to a temperature range of 0–100°C, converting temperature readings into electrical signals (voltage).

The probe was connected to a signal conditioning, which scaled the probe's voltage signal to ensure it corresponded accurately to the temperature range device (2 V for 0°C and 10 V for 100°C).

The signal conditioning device was linked to an analog input module and a power supply unit. The power supply provided the necessary necessary voltage and current for proper operation and allowed real-time monitoring of system stability to operate properly (e.g. 24.75 V for voltage output).

The analog input module converted the conditioned analog voltage signal into a digital signal, which was ten processed by a computer containing Delft Measure software. This software logged temperature data in real time.

The probe continuously measured the sample's temperature as it cooled. Over approximately one hour, the temperature gradually decreased until it stabilized at around 21°C, close to room temperature.

3.5. Data analyses

Computational and statistical analyses were performed using Python version 3.11.5. The Pandas and NumPy libraries were used for data modification, while SciPy and statsmodels were utilized for statistical testing. Data visualization, including boxplots, scatterplots, and histograms, was conducted using Matplotlib.pyplot and Seaborn. Additionally, the os module was used for saving and organizing data files.

Scatterplots were created to visualize differences between the nesting- and shoreline and to explore relations between latitude and sediment characteristics; species and sediment characteristics; and helium gas pycnometer and water displacement methods. In the scatterplots comparing the nesting- and shoreline, each dot represented the beach where the sample was collected. The x-axis displayed the

value of a given sediment characteristic at the nesting line, while the y-axis showed the same characteristic at the shoreline. A dashed line was included as a reference line indicating equal values between the two locations. Dots positioned on this line signifies that the sediment characteristic was identical at both locations. If a dot appeared above the dashed line, the sediment characteristic at the shoreline was greater than at the nesting line. A similar scatterplot was obtained to visualize differences between the helium gas pycnometer and water displacement methods. In this case, the x-axis represented the solid particle density measured using the helium gas pycnometer, and the y-axis represented the solid particle density measured using the water displacement method.

3.5.1. Particle Size Distribution

Cumulative passing distribution curves are a common approach in sedimentology, allowing the derivation of many critical and statistical parameters. In these curves, the vertical axis is labeled with the term Q_3, which represents cumulative distribution based on mass or volume. The subscript '3' indicates that the cumulative curve is associated with mass or volume measurements. The output of dry sieving is based on mass percentages, while DIA (using CPA) and SLS (using Mastersizer) provide volume-based outputs.

A cumulative PSD curve can be interpreted as follows: at a given percentage X% of Q_3, the corresponding particle size represents the particle size at which X% of the sample is finer. Each curve is represented by dots. The x-values of these dots correspond to the specific sieve or particle sizes used during the sieving test, while the y-values represent the cumulative percentage of particles finer than the respective sieve size. The median particle diameter (D_{50}) represents the particle size for which 50% of the sample's total weight consists of finer particles. Based on the Wentworth classification shown in Figure 2.1, the samples can be classified by particle size using D_{50}, as it accurately reflects the PSD determined through dry sieving.

To quantify the gradation of the cumulative PSD curves, the Coefficient of Uniformity (Cu) and the Coefficient of Curvature (Cc) are employed. These parameters are directly related to D_{10}, D_{30}, D_{60}, and can be calculated using Equations 3.3 and 3.4 (Kalore and Babu 2023).

$$Cu = \frac{D_{60}}{D_{10}} \tag{3.3}$$

$$Cc = \frac{(D_{30})^2}{D_{10} \cdot D_{60}} \tag{3.4}$$

The Coefficient of Uniformity (Cu) represents the overall range of particle sizes and is visually reflected in the slope of the cumulative curve. A high Cu indicates a wider range of particle sizes (poorly sorted or well-graded), whereas a low Cu indicates a narrower range of particle sizes (well-sorted or poorly graded). Cu values higher than four for gravel and higher than six for sand are classified as poorly sorted (Kalore and Babu 2023), while values lower than four for gravel and lower than six for sand are classified as well-sorted (Kalore and Babu 2023). High Cu values correspond to a flatter PSD curve, whereas low Cu values correspond to a steeper curve.

The Coefficient of Curvature (Cc) relates to the shape of the middle section of the PSD curve, reflecting the distribution of intermediate particle sizes. A Cc value between one and three indicates well-graded

material, while values outside this range suggest poor gradation, such as gap-graded distributions, where intermediate particle sizes are missing (Kalore and Babu 2023). A PSD curve with a Cc value between 1 and 3 typically exhibits a smooth shape. In contrast, curves with Cc values less than 1 or greater than 3 often display irregularities, indicating gap-graded or poorly distributed intermediate sizes.

Another method to quantify particle size distribution curves is the Method of Moments by Folk and Ward, which uses percentiles expressed in φ. The φ-diameter is calculated by taking the negative logarithm of the particle diameter in millimeters. This method derives key statistical parameters, including graphic mean (M), standard deviation (SD), sorting (S_r), skewness (S_k), and kurtosis (K). The formulae for these parameters are provided in Equations 3.5, 3.6, 3.7, 3.8 and 3.9 (OLADIPO et al. 2018).

$$M = \frac{\varphi_{60} + \varphi_{50} + \varphi_{84}}{3} \tag{3.5}$$

$$SD = \frac{\varphi_{84} - \varphi_{16}}{4} \tag{3.6}$$

$$S_r = \frac{\varphi_{84} - \varphi_{16}}{4} + \frac{\varphi_{95} - \varphi_5}{6.6} \tag{3.7}$$

$$S_k = \frac{\varphi_{84} + \varphi_{16} - 2\varphi_{50}}{2(\varphi_{84} - \varphi_{16})} + \frac{\varphi_5 + \varphi_{95} - 2\varphi_{50}}{2(\varphi_{95} - \varphi_5)} \tag{3.8}$$

$$K = \frac{\varphi_{95} - \varphi_5}{2.44(\varphi_{75} - \varphi_{25})} \tag{3.9}$$

Skewness measures the asymmetry of the particle size distribution. Positive skewness indicates a dominance of finer particles, while negative skewness indicates a dominance of coarser particles (Kalore and Babu 2023). Tables 3.5 and 3.6 present the classifications for the degree of sorting and kurtosis values typically used in sedimentology.

$\mathbf{S_r}$	**Characterization**
> 4	Extremely poorly sorted
2 - 4	Very poorly sorted
1 - 2	Poorly sorted
0.71 - 1	Moderately sorted
0.50 - 0.71	Moderately well sorted
0.35 - 0.5	Well sorted
<0.35	Very well sorted

Table 3.5: Classification of the degree of sorting (OLADIPO et al. 2018).

K	Characterization	Explanation
< 0.67	Very platykurtic	Very flat frequency distribution
0.67 - 0.90	Platykurtic	Flat
0.90 - 1.11	Mesokurtic	Not especially peaked, normal
1.11 - 1.50	Leptokurtic	Highly peaked
> 1.50	Very leptokurtic	Very highly peaked

Table 3.6: Classification of kurtosis values (OLADIPO et al. 2018)

3.5.2. Roundness, circularity and sphericity

The HAVER CPA 2-1 generated a text file (TXT format) containing roundness, circularity and sphericity. Roundness quantifies how closely the shape of a particle's projection matches the shape of a circle. The CPA calculats the roundness using Equation 3.10:

$$Roundness, (R_n) = \frac{4A}{\pi x_{Fmax}^2} \tag{3.10}$$

Where A is the area of the particle's projection, and x_{Fmax} represents the maximum Feret diameter, which is the largest particle dimension. A higher roundness indicates that the shape is closer to a circle, with values approaching 1. A lower roundness (close to 0) signifies that the particle is more irregular and elongated.

Circularity measures the comparison between the circumference of a circle with the same projection area as the particle and the actual circumference of the particle. The CPA determines circularity as shown in Equation 3.11:

$$Circularity, (\psi) = \frac{2\sqrt{\pi A_1}}{U_p} \tag{3.11}$$

Where A_1 is the measured projection area and U_p the measured projection area circumference (perimeter). Circularity provides information about about how circular the particle is. A perfect circle has a circularity of 1. Irregularities like elongation or jagged edges are indicated by deviations from 1.

Sphericity compares the surface area of a sphere with the same volume as the particle to the actual surface area of the particle. This measure indicates how closely the particle's 3D shape resembles a perfect sphere. The uniformity index is calculated as the ratio of the particle size at D_5 to the particle size at D_{90}, multiplied by 100. Here, D_5 and D_{90} are determined from internal values provided by the CPA.

3.5.3. Statistical analyses

Prior to statistical analyses, all data for each sediment characteristic were tested for normality and homogeneity of variance. Group means were used to compare data that were normally distributed, whereas group medians were used to compare data that were not. The datasets for the nesting line and shoreline were tested separately for normality for each sediment characteristic. The Shapiro-Wilk test was used to assess whether the data were normally distributed. Levene's test was used to evaluate the homogeneity of variance between the nesting line and shoreline for each characteristic.

Relations between various sediment characteristics at the nesting line were assessed using Spearman's correlation coefficient. This non-parametric approach was chosen because not all sediment characteristics met the assumption of normality. Spearman's correlation examines if there is a consistent increase or decrease in one variable with another. Pearson's correlation coefficient, which assumes normality, was therefore not used.

To compare cumulative PSD between the nesting line and shoreline, the maximum distance (D_{max}) based on the Kolmogorov–Smirnov test was calculated. Higher D_{max} values indicate greater differences in PSDs between the nesting line and the shoreline at a given beach. The D_{max} results provided quantitative insights into the differences between the nesting line and shoreline cumulative distributions. This approach was also used to compare the cumulative distributions obtained through dry sieving, DIA and SLS. However, D_{max} only quantify the largest gap between the distributions and do not directly indicate statistical significance.

To assess whether there were significant differences in key sediment characteristics (D_{50}, ψ, R_n, $\rho_{average}$, ρ_s, angle of repose and average porosity) between the nesting line and shoreline, different statistical methods were used depending on the data of the characteristics. All nesting line samples were grouped separately from all shoreline samples. This study focused on overall trends between the two environments, rather than differences between nesting- and shoreline on each beach. For data that were normally distributed with homogeneous variances and independent groups, an unpaired t-test was applied. The nesting- and shoreline were considered independent groups, as samples were taken from distinct environments and did not influence each other. When comparing two independent groups with not normally distributed data, the Mann-Whitney U test was used.

To assess significant differences between measurements obtained from the helium gas pycnometer and the water displacement method, a paired t-test was performed. This test is applied when the same samples are measured under two different conditions, assuming normal distributions with homogeneity of variances.

For all statistical tests, the significance level (α) was set at 0.05. If the p-value was higher than the significance level, the null hypothesis was not rejected (indicating no statistically significant difference). If the p-value was less than 0.05, the null hypothesis was rejected, indicating a statistically significant result.

4

Results

4.1. Qualitative analyses

The results of the qualitative analyses on a macroscopic level are shown in Appendix B. In addition, all sediment samples were also examined at a microscopic level utilizing the LEICA digital microscope, providing a clearer view. These images are shown in Appendix C.

Using the Munsell color chart, for both NL and SL samples, 62.50% of the sediments fell within the hue 10YR category. Value ranged from 4 to 9.5, with 7 being the most dominant (37.50% in NL and 31.25% in SL). Lower values correspond to darker sands, while higher values correspond to lighter sands. Chroma ranged from 1 to 4, indicating relatively low to moderate color intensity. Among all sample groups, only CA/NE/I showed noticeable color variation, suggesting local differences in sand composition.

The qualitative particle shape analysis was conducted using the Power Scale. Particles exhibited a balanced distribution of high and low sphericity, each making up approximately 50% in both NL and SL. Roundness varied across the ranges 0.17–0.25, 0.25–0.35, 0.35–0.49, and 0.49–0.70. This variation indicated that no particles were classified as either very angular or well-rounded. The majority of the particles fell within the range 0.35–0.49, suggesting that most samples consisted of sub-rounded particles in both NL and SL.

For particle size and grading, all sediments in the dataset were categorized as well-sorted sand. Therefore, all quantitative methods used in this study were primarily designed for sand.

4.2. Quantitative analyses

All quantitative analyses included dry sieving, DIA, SLS, the free-fall and vibration table method, water displacement volume measurement, helium gas displacement pycnometry, image-based angle of repose analysis, and thermal retention analysis (see Table 3.3). The nesting line samples were analyzed separately from the shoreline samples.

4.2.1. Particle size and grading

The particle size and grading were analyzed using dry sieving, DIA, and SLS. With each of these methods, the particle size distribution (PSD) and other critical parameters were obtained. All statistical parameters of the PSD are provided in Appendix D.

A. Dry Sieving

Figure 4.1 illustrates the cumulative distribution curves for the **nesting line** of sixteen beaches.

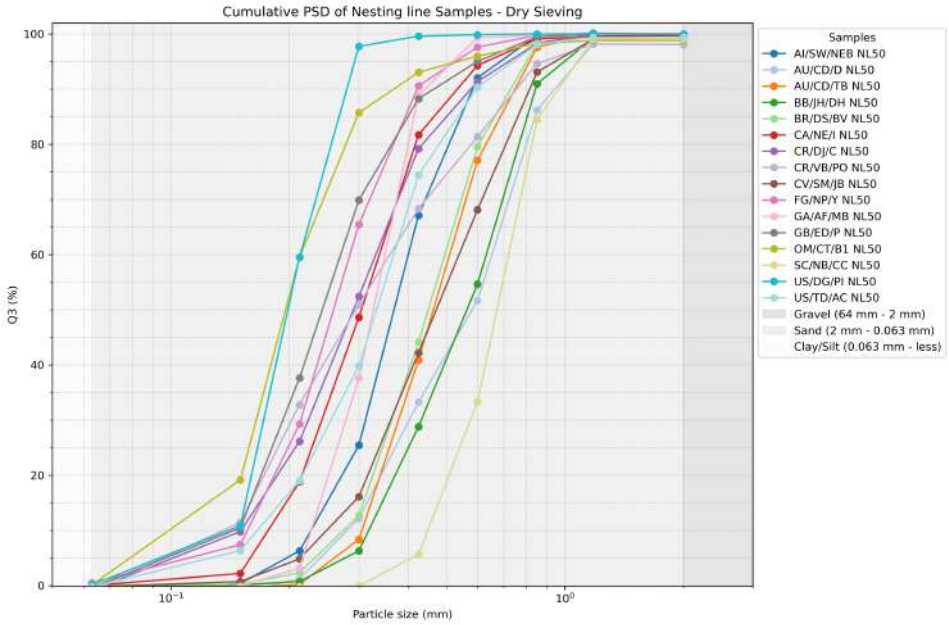

Figure 4.1: The cumulative particle size distribution of the sixteen sea turtle nesting line samples was determined using the dry sieving method. The x-axis represents particle size in mm, while the y-axis represents Q_3 in the context of cumulative mass (%) distribution. Abbreviations: mm = Millimeter, NL = Nesting Line, PSD = Particle Size Distribution.

All curves fell within the sand range (2 mm to 0.063 mm; see Figure 2.1), confirming the results of the qualitative analysis of particle size. D_{50}, Cu, and Cc, derived from the PSD for the sixteen NL samples, are presented in Table 4.1.

Sample code	D_{50} (mm)	Cu (-)	Cc (-)	Wentworth classification
AI/SW/NEB NL50	0.374	1.762	1.064	Medium sand
AU/CD/D NL50	0.584	2.338	0.882	Coarse sand
AU/CD/TB NL50	0.469	1.689	0.926	Medium sand
BB/JH/DH NL50	0.569	1.987	0.919	Coarse sand
BR/DS/BV NL50	0.454	1.817	0.975	Medium sand
CA/NE/I NL50	0.305	1.915	0.977	Medium sand
CR/DJ/C NL50	0.292	2.225	1.001	Medium sand
CR/VB/PO NL50	0.295	2.608	0.814	Medium sand
CV/SM/JB NL50	0.478	2.162	0.977	Medium sand
FG/NP/Y NL50	0.262	1.822	1.013	Medium sand
GA/AF/MB NL50	0.330	1.546	0.967	Medium sand
GB/ED/P NL50	0.246	1.866	0.948	Fine sand
OM/CT/B1 NL50	0.197	1.975	1.202	Fine sand
SC/NB/CC NL50	0.682	1.615	1.014	Coarse sand
US/DG/PI NL50	0.200	1.489	0.997	Fine sand
US/TD/AC NL50	0.337	2.221	1.067	Medium sand

Table 4.1: The critical particle size distribution parameters (D_{50}, Cu and Cc) for the sixteen sea turtle nesting line samples were calculated based on the PSD, which was determined using the dry sieving method (Kalore and Babu 2023). Abbreviations: D_{50} = Median particle diameter, Cu = Coefficient of Uniformity, Cc = Coefficient of Curvature, mm = Millimeter, NL = Nesting Line, PSD = Particle Size Distribution.

The median particle size D_{50} for the nesting line samples ranged from 0.197 mm to 0.682 mm. This confirmed that all nesting line samples were dominated by sand-sized particles, with negligible amounts of finer or coarser materials. According to the Wentworth classification, sand was further categorized into fine, medium, and coarse fractions (Figure 2.1). Each sample's classification is provided in Table 4.1. The coefficient of uniformity (Cu) values ranged from 1.49 to 2.61, indicating a narrow particle size range. Since all Cu values were below six, the samples were classified as well-sorted (or poorly graded), meaning they primarily consisted of particles of similar sizes. The coefficient of curvature (Cc) values ranged from 0.81 to 1.20. Cc values close to one indicate a narrowly graded distribution. Samples with Cc values close to one, indicated a gradual and smooth PSD distribution curve, meaning there was no significant gap in particle sizes. If Cc was below one, there could have been gap grading, meaning some intermediate particle sizes were missing. In this dataset, most of the samples likely exhibited a relatively smooth PSD curve. However, some samples showed slight signs of gap grading.

The Method of Moments by Folk and Ward provides a more comprehensive statistical approach to analyzing sediment size distributions. These parameters are presented in Appendix D Table D.1. In the nesting line dataset, all samples were classified as very well-sorted, indicating that the sediments were uniformly distributed, confirming the results obtained from Cu. The S_k values in this dataset included both positive and negative skewness. Some values were very close to zero, implying near-symmetrical distributions. The majority of the samples exhibited a near-normal distribution of particle sizes (mesokurtic profile).

Figure 4.2 illustrates the cumulative distribution curves for the **shoreline** of sixteen beaches. Similar to the distribution curves at the nesting line, the particle sizes of the shoreline samples also fell within the sand range.

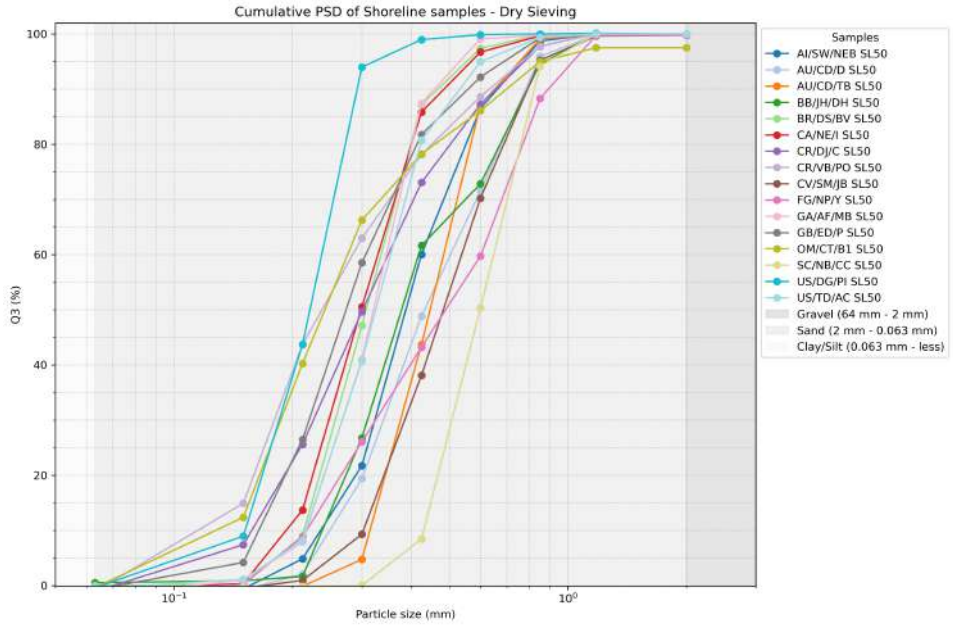

Figure 4.2: The cumulative particle size distribution of the sixteen sea turtle shoreline samples was determined using the dry sieving method. The x-axis represents particle size in mm, while the y-axis represents Q_3 in the context of cumulative mass (%) distribution. bbreviations: mm = Millimeter, PSD = Particle Size Distribution, SL = Shoreline.

The critical PSD parameters of the shoreline samples are summarized in Table 4.2. The D_{50} values, ranged from 0.223 to 0.599 mm, confirmed that all samples fall within the sand range. The majority of the samples fell within the medium sand category of the Wentworth classification. The gradation of all samples was classified as well-sorted, as all Cu values (1.52-2.76) were below six. Most samples likely exhibited a relatively smooth PSD curve, as the Cc values (0.82-1.05) were very close to one. However, some samples showed slight signs of gap grading.

Sample code	D_{50} (mm)	Cu (-)	Cc (-)	Wentworth classification
AI/SW/NEB SL50	0.392	1.779	1.053	Medium sand
AU/CD/D SL50	0.434	2.026	0.924	Medium sand
AU/CD/TB SL50	0.450	1.549	0.934	Medium sand
BB/JH/DH SL50	0.383	1.738	0.960	Medium sand
BR/DS/BV SL50	0.309	1.587	0.931	Medium sand
CA/NE/I SL50	0.299	1.712	0.969	Medium sand
CR/DJ/C SL50	0.302	2.236	0.922	Medium sand
CR/VB/PO SL50	0.241	2.323	0.944	Fine sand
CV/SM/JB SL50	0.490	1.796	0.921	Medium sand
FG/NP/Y SL50	0.497	2.762	0.822	Medium sand
GA/AF/MB SL50	0.324	1.614	0.959	Medium sand
GB/ED/P SL50	0.277	1.854	0.960	Medium sand
OM/CT/B1 SL50	0.245	2.084	0.960	Fine sand
SC/NB/CC SL50	0.599	1.519	0.938	Coarse sand
US/DG/PI SL50	0.223	1.583	0.963	Fine sand
US/TD/AC SL50	0.329	1.660	0.940	Medium sand

Table 4.2: The critical particle size distribution parameters (D_{50}, Cu and Cc) for the sixteen sea turtle shoreline samples were calculated based on the PSD, which was determined using the dry sieving method (Kalore and Babu 2023). Abbreviations: D_{50} = Median particle diameter, Cu = Coefficient of Uniformity, Cc = Coefficient of Curvature, mm = Millimeter, PSD = Particle Size Distribution, SL = Shoreline.

Table D.2 in Appendix D provides an overview of the statistical parameters for the sixteen shoreline samples. The SD and S_r values indicated that all shoreline samples fell into the category of very well sorted, consistent with the Cu values. The majority of the S_k values were positive, suggesting that the samples were slightly skewed toward finer particles. Furthermore, K values showed that most samples exhibited a relatively normal distribution of particle sizes (mesokurtic profile).

B. Dynamic Image Analysis by CPA

The cumulative PSD of the sixteen **nesting line** samples analyzed using DIA by CPA is shown in Figure 4.3. All PSD curves fell within the sand domain. Compared to Figure 4.1, which presents results from dry sieving, no significant differences were observed.

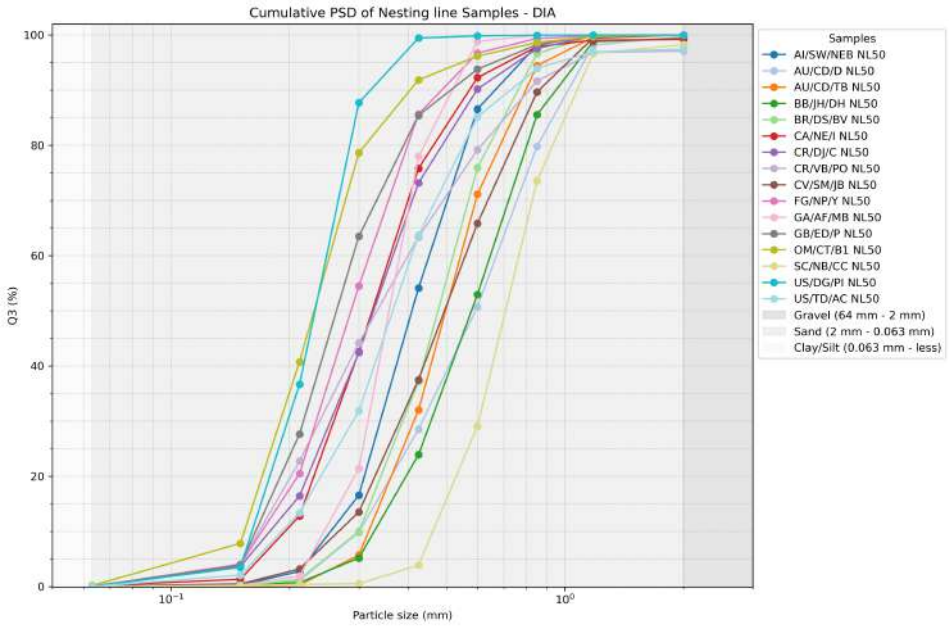

Figure 4.3: The cumulative particle size distribution of the sixteen sea turtle nesting line samples was determined using Dynamic Image Analysis by a Computerized Particle Analyzer. The x-axis represents particle size in mm, while the y-axis represents Q_3 in the context of cumulative volume (%) distribution. Abbreviations: mm = Millimeter, NL = Nesting Line, PSD = Particle Size Distribution.

The critical PSD parameters of the nesting line samples analyzed using DIA are summarized in Table 4.3. The D_{50} values, ranging from 0.233 to 0.718 mm, confirmed that all samples fell within the sand range, consistent with the PSD results obtained from dry sieving. The majority of the samples fell within the medium sand category of the Wentworth classification. The gradation of all samples was classified as well-sorted, as all Cu values (1.55–2.38) were below six. The Cc values (0.86–1.07) were very close to one, indicating a relatively smooth PSD curve. However, some samples showed slight signs of gap grading.

Sample code	D_{50} (mm)	Cu (-)	Cc (-)	Wentworth classification
AI/SW/NEB NL50	0.411	1.770	1.008	Medium sand
AU/CD/D NL50	0.594	2.258	0.933	Coarse sand
AU/CD/TB NL50	0.506	1.717	0.979	Coarse sand
BB/JH/DH NL50	0.582	1.969	0.982	Coarse sand
BR/DS/BV NL50	0.483	1.760	0.970	Medium sand
CA/NE/I NL50	0.328	1.857	0.960	Medium sand
CR/DJ/C NL50	0.331	2.054	0.990	Medium sand
CR/VB/PO NL50	0.338	2.376	0.855	Medium sand
CV/SM/JB NL50	0.502	2.089	0.978	Coarse sand
FG/NP/Y NL50	0.288	1.867	1.008	Medium sand
GA/AF/MB NL50	0.363	1.550	1.063	Medium sand
GB/ED/P NL50	0.267	1.756	0.981	Medium sand
OM/CT/B1 NL50	0.233	1.666	0.930	Fine sand
SC/NB/CC NL50	0.718	1.655	1.012	Coarse sand
US/DG/PI NL50	0.235	1.555	0.973	Fine sand
US/TD/AC NL50	0.371	2.121	1.068	Medium sand

Table 4.3: The critical particle size distribution parameters (D_{50}, Cu and Cc) for the sixteen sea turtle nesting line samples were calculated based on the PSD, which was determined using Dynamic Image Analysis by a Computerized Particle Analyzer (Kalore and Babu 2023). Abbreviations: D_{50} = Median particle diameter, Cu = Coefficient of Uniformity, Cc = Coefficient of Curvature, mm = Millimeter, NL = Nesting line, PSD = Particle Size Distribution.

Table D.3 in Appendix D provides an overview of the statistical parameters for the sixteen nesting samples analyzed using DIA by CPA. The SD and S_r values indicated that all nesting line samples fell into the category of very well sorted, consistent with the Cu values. The S_k values were close to zero, suggesting a near-symmetrical distribution for the majority of the samples, though some PSD curves showed slight skewness toward either finer or coarser particles. Most K values indicate that the samples exhibited a relatively normal distribution of particle sizes (mesokurtic profile).

Figure 4.4 illustrates the cumulative distribution curves for the **shoreline** of sixteen beaches. It shows that all curves also fell within the sand domain.

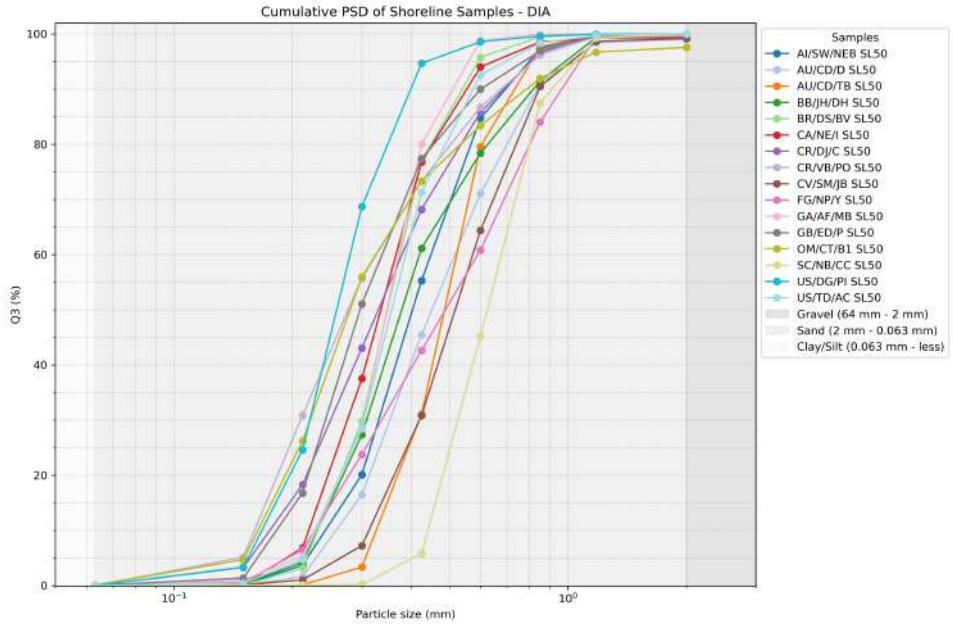

Figure 4.4: The cumulative particle size distribution of the sixteen sea turtle shoreline samples was determined using Dynamic Image Analysis by a Computerized Particle Analyzer. The x-axis represents particle size in mm, while the y-axis represents Q_3 in the context of cumulative volume (%) distribution. Abbreviations: DIA = Dynamic Image Analysis, mm = Millimeter, PSD = Particle Size Distribution, SL = Shoreline.

The D_{50} values (0.280-0.628 mm) classified all samples as medium sand according to the Wentworth classification, except for SC/NB/CC, which was categorized as coarse sand. All Cu values (1.55-2.58) were below six, indicating that all samples were classified as well-sorted. The Cc values (0.83-1.07) were very close to one, suggesting a relatively smooth PSD curve. However, some samples showed slight signs of gap grading (see Table 4.4).

Sample code	D_{50} (mm)	Cu (-)	Cc (-)	Wentworth classification
AI/SW/NEB SL50	0.406	1.843	1.009	Medium sand
AU/CD/D SL50	0.456	2.004	0.936	Medium sand
AU/CD/TB SL50	0.493	1.604	1.011	Medium sand
BB/JH/DH SL50	0.384	1.798	0.975	Medium sand
BR/DS/BV SL50	0.354	1.620	1.013	Medium sand
CA/NE/I SL50	0.340	1.680	0.944	Medium sand
CR/DJ/C SL50	0.334	2.162	0.942	Medium sand
CR/VB/PO SL50	0.280	2.043	0.825	Medium sand
CV/SM/JB SL50	0.525	1.834	0.975	Medium sand
FG/NP/Y SL50	0.496	2.576	0.856	Medium sand
GA/AF/MB SL50	0.352	1.638	1.066	Medium sand
GB/ED/P SL50	0.297	1.854	0.956	Medium sand
OM/CT/B1 SL50	0.282	1.992	0.917	Medium sand
SC/NB/CC SL50	0.628	1.549	0.930	Coarse sand
US/DG/PI SL50	0.263	1.668	1.037	Medium sand
US/TD/AC SL50	0.362	1.694	1.017	Medium sand

Table 4.4: The critical particle size distribution parameters (D_{50}, Cu and Cc) for the sixteen sea turtle shoreline samples were calculated based on the PSD, which was determined using Dynamic Image Analysis by a Computerized Particle Analyzer (Kalore and Babu 2023). Abbreviations: D_{50} = Median particle diameter, Cu = Coefficient of Uniformity, Cc = Coefficient of Curvature, mm = Millimeter, PSD = Particle Size Distribution, SL = Shoreline.

Table D.4 in Appendix D provides an overview of the statistical parameters for the sixteen shoreline samples analyzed using DIA by CPA. The SD and S_r values indicated that all shoreline samples fell into the category of very well sorted, consistent with the Cu values. The majority of the S_k values were positive, suggesting that the samples were slightly skewed toward finer particles. Most K values indicated that the samples exhibited a relatively normal distribution of particle sizes (mesokurtic profile).

C. Static Light Scattering by Mastersizer 2000

The Mastersizer performed eight measuring cycles, calculating the volume percentages per particle size during each cycle. Figures 4.5 and 4.6 illustrate the particle size distributions for the nesting line and shoreline across the eight cycles. It was observed that some cycles produced significantly different results, as seen in samples AU/CD/D NL50 and FG/NP/Y SL50. Consequently, the cycle closest to the median cycle was selected for further analysis. The closest distance to the median was determined by calculating the Euclidean distance.

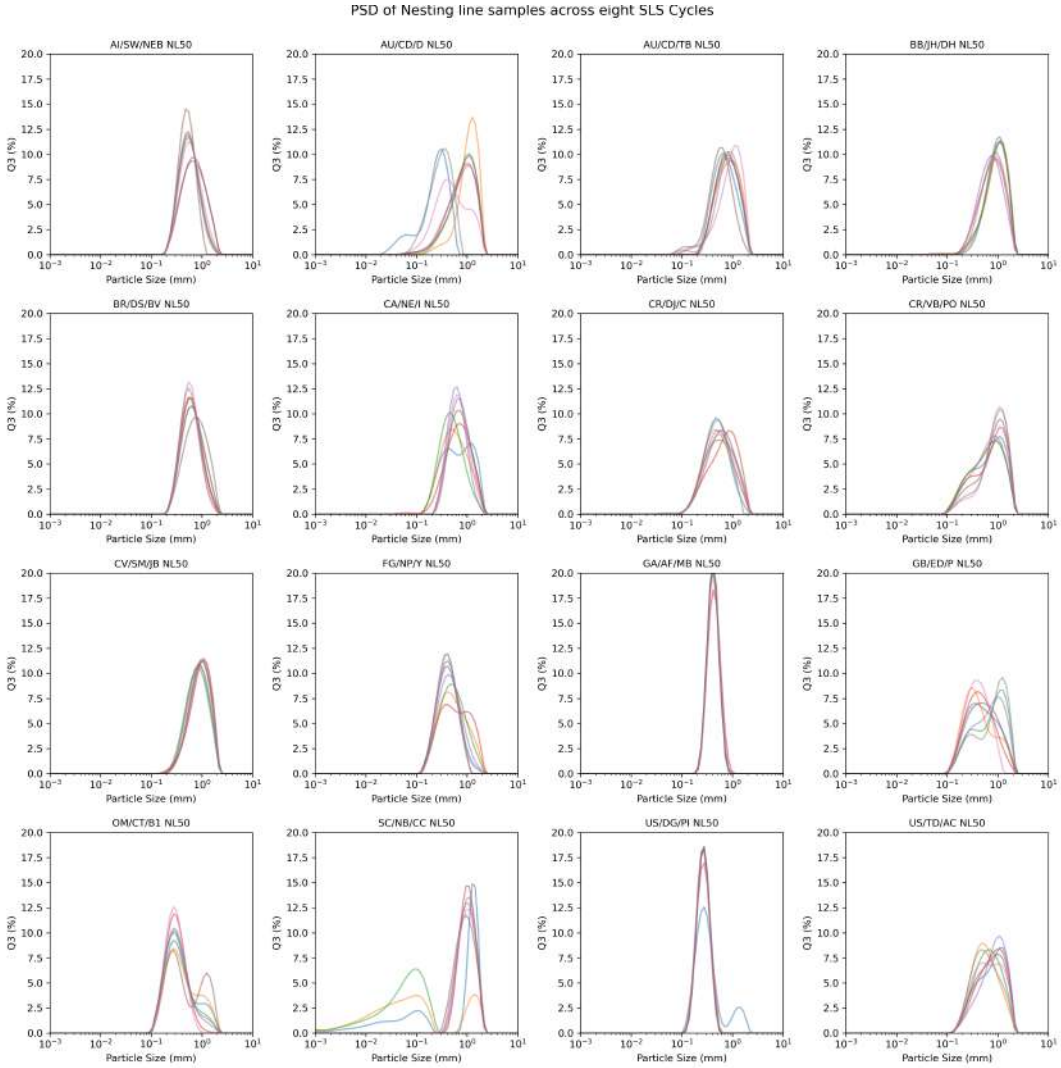

Figure 4.5: The particle size distributions of sixteen nesting line samples, each measured across eight cycles using the Mastersizer 2000. Abbreviations: mm = Millimeter, NL = Nesting line, PSD = Particle Size Distribution, SLS = Static Light Scattering.

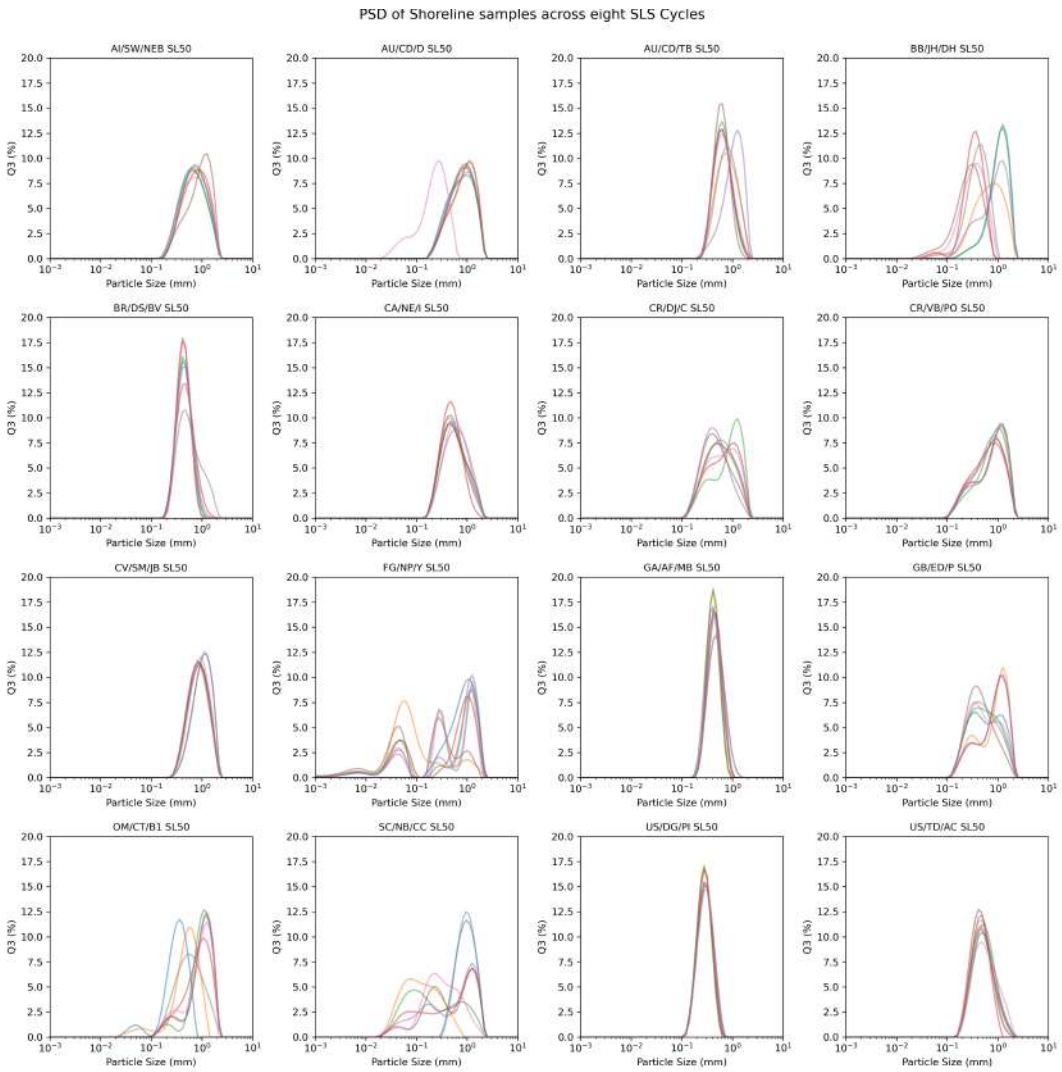

Figure 4.6: The particle size distributions of sixteen shoreline samples, each measured across eight cycles using the Mastersizer 2000. Abbreviations: mm = Millimeter, PSD = Particle Size Distribution, SL = Shoreline, SLS = Static Light Scattering.

The cumulative PSD of the sixteen **nesting line** samples analyzed using SLS by Mastersizer 2000 is shown in Figure 4.7. All PSD curves fell within the particle size range of sand, although some samples contained also proportions of fine particles.

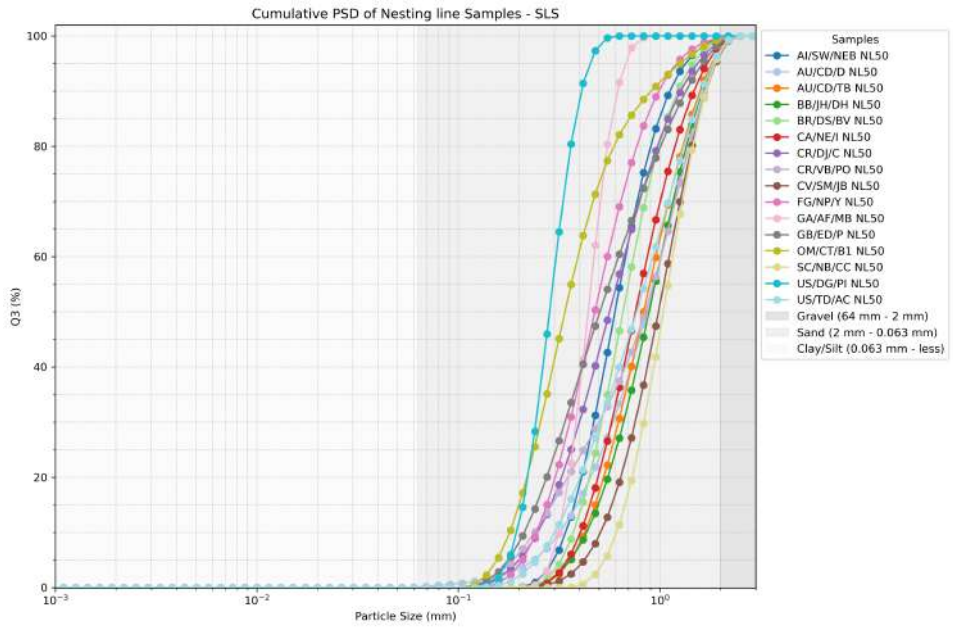

Figure 4.7: The cumulative particle size distribution of the sixteen sea turtle nesting line samples was determined using Static Light Scattering by the Mastersizer 2000. The x-axis represents particle size in millimeters (mm), while the y-axis represents Q_3 in the context of cumulative volume (%) distribution. Abbreviations: mm = Millimeter, NL = Nesting Line, PSD = Particle Size Distribution, SLS = Static Light Scattering.

The critical PSD parameters of the nesting line samples analyzed using SLS are summarized in Table 4.5. The D_{50} values, ranging from 0.284 to 1.044 mm, confirmed that all samples fell within the sand range, consistent with the PSD results obtained from dry sieving. However, the majority of the samples were classified as coarse sand according to the Wentworth classification, which contradicts the dry sieving results, where most samples were categorized as medium sand. The gradation Cu values (1.49–4.25) classified all samples as well-sorted. Compared to the Cu values from dry sieving, the Cu values from the Mastersizer were slightly higher. The Cc values (0.86–1.05) were very close to one, indicating a relatively smooth PSD curve. Some samples exhibited slight signs of gap grading, similar to the results from dry sieving.

Sample code	D_{50} (mm)	Cu (-)	Cc (-)	Wentworth classification
AI/SW/NEB NL50	0.601	1.989	0.959	Coarse sand
AU/CD/D NL50	0.865	3.187	1.054	Coarse sand
AU/CD/TB NL50	0.832	2.254	0.960	Coarse sand
BB/JH/DH NL50	0.888	2.343	0.994	Coarse sand
BR/DS/BV NL50	0.659	1.993	0.961	Coarse sand
CA/NE/I NL50	0.760	2.153	0.949	Coarse sand
CR/DJ/C NL50	0.564	2.689	0.966	Coarse sand
CR/VB/PO NL50	0.848	4.255	1.029	Coarse sand
CV/SM/JB NL50	0.987	2.191	1.009	Coarse sand
FG/NP/Y NL50	0.477	2.246	0.954	Medium sand
GA/AF/MB NL50	0.442	1.491	0.987	Medium sand
GB/ED/P NL50	0.506	2.938	0.864	Coarse sand
OM/CT/B1 NL50	0.339	2.186	0.926	Medium sand
SC/NB/CC NL50	1.044	1.903	0.981	Coarse sand
US/DG/PI NL50	0.284	1.574	0.992	Medium sand
US/TD/AC NL50	0.771	3.074	0.935	Coarse sand

Table 4.5: The critical particle size distribution parameters (D_{50}, Cu and Cc) for the sixteen sea turtle nesting line samples were calculated based on the PSD, which was determined using Statistic Light Scattering by the Mastersizer 2000 (Kalore and Babu 2023). Abbreviations: D_{50} = Median particle diameter, Cu = Coefficient of Uniformity, Cc = Coefficient of Curvature, mm = Millimeter, PSD = Particle Size Distribution.

Table D.5 in Appendix D provided an overview of the statistical parameters for the sixteen nesting line samples analyzed using SLS by Mastersizer 2000. The SD and S_r values indicated that all shoreline samples fell into the category of very well sorted, consistent with the Cu values. The majority of the S_k values were negative, suggesting that the samples were slightly skewed toward coarser particles. However, most values were close to zero, indicating that many samples have a near-symmetrical PSD. Most K values suggested that the samples exhibited a relatively normal distribution of particle sizes (mesokurtic profile).

Figure 4.8 illustrates the cumulative distribution curves for the **shoreline** of sixteen beaches. It shows that all curves also fell within the sand domain. There is no significant gravel or clay/silt fraction in most samples, with a couple of exceptions, like FG/NP/Y.

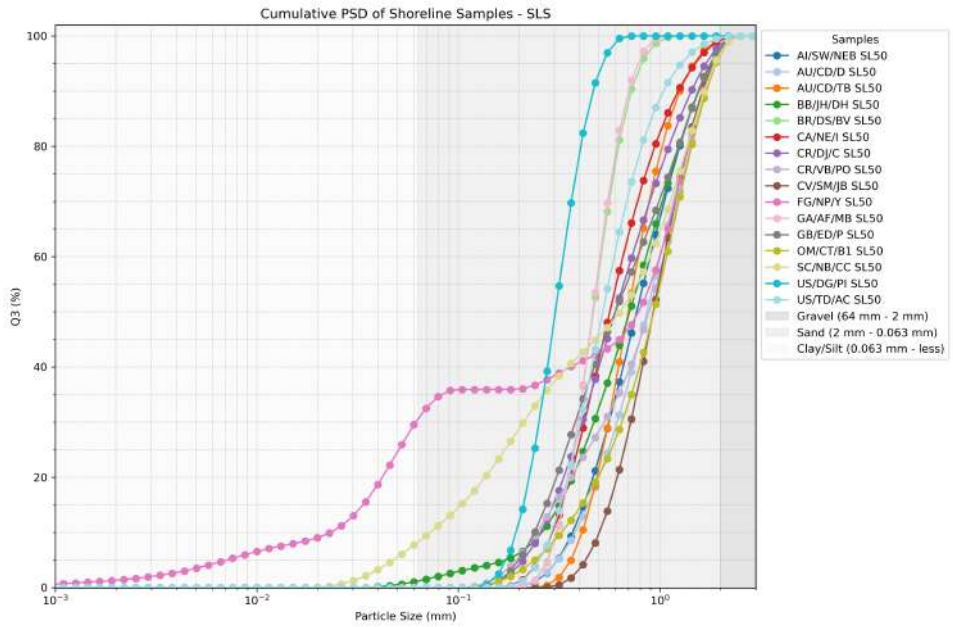

Figure 4.8: The cumulative particle size distribution of the sixteen sea turtle shoreline samples was determined using Static Light Scattering by the Mastersizer 2000. The x-axis represents particle size in millimeters (mm), while the y-axis represents Q_3 in the context of cumulative volume (%) distribution. Abbreviations: mm = Millimeter, PSD = Particle Size Distribution, SL= Shoreline, SLS = Static Light Scattering.

The critical PSD parameters of the shoreline samples analyzed using SLS are summarized in Table 4.6. The D_{50} values, ranging from 0.304 to 0.936 mm, confirmed that all samples fall within the sand range, consistent with the PSD results obtained from dry sieving. However, all samples were classified as coarse sand according to the Wentworth classification, which contradicted the dry sieving results. The gradation could be classified as well-sorted, except for two samples: FG/NP/Y and SC/NB/CC. These samples had Cu values above six, indicating a broad range of particle sizes. FG/NP/Y had an extremely high Cu value, indicating that it was very poorly sorted and reflects a mix of both very fine and very coarse particles. Most samples exhibit Cc values very close to one, indicating a relatively smooth PSD curve. However, FG/NP/Y, GB/ED/P, and SC/NB/CC SL50 had very low Cc values, suggesting the presence of gap grading. In particular, FG/NP/Y reflected extreme gap grading, with significant missing intermediate particle sizes.

Sample code	D_{50} (mm)	Cu (-)	Cc (-)	Wentworth classification
AI/SW/NEB SL50	0.770	2.431	0.945	Coarse sand
AU/CD/D SL50	0.865	2.649	0.988	Coarse sand
AU/CD/TB SL50	0.699	1.903	0.957	Coarse sand
BB/JH/DH SL50	0.711	3.296	0.998	Coarse sand
BR/DS/BV SL50	0.468	1.665	0.976	Coarse sand
CA/NE/I SL50	0.566	2.244	0.929	Coarse sand
CR/DJ/C SL50	0.603	2.843	0.911	Coarse sand
CR/VB/PO SL50	0.885	4.267	1.089	Coarse sand
CV/SM/JB SL50	0.930	2.098	0.977	Coarse sand
FG/NP/Y SL50	0.787	43.097	0.164	Coarse sand
GA/AF/MB SL50	0.466	1.639	0.980	Coarse sand
GB/ED/P SL50	0.603	3.258	0.782	Coarse sand
OM/CT/B1 SL50	0.936	3.327	1.203	Coarse sand
SC/NB/CC SL50	0.637	12.395	0.682	Coarse sand
US/DG/PI SL50	0.304	1.718	0.985	Coarse sand
US/TD/AC SL50	0.523	2.051	0.948	Coarse sand

Table 4.6: The critical particle size distribution parameters (D_{50}, Cu and Cc) for the sixteen sea turtle shoreline samples were calculated based on the PSD, which was determined using Statistic Light Scattering by the Mastersizer 2000 (Kalore and Babu 2023). Abbreviations: D_{50} = Median particle diameter, Cu = Coefficient of Uniformity, Cc = Coefficient of Curvature, mm = Millimeter, PSD = Particle Size Distribution.

Table D.6 in Appendix D provides an overview of the statistical parameters for the sixteen shoreline samples analyzed using SLS by Mastersizer 2000. The SD and S_r values indicated that all shoreline samples fell into the category of very well sorted. This was almost consistent with the Cu values, except for FG/NP/Y and SC/NB/CC, where Cu values indicated poorly sorted samples. This inconsistency arises because Cu is based on on only two values: D_{10} and D_{60}, making it sensitive to extreme values. If a sample contains even a small proportion of very coarse or very fine particles, the D_{10} and D_{60} values become widely separated, influencing the Cu value. In contrast, the standard deviation and sorting parameters consider the entire particle size distribution, reflecting how all particle sizes are distributed relative to the mean particle size. The curve of sample FG/NP/Y indicated the presence of very fine sediment, resulting in a high Cu value. The majority of the S_k values were negative, suggesting that the samples were slightly skewed toward coarse particles. However, most values were close to zero, indicating that many samples exhibited a near-symmetrical PSD. Some K values indicated that the samples exhibited a relatively normal distribution of particle sizes (mesokurtic profile), while other samples showed platykurtic distributions, where the PSD was flatter and less peaked.

4.2.2. Particle shape

The CPA quantifies particle shape using roundness (R_n), circularity (ψ), and sphericity. This study focused on the 2D analysis of particle shape; therefore, only roundness and circularity were analyzed.

Figure 4.9 illustrates the relationship between roundness and circularity for sediment particles from sixteen sea turtle nesting beaches at the **nesting line**. The x-axis represents roundness at the median particle size, while the y-axis represents circularity at the median particle size. For each sediment sample, microscopic images of the particles were included to provide better visualization.

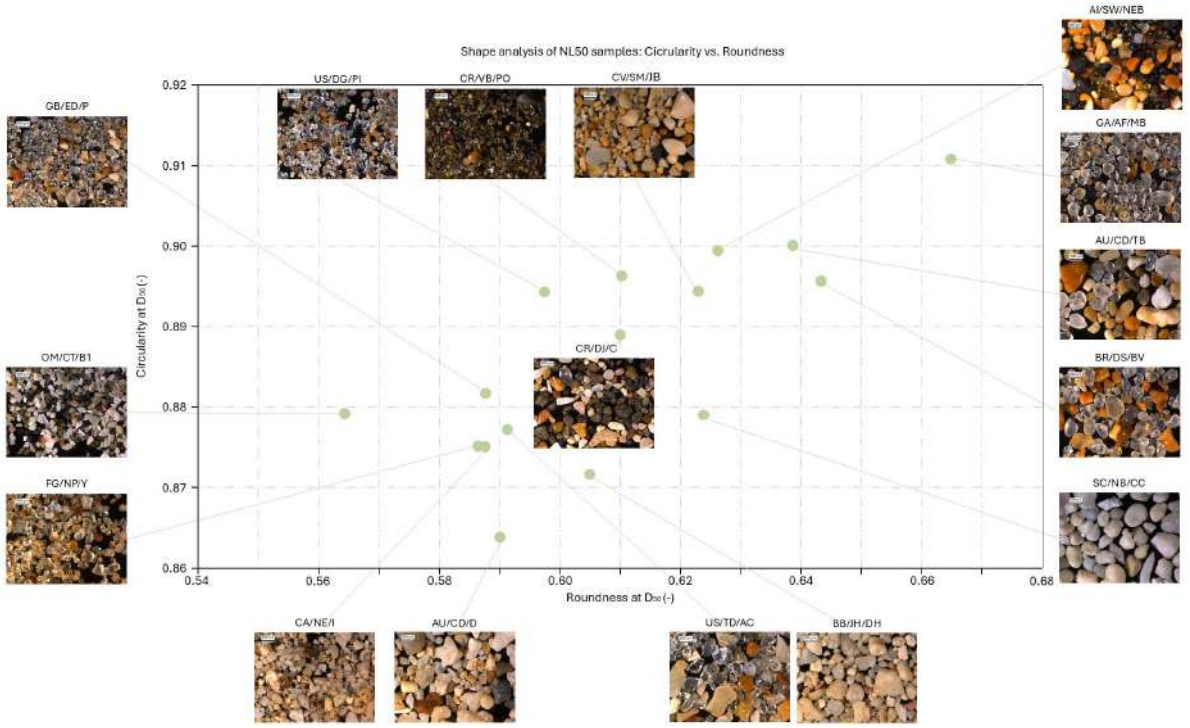

Figure 4.9: Shape analysis of the sixteen sea turtle nesting line samples: circularity (ψ) vs. roundness (R_n) with representative microscope images. The values represent the shape characteristics of the median particles.

Roundness measured the smoothness and compactness of a particle's projection by assessing how closely its overall geometry resembles a circle. Figure 4.9 shows that all samples had a roundness values above 0.56, indicating that the particles were not highly irregular or elongated. The upper limit of roundness in the dataset was 0.67, suggesting that none of the particles were near-perfect circles. This implies that while the particles were moderately compact, they still exhibited slight irregularities or elongation. Circularity focused on the smoothness of the particle's boundary, measuring how consistent the circumference was relative to a perfect circle. The circularity values for the samples ranged from 0.86 to 0.92, indicating that the particles had relatively smooth edges with minimal boundary irregularities.

The combination of moderate roundness (0.56–0.67) and high circularity (0.86–0.92) suggested that the particles generally had smooth edges and moderately compact, but were slightly elongated or irregular in shape. Figure 4.9 revealed a slight trend, where higher roundness values were associated with higher circularity values. Microscope images in Figure 4.9 provide a clear visualization of the analyzed samples. For example, comparing the roundness in samples OM/CT/B1 and SC/NB/CC, which had the same circularity, it could be observed that SC/NB/CC contained more circular particles than OM/CT/B1. Similarly, when analyzing the circularity of AU/CD/D and US/DG/PI, AU/CD/D exhibited more irregular edges, despite having approximately the same roundness.

The roundness and circularity of the **shoreline** samples from the sixteen sea turtle nesting beaches are shown in Figure 4.10. Microscope images of the shoreline samples can be viewed in greater detail in Appendix C.2.

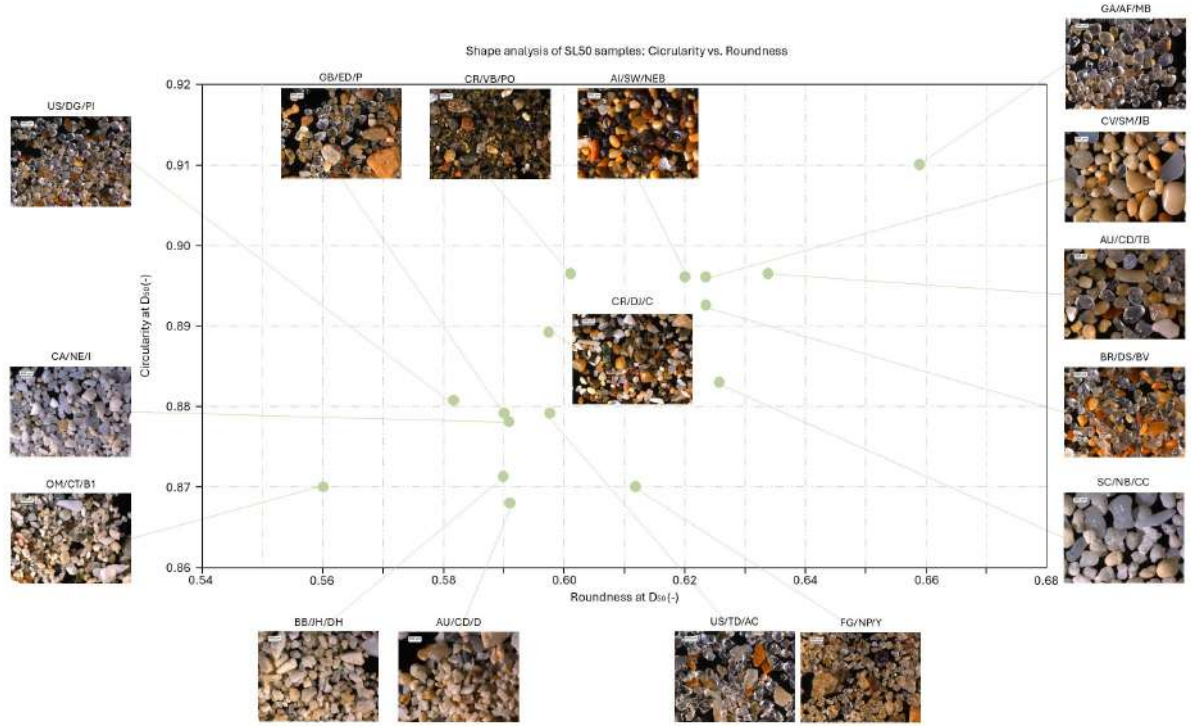

Figure 4.10: Shape analysis of the sixteen sea turtle shoreline samples: circularity (ψ) vs. roundness (R_n) with representative microscope images. The circularity and roundness values are derived from the median. The values represent the shape characteristics of the median particles.

The figure shows that the particles in the shoreline samples exhibited a combination of moderate roundness and high circularity. Similar to the shape analysis of the nesting line, the particles in the shoreline samples generally had smooth edges and were moderately compact. However, the roundness values suggested that the particles were slightly elongated or irregular in their overall shape. Additionally, a slight trend was observed, where higher roundness values were associated with higher circularity values.

4.2.3. Bulk density

Bulk density (ρ_b) is defined as the mass per unit volume of dry soil in its natural condition. The bulk density of surface mineral soil typically ranges from 1.0 to 1.6 g/cm^3, with key influencing factors including pore space, texture, organic matter, and soil depth (Walters 2021). More specifically, the bulk density of clay to sand varies between 1.35 and 1.65 g/cm^3 (Zeri et al. 2018).

This study measured the minimum and maximum bulk density of 32 samples. The minimum density represented the loosest condition the sample can attain, while the maximum density represented the densest condition. The bulk densities of the sixteen sea turtle **nesting line** samples are illustrated in Figure 4.11. The y-axis starts at 1.0 g/cm^3, with a dashed line at 1.6 g/cm^3 indicating the upper end of the typical bulk density range for surface mineral soils.

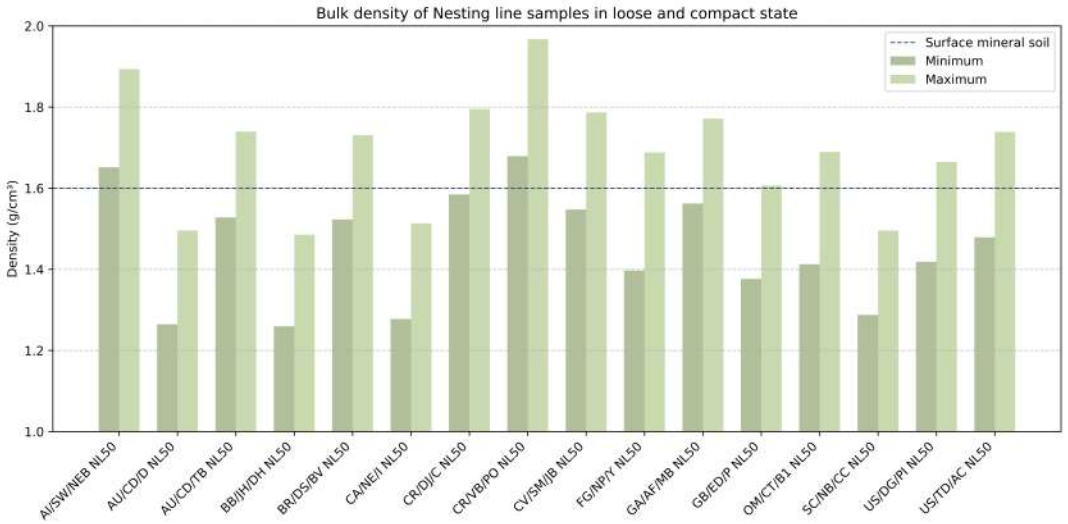

Figure 4.11: The bulk densities of the sixteen sea turtle nesting line samples. The minimum density (dark green) indicates the bulk density in loose state and the maximum density (light green) indicates the bulk density in compact state. The dashed line is the upper end of the typical bulk density range for surface mineral soil.

The minimum densities of the nesting line samples ranged from 1.26 to 1.68 g/cm^3, while the maximum densities ranged from 1.49 to 1.97 g/cm^3. CR/VB/PO and AI/SW/NEB exhibited the highest minimum and maximum densities compared to the other samples. Most minimum bulk density values fall within the typical range for surface mineral soils, whereas the majority of maximum values exceed this range. Some samples, such as AU/CD/D, had relatively low minimum bulk densities compared to the general density of sand. Additionally, Figure 4.11 shows that the differences between the loose and compact states were relatively consistent across all samples.

The bulk density of the **shoreline** samples is presented in Figure 4.12.

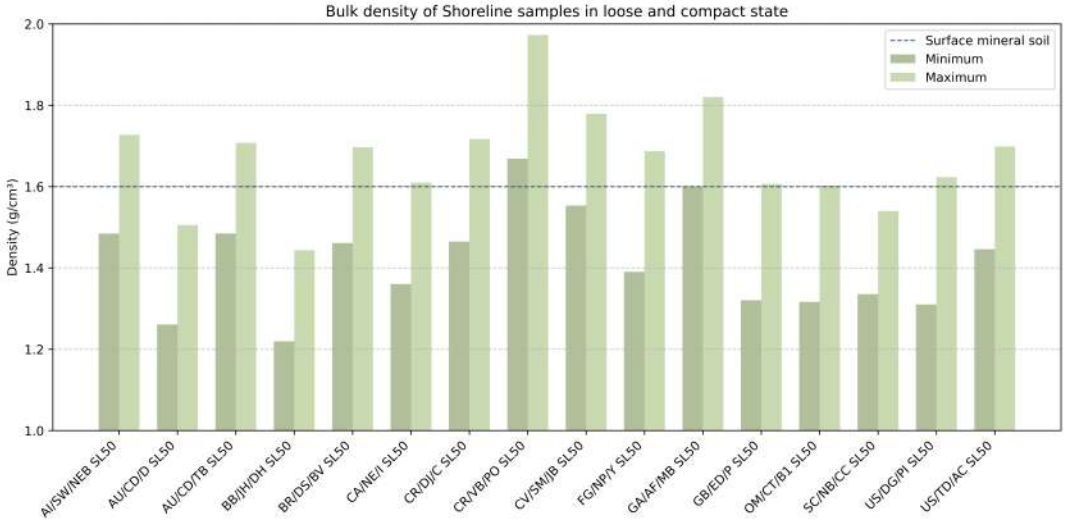

Figure 4.12: The bulk densities of the sixteen sea turtle shoreline samples. The minimum density (dark green) indicates the bulk density in loose state and the maximum density (light green) indicates the bulk density in compact state. The dashed line is the upper end of the typical bulk density range for surface mineral soil.

The minimum density of the shoreline samples varied between 1.22 to 1.67 g/cm^3, while the maximum

density varied between 1.44 to 1.97 g/cm^3. These ranges were similar to those observed in the nesting line samples. In this dataset, CR/VB/PO and GA/AF/MB exhibited the highest minimum and maximum densities among the shoreline samples. Additionally, similar to the nesting line, the difference between the two density states was approximately uniform across all samples.

4.2.4. Solid particle density

The solid particle density was determined using two different methods: the helium gas displacement pycnometer and the volume of water displacement method. Since the helium pycnometer at Deltares was outdated and the required operation by an extern, only seven nesting line samples were tested using this method.

The solid particle density of mineral particles (sand) typically ranges between 2.60 and 2.75 g/cm^3, with 2.65 g/cm^3 often used as an average reference value, representing the density of pure quartz. Mineral particles generally have higher densities than organic matter, which has a particle density ranging from 0.9 to 1.3 g/cm^3 (Walters 2021).

Helium gas displacement pycnometer

The seven nesting line samples tested using the helium pycnometer include: AI/SW/NEB, AU/CD/D, BB/JH/DH, CR/DJ/C, GA/AF/MB, SC/NB/CC, and US/TD/AC. Figure 4.13 presents the solid particle densities of each nesting line sample. They y-axis starts at 2.0 g/cm^3.

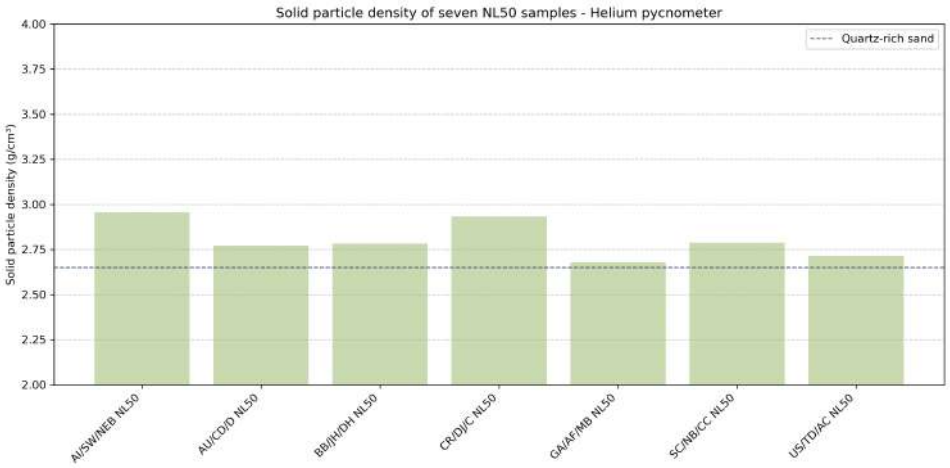

Figure 4.13: Solid particle densities of seven sea turtle nesting line samples obtained from the helium gas displacement pycnometer method. The dashed line is the average reference density value of sand consisted of pure quartz (2.65 g/cm^3). Abbreviations: NL = Nesting line.

The lowest particle density was 2.69 g/cm^3 for GA/AF/MB, which was close to the average density of quartz-based sand. The highest density observed was 2.96 g/cm^3 of AI/SW/NEB, which was relatively high compared to the typical density range of mineral particles.

Volume of water displacement method

Figure 4.14 illustrates the solid particle densities of the **nesting line** samples from all sea turtle nesting beaches, determined using the volume of water displacement method. They y-axis starts at 2.0 g/cm^3.

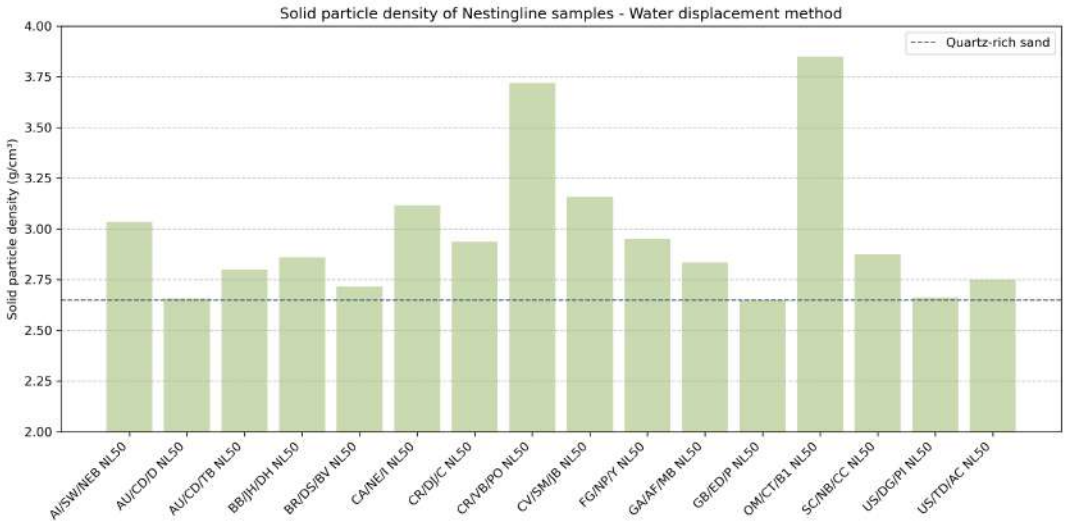

Figure 4.14: Solid particle densities of the sixteen sea turtle nesting line samples obtained from the volume of water displacement method. The dashed line is the average reference density value of sand consisted of pure quartz (2.65 g/cm^3). Abbreviations: NL = Nesting line.

There was noticeable variation in densities across the samples. Some samples, such as CR/VB/PO and OM/CT/B1, exhibited significantly higher densities than others. Only a few samples fell within the typical density range of mineral particles, while most samples have densities higher than 2.75 g/cm^3.

The solid particle densities for the **shoreline** samples are illustrated in Figure 4.15. They y-axis starts at 2.0 g/cm^3.

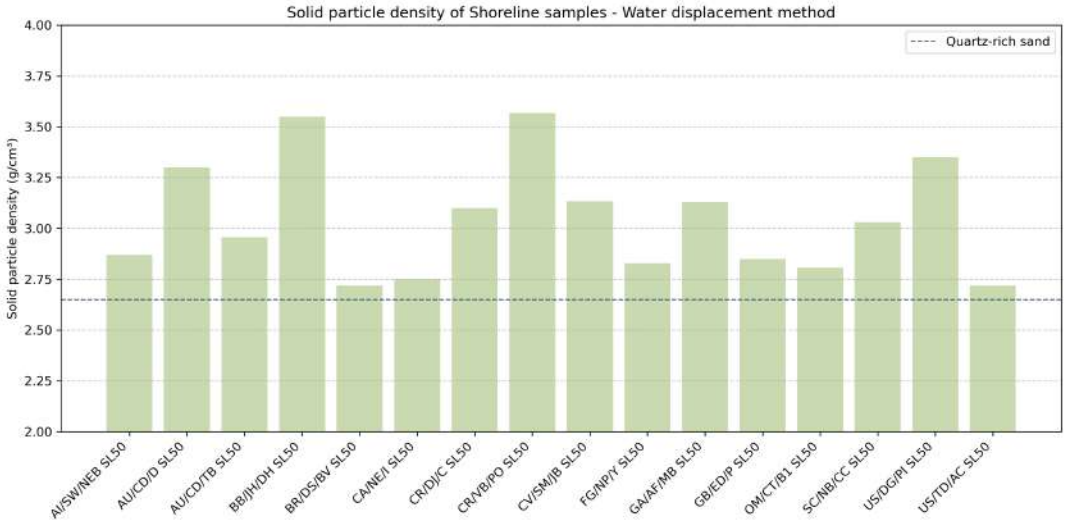

Figure 4.15: Solid particle densities of the sixteen sea turtle shoreline samples obtained from the volume of water displacement method. The dashed line is the average reference density value of sand consisted of pure quartz (2.65 g/cm^3). Abbreviation: SL = Shoreline.

Similar to the nesting line samples, most shoreline samples exhibited solid particle densities higher than 2.75 g/cm^3. This suggested that the shoreline samples did not consist entirely of quartz. The highest particle densities among the shoreline samples were found in BB/JH/DH and CR/VB/PO. The lowest particle densities among the shoreline samples were found in BR/DS/BV and US/TD/AC.

4.2.5. Angle of repose

The angle of repose was determined using photographic documentation. By averaging two measured angles, the angle of repose was derived from the conical deposition of sand. In general, the angle of repose for sand ranges from 30° to 35° (Al-Hashemi and Al-Amoudi 2018).

The angles of repose for the **nesting line** samples from all sea turtle nesting beaches are illustrated in Figure 4.16. The measured angles ranged from 16.69° to 26.48°, indicating variability across the samples. All measured angles in this dataset were lower than the general angle of repose for sand. The samples AU/CD/D and BB/JH/DH exhibited the highest angles. Several sediment characteristics could influence the angle of repose, including: particle surface texture, particle shape and particle sizes.

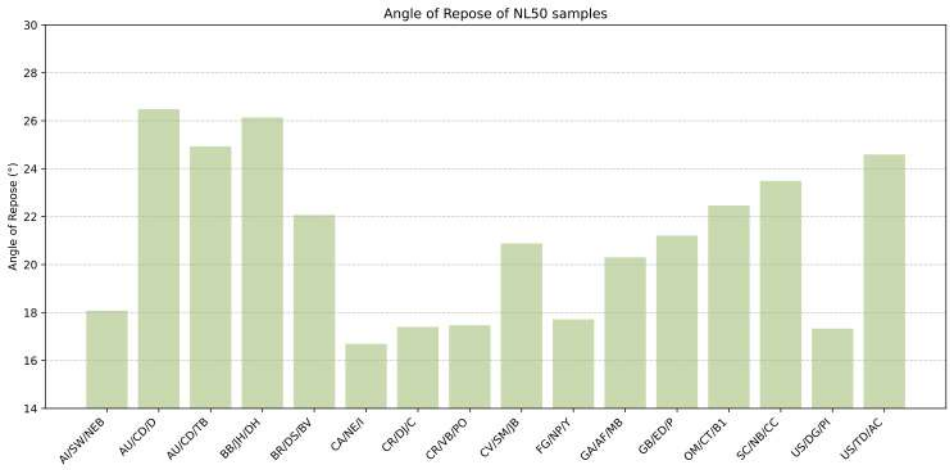

Figure 4.16: Angle of repose (°) of all sixteen sea turtle nesting line samples analyzed using Image-Based Angle of Repose Analysis. Abbreviations: NL = Nesting Line.

Figure 4.17 illustrates the angles of repose for the **shoreline** samples from the analyzed sea turtle beaches. The angles range from 16.55° to 28.26°, with AU/CD/D and OM/CT/B1 exhibiting the highest angles. Similar to the nesting line samples, all shoreline samples exhibited lower angles of repose than the typical range for sand.

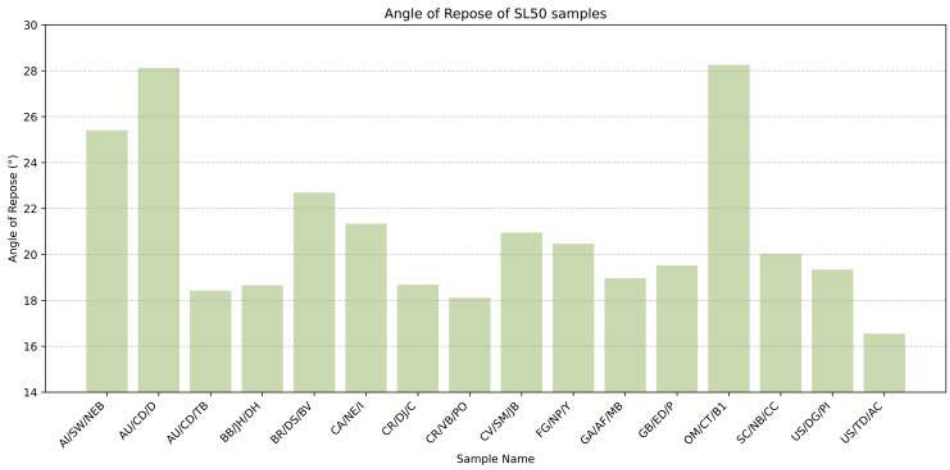

Figure 4.17: Angle of repose (°) of all sixteen sea turtle shoreline samples analyzed using Image-Based Angle of Repose Analysis. Abbreviations: SL = Shoreline.

4.2.6. Thermal retention

The thermal retention is determined exclusively for the nesting line of the sea turtle beaches. In Figure 4.18, the cooling process for each sample are represented, with time (minutes) on the x-axis and temperature (°C) on the y-axis. Each curve corresponds to a different sample.

Initially, the temperature of all samples started between 80-100°C, then cool gradually toward room temperature (21°C). The little bulb at the beginning was where the temperature probe was put in the sample, therefore the temperature first increased a little bit. The curves showed an exponential decay pattern, where they approached equilibrium with the environment. Around an hour, the temperatures of the samples varied from approximately 21-27°C. Samples such as CR/VB/PO, CR/DJ/C and AI/SW/NEB, exhibited the highest temperatures, indicating that these samples retained heat longer than other samples, while samples such as FG/NP/Y showed lower temperatures, suggesting a poorer heat retention. These differences could be influenced by factors including, mineral and organic content and bulk density (Abu-Hamdeh 2003).

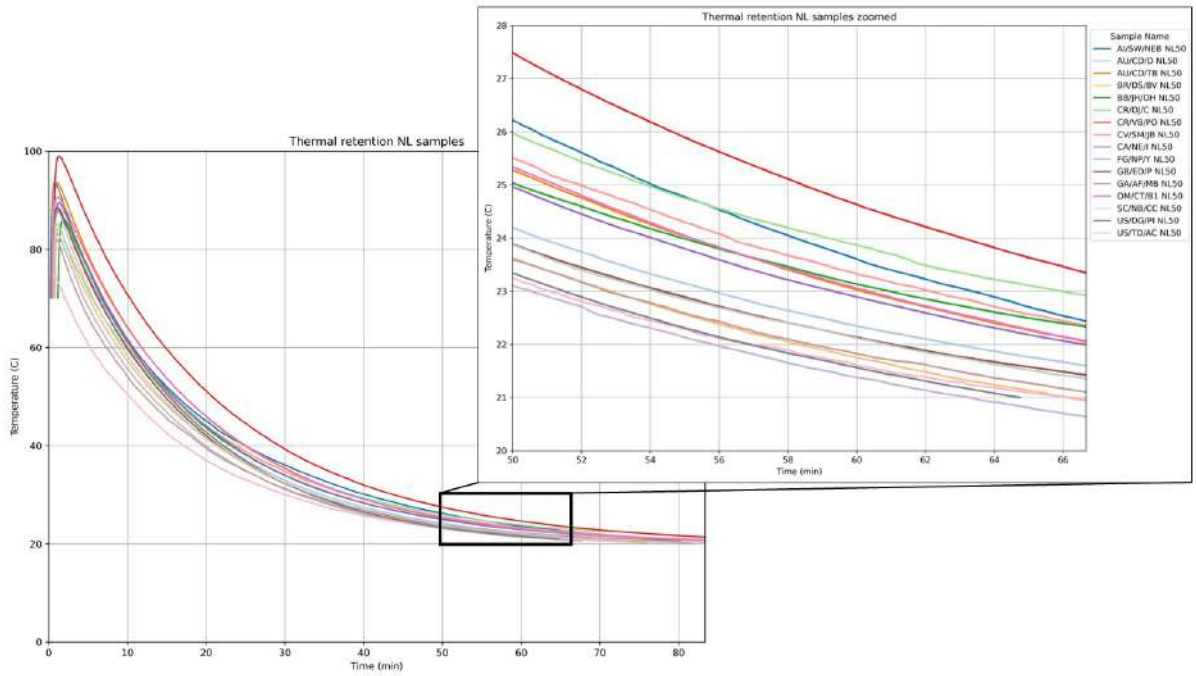

Figure 4.18: Zoomed-in view of the thermal retention curves for the sixteen sea turtle nesting line samples, focusing on the temperature trends around the 60-minutes mark. Abbreviations: NL = Nesting Line.

4.2.7. Porosity

The porosity was calculated using Equation 2.4. Porosity values typically fall between 30-60%, while sand soils often vary in total pore space from 30-50% (Walters 2021). It depends on the arrangement of particles, particle sizes, and particle shapes (Sweijen et al. 2019). The minimum density gives the highest porosity condition of a sample, while the maximum density gives the lowest porosity condition of the sample. The solid particle density was determined by two methods. Therefore this distinguish was also made when calculating the porosity.

Helium gas displacement pycnometer

Figure 4.19 illustrate the porosity of seven nesting line samples (AI/SW/NEB, AU/CD/D, BB/JH/DH, CR/DJ/C, GA/AF/MB, SC/NB/CC, and US/TD/AC). The porosity ranged from 34-55%, which is in the same range of the general porosity value of sand soils.

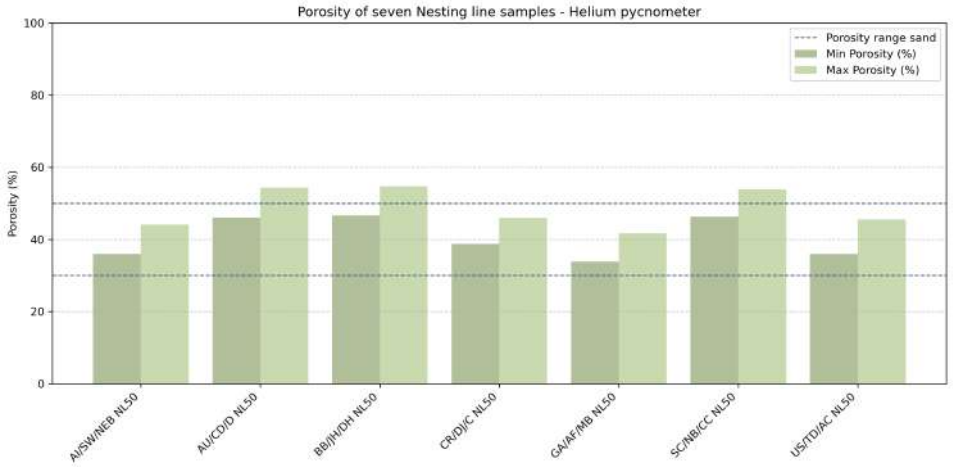

Figure 4.19: Porosity (%) of seven sea turtle nesting line samples analyzed using a helium pycnometer. Abbreviations: NL = Nesting Line.

Volume of water displacement method

Figure 4.20 illustrate the porosity of the sixteen **nesting line** samples. The porosity ranged from 36-63%. OM/CT/B1 gave the highest minimum and maximum porosity of the dataset.

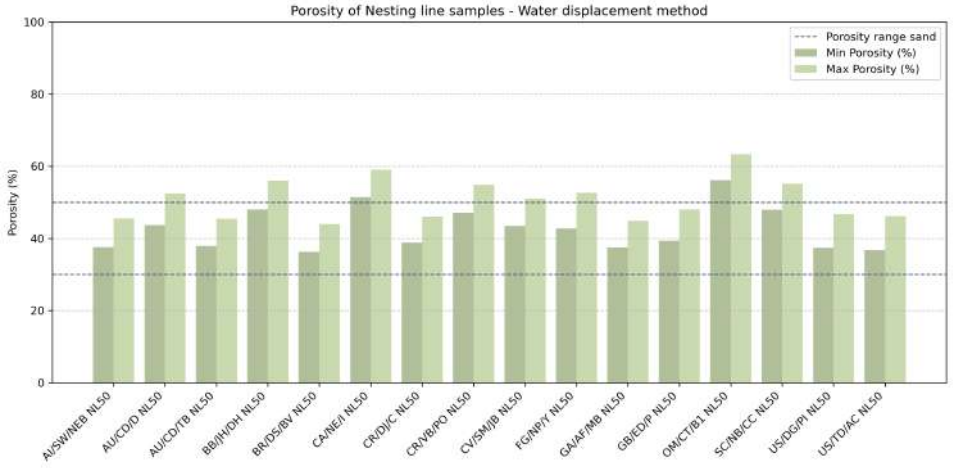

Figure 4.20: Porosity (%) of the sixteen sea turtle nesting line samples analyzed using the Volume of water displacement method. Abbreviations: NL = Nesting Line.

Figure 4.21 illustrate the porosity of the sixteen **shoreline** samples. The porosity ranged from 38-66%. BB/JH/DH gave the highest minimum and maximum porosity of the dataset. This dataset was also within in the typically range of porosity of sand.

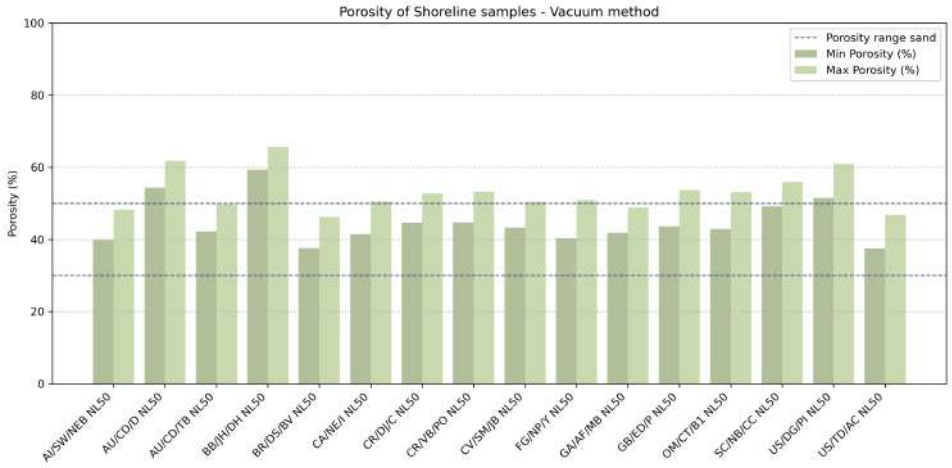

Figure 4.21: Porosity (%) of the sixteen sea turtle shoreline samples analyzed using the Volume of water displacement method. Abbreviations: SL = Shoreline.

4.2.8. Summary

Table 4.7 summarizes the results of the tested sediment characteristics from 32 samples collected at sea turtle nesting beaches.

Sample code	Site	D_{50} (mm)	Grading	ψ (-)	R_n (-)	$\rho_{b,avg}$ (g/cm^3)	ρ_s (g/cm^3)	Angle of Repose (°)	Temperature (°C)	Avg. porosity (%)
AI/SW/NEB	Nesting line	0.37	Very well sorted	0.90	0.63	1.82	3.03	18.08	23.61	41.56
	Shoreline	0.39	Very well sorted	0.90	0.62	1.61	2.87	25.41		44.05
AU/CD/D	Nesting line	0.58	Very well sorted	0.86	0.59	1.38	2.66	26.48	22.35	48.05
	Shoreline	0.43	Very well sorted	0.87	0.59	1.38	3.30	28.12		58.09
AU/CD/TB	Nesting line	0.47	Very well sorted	0.90	0.64	1.63	2.80	24.92	23.03	41.65
	Shoreline	0.45	Very well sorted	0.90	0.63	1.60	2.96	18.42		46.00
BB/JH/DH	Nesting line	0.57	Very well sorted	0.87	0.60	1.37	2.86	26.13	23.13	52.01
	Shoreline	0.38	Very well sorted	0.87	0.59	1.33	3.55	18.66		62.49
BR/DS/BV	Nesting line	0.45	Very well sorted	0.90	0.64	1.63	2.72	22.06	21.76	40.11
	Shoreline	0.31	Very well sorted	0.89	0.62	1.58	2.72	22.70		41.92
CA/NE/I	Nesting line	0.31	Very well sorted	0.88	0.59	1.40	3.12	16.69	22.90	55.22
	Shoreline	0.30	Very well sorted	0.88	0.59	1.58	2.75	21.34		45.99
CR/DJ/C	Nesting line	0.29	Very well sorted	0.89	0.61	1.69	2.94	17.40	23.87	42.47
	Shoreline	0.30	Very well sorted	0.89	0.60	1.59	3.10	18.68		48.68
CR/VB/PO	Nesting line	0.30	Very well sorted	0.90	0.61	1.82	3.72	17.47	24.62	50.99
	Shoreline	0.24	Very well sorted	0.90	0.60	1.82	3.57	18.11		48.95
CV/SM/JB	Nesting line	0.48	Very well sorted	0.89	0.62	1.67	3.16	20.88	23.32	47.22
	Shoreline	0.49	Very well sorted	0.90	0.62	1.67	3.13	20.95		46.82
FG/NP/Y	Nesting line	0.26	Very well sorted	0.88	0.59	1.54	2.95	17.71	21.37	47.71
	Shoreline	0.50	Very well sorted	0.87	0.61	1.54	2.83	20.46		45.60
GA/AF/MB	Nesting line	0.33	Very well sorted	0.91	0.66	1.67	2.83	20.30	21.82	41.20
	Shoreline	0.32	Very well sorted	0.91	0.66	1.71	3.13	18.96		45.33
GB/ED/P	Nesting line	0.25	Very well sorted	0.88	0.59	1.49	2.65	21.20	22.13	43.71
	Shoreline	0.28	Very well sorted	0.88	0.59	1.46	2.85	19.52		48.65
OM/CT/B1	Nesting line	0.20	Very well sorted	0.88	0.56	1.55	3.85	22.46	23.06	59.72
	Shoreline	0.24	Very well sorted	0.87	0.56	1.46	2.81	28.26		48.00
SC/NB/CC	Nesting line	0.68	Very well sorted	0.88	0.62	1.39	2.88	23.49	21.61	51.60
	Shoreline	0.60	Very well sorted	0.88	0.63	1.44	3.03	20.04		52.55
US/DG/PI	Nesting line	0.20	Very well sorted	0.89	0.60	1.54	2.66	17.33	21.56	42.06
	Shoreline	0.22	Very well sorted	0.88	0.58	1.47	3.35	19.34		56.21
US/TD/AC	Nesting line	0.34	Very well sorted	0.88	0.59	1.61	2.75	24.59	22.11	41.50
	Shoreline	0.33	Very well sorted	0.88	0.60	1.57	2.72	16.55		42.17

Table 4.7: Overview of sediment characteristics from 32 samples collected at the key sea turtle nesting beaches. The values of the solid particle density were obtained using the volume of water displacement method, as this experiment analyzes all 32 samples. The thermal retention was determined 60 minutes after inserting the temperature probe. Analyzing the temperature at this time ensured that the sample had reached approximate thermal equilibrium, minimizing the influence of initial temperature fluctuations. This approach allowed for better comparability between samples.

4.3. Comparative analyses

4.3.1. Relationships between key sediment characteristics

To further explore the interactions between sediment characteristics across the nesting line of the sixteen nesting beaches, a correlation analysis was performed. This analysis examined the potential relationships between particle size, grading, densities, angle of repose, thermal retention, and porosity. The correlation matrix (Figure 4.22) summarizes the strength and direction of these relationships.

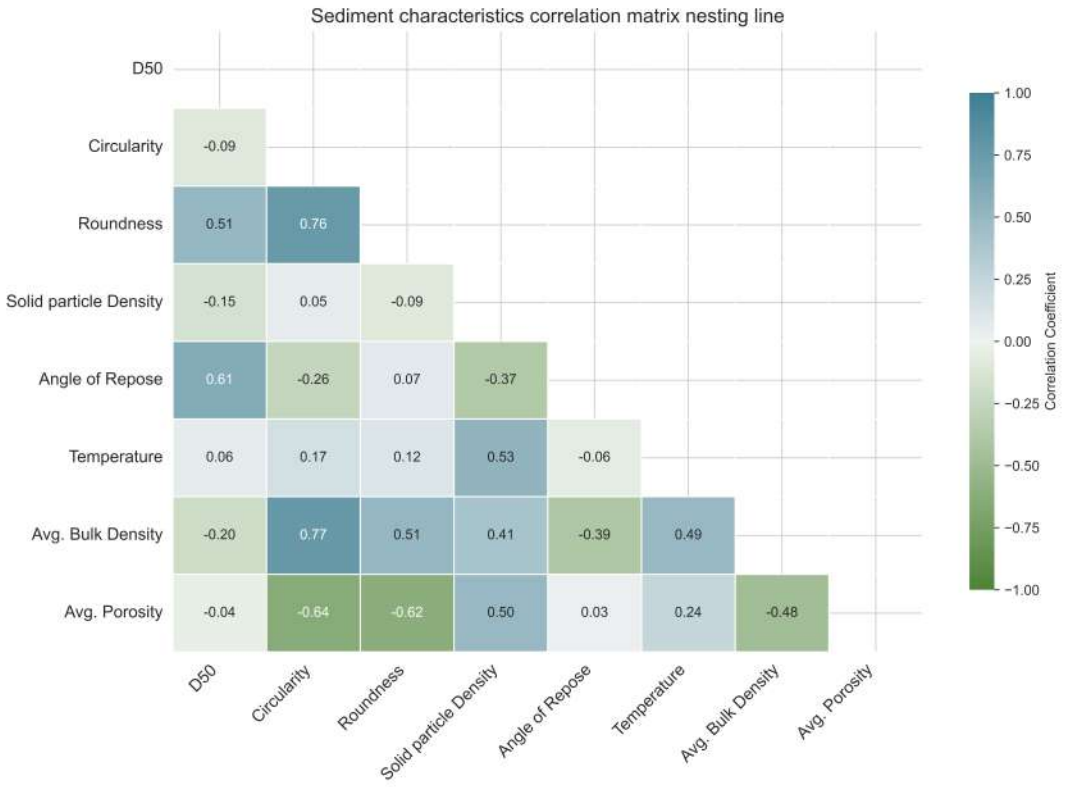

Figure 4.22: Spearman correlation matrix of key sediment characteristics measured at the sixteen nesting beaches at the nesting line. The matrix illustrates how strongly and in which direction the variables are related. Blue colors indicate strong positive correlations and green colors represent strong negative correlations.

A strong positive correlation was observed between the circularity and the average bulk density, suggesting that particles having more smooth boundaries tend to have higher bulk density. Furthermore, there was a positive correlation between the median particle size and angle of repose, suggesting that coarser sediments tend to form a steeper slope. A positive correlation could also be found between the solid density and temperature, suggesting that denser particles may facilitate better heat retention or conduction within the sediment. Lastly, positive correlation between porosity and solid density suggested that sediments with denser particles also tend to have higher porosity.

Negative correlations were observed between the porosity and particle shape (circularity -0.64 and roundness -0.62). This indicated that if the particles became more circular and/or smoother, particles tend to reduce porosity. A negative correlation between porosity and bulk density confirmed that denser sediments generally have lower porosity. A slight negative correlation between bulk density and median particle size suggested that coarser particle sediments tend to have lower bulk density. This may be due to the fact that larger particles result in more loosely packed structures with greater void space,

while finer particles compact more effectively.

4.3.2. Nesting line versus shoreline

This study focused on overall trends between the two environments, rather than differences between nesting- and shoreline on each beach. Understanding this broader patterns is useful for guiding large-scale research. If no consistent differences exist between the nesting zone and the shoreline across locations, large-scale research could initially focus on just one of these environments. Table 4.8 presents the results of this maximum distance. Beach FG/NP/Y exhibited the largest difference, suggesting greater variation in PSD between the nesting line and the shoreline. In contrast, lower D_{max} values, such as those observed at GA/AF/MB, indicate more uniform PSDs.

Sample code	D_{max} **(%)**
AI/SW/NEB	7.081
AU/CD/D	19.895
AU/CD/TB	10.058
BB/JH/DH	32.846
BR/DS/BV	43.074
CA/NE/I	5.123
CR/DJ/C	6.134
CR/VB/PO	12.036
CV/SM/JB	6.819
FG/NP/Y	47.348
GA/AF/MB	4.695
GB/ED/P	11.385
OM/CT/B1	19.482
SC/NB/CC	16.992
US/DG/PI	15.790
US/TD/AC	10.835

Table 4.8: Maximum distance (%) between the cumulative particle size distributions at the nesting line and shoreline.

Furthermore, potential differences in other sediment characteristics between the two locations were also investigated using statistical tests. Table 4.9 summarizes the results of these tests. The p-values for all sediment characteristics in the table were higher than the significance level ($p > 0.05$), indicating that there were no significant differences between the sediment characteristics of the nesting line and the shoreline.

Sediment characteristic	**Statistic test**	**p-value**	**Significant difference between NL and SL?**
Particle size (D_{50})	Unpaired t-test	0.699	No significant difference
Particle shape (ψ)	Unpaired t-test	0.705	No significant difference
Particle shape (R_n)	Unpaired t-test	0.723	No significant difference
Avg. bulk density ($\rho_{b,avg}$)	Unpaired t-test	0.555	No significant difference
Solid particle density (ρ_s)	Mann-Whitney U test	0.309	No significant difference
Angle of Repose	Mann-Whitney U test	0.985	No significant difference
Avg. porosity	Mann-Whitney U test	0.207	No significant difference

Table 4.9: Statistical tests comparing sediment characteristics between the nesting line and the shoreline.

Although it could be concluded that there were no statistically significant differences between the sediment characteristics of the nesting line and shoreline, visible differences might still have been present,

including variations in spread, median, and the presence of outliers.

Figure 4.23 compares D_{50}, ψ, and R_n between the nesting line and shoreline. Additional sediment characteristics are presented in Appendix D Figure D.1. The majority of the D_{50} values clustered near the dashed line, suggesting that in most cases, D_{50} was similar between the two locations. Some dots slightly above or below the line indicated localized variations between the nesting line and shoreline. The values of ψ and R_n for both locations were highly similar, as all dots were close to the dashed line. While ψ showed no local variation, R_n exhibited slight variation.

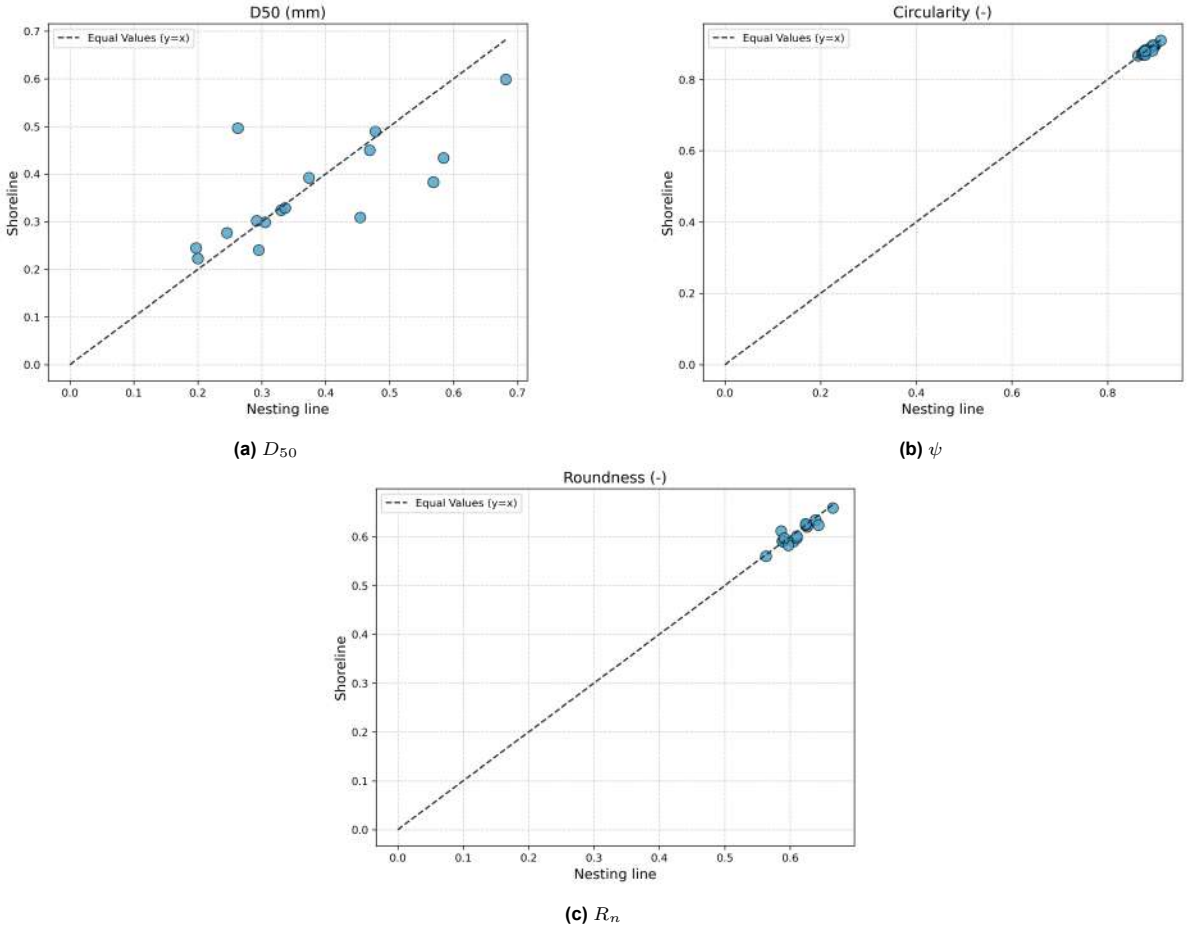

(a) D_{50} **(b)** ψ

(c) R_n

Figure 4.23: Scatterplot comparisons between nesting line and shoreline for median particle size (D_{50}), circularity (ψ), and roundness (R_n). The x-axis displayed the value of a given key sediment characteristic at the nesting line, while the y-axis showed the same key characteristic at the shoreline. A dashed line was included as a reference line indicating equal values between the two locations.

Figure 4.24 displays boxplots of bulk densities, solid particle density, angle of repose, and porosity for both the nesting- and shoreline. Boxplots of the remaining key sediment characteristics are shown in Appendix D Figure D.2. Both environments had similar median values for bulk density, but the nesting line had slightly higher upper values. Because the distributions overlap, no strong differences were suggested. In the case of solid particle density, a few outliers were presented at the nesting line, indicating some variation in the data. However, the overall distribution between the two locations was relatively similar, but the median value at the shoreline was higher than at the nesting line. The inter-quartile range for the angle of repose was larger at the nesting line than at the shoreline, suggesting greater variability. In contrast, the shoreline showed a more compact distribution, with a few high

outliers. The porosity values at the nesting line exhibit a greater spread, but a lower median compared to those at the nesting line.

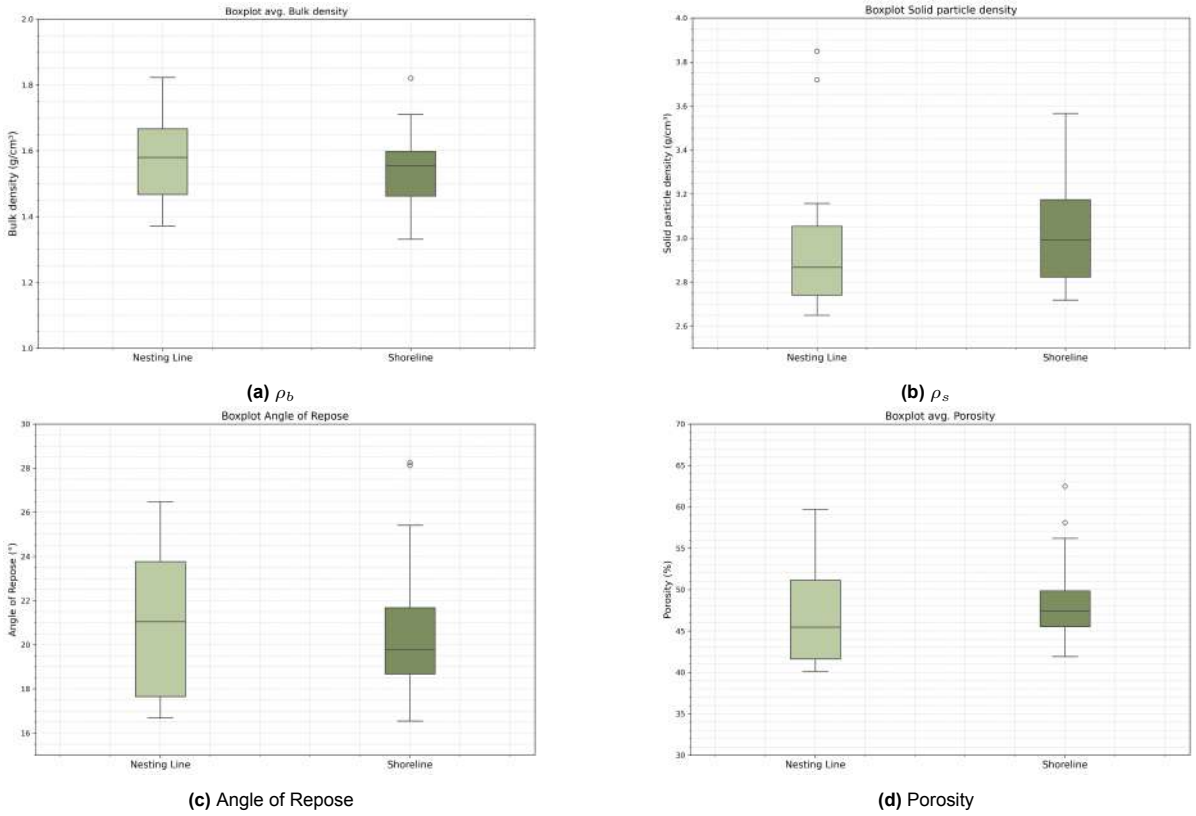

(a) ρ_b **(b)** ρ_s

(c) Angle of Repose **(d)** Porosity

Figure 4.24: Boxplot comparisons between nesting line and shoreline for bulk density ($\rho_{b,avg}$), solid particle density (ρ_s), angle of repose and porosity.

4.3.3. Relationships between latitude and sediment characteristics

Latitude variation influences climate differences across the world, which in turn can affect beach composition. Therefore, the latitudes of the sixteen sea turtle nesting beaches were compared with the key sediment characteristics. Figure 4.25 presents the distribution of D_{50} and $\rho_{b,avg}$ sediment characteristics at the nesting line (x-axis) across latitude (y-axis). No clear trend in all key sediment characteristics along latitude was observed. The remaining key sediment characteristics are shown in Appendix D Figure D.3.

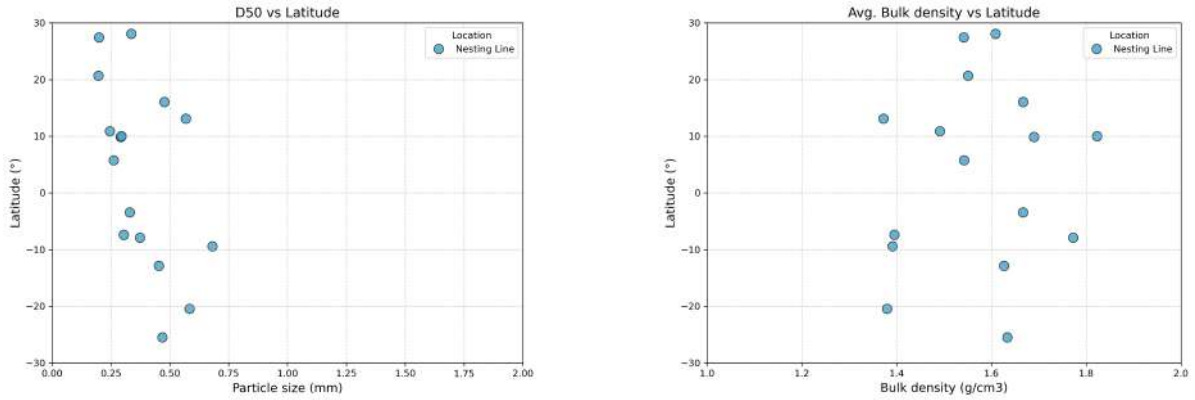

(a) D_{50} **(b)** $\rho_{b,avg}$

Figure 4.25: Distribution of median particle size (D_{50}) and average bulk density ($\rho_{b,avg}$) across latitude at the nesting line. The x-axis displayed the value of a given key sediment characteristic at the nesting line, while the y-axis showed the latitude coordinates.

4.3.4. Relationships between species and key sediment characteristics

Table 3.2 presents the distribution of sea turtle species across different beaches. To analyze the habitat preferences of each species, Table 4.10 summarizes the mean values of key sediment characteristics at the nesting line for each sea turtle species. Additionally, scatterplots were generated for all key sediment characteristics to visualize trends, outliers and potential relationships per species (x-axis). Figure 4.26 presents the scatterplots for D_{50} and $\rho_{b,avg}$, while the remaining scatterplots are provided in Appendix D Figure D.4.

Specie	Beaches*	D_{50} (mm)	Classification	Grading	ψ (-)	R_n (-)	$\rho_{b,avg.}$ (g/cm^3)	ρ_s (g/cm^3)	Angle of Repose (°)	Temperature (°C)	Avg. porosity (%)
CM	11	0.38	Medium sand	Very well sorted	0.89	0.61	1.58	2.93	20.50	22.56	45.83
EI	6	0.36	Medium sand	Very well sorted	0.88	0.60	1.52	2.84	20.26	22.39	46.21
ND	1	0.58	Coarse sand	Very well sorted	0.86	0.59	1.38	2.66	26.48	22.34	48.05
CC	5	0.39	Medium sand	Very well sorted	0.89	0.61	1.62	3.05	22.98	22.66	46.04
DC	3	0.40	Medium sand	Very well sorted	0.89	0.63	1.58	2.88	21.28	22.94	45.23
LO	5	0.33	Medium sand	Very well sorted	0.89	0.62	1.67	3.03	18.99	22.69	44.50
LK	1	0.20	Medium sand	Very well sorted	0.89	0.60	1.54	2.66	17.33	21.56	42.06

Table 4.10: Overview of the average sediment characteristics for each sea turtle species. Wentworth classification was used to classify D_{50}. *Beaches indicate the number of beaches where each sea turtle species nests, based on the analyzed samples.

The CM species nests at most of the key nesting beaches, with a total of eleven sites. In contrast, ND and LK each nest on only one of the analyzed beaches. The scatterplots indicated no distinct preference for any specific sea turtle species, as the data points were evenly distributed across all sediment characteristics.

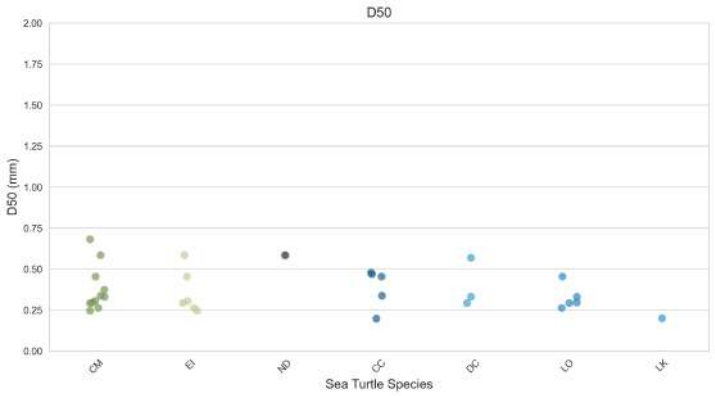

(a) D_{50}

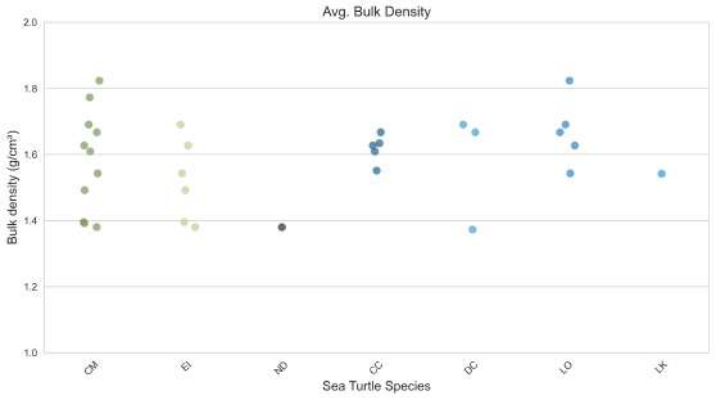

(b) $\rho_{b,avg}$

Figure 4.26: Scatterplots of median particle size (D_{50}) and average bulk density ($\rho_{b,avg}$) per sea turtle species at the nesting line. The x-axis displayed the sea turtle species, while the y-axis showed the value of a given key sediment characteristic at the nesting line.

4.3.5. Comparisons of different methods for particle size and particle density measurements

Dry sieving, DIA (CPA), and SLS (Mastersizer) all provided particle size distributions, while the helium pycnometer and water displacement methods determined solid particle densities.

Particle size distributions

Dry sieving was considered the gold standard, as multiple studies have shown it to be the most accurate method. To quantify the differences between the cumulative distributions, D_{max} was determined by comparing the distributions of DIA and SLS with the sieving distributions (Table 4.11).

Sample code	Location	$D_{max,DIA}$ (%)	$D_{max,SLS}$ (%)
AI/SW/NEB	Nesting line	13.02	44.72
	Shoreline	4.77	52.45
AU/CD/D	Nesting line	6.41	37.26
	Shoreline	4.91	47.00
AU/CD/TB	Nesting line	8.89	49.65
	Shoreline	12.66	50.77
BB/JH/DH	Nesting line	5.42	44.07
	Shoreline	5.58	36.18
BR/DS/BV	Nesting line	6.94	37.42
	Shoreline	17.31	48.50
CA/NE/I	Nesting line	6.05	69.61
	Shoreline	13.01	55.65
CR/DJ/C	Nesting line	9.98	45.90
	Shoreline	7.33	41.57
CR/VB/PO	Nesting line	10.07	45.69
	Shoreline	12.84	54.99
CV/SM/JB	Nesting line	4.68	54.80
	Shoreline	7.32	52.54
FG/NP/Y	Nesting line	10.93	48.83
	Shoreline	4.29	35.74
GA/AF/MB	Nesting line	16.20	44.68
	Shoreline	12.57	48.44
GB/ED/P	Nesting line	9.99	46.80
	Shoreline	9.71	46.70
OM/CT/B1	Nesting line	18.77	44.57
	Shoreline	14.06	62.39
SC/NB/CC	Nesting line	10.89	52.93
	Shoreline	6.66	37.34
US/DG/PI	Nesting line	22.86	43.58
	Shoreline	25.27	45.45
US/TD/AC	Nesting line	10.67	52.90
	Shoreline	11.99	47.08

Table 4.11: Maximum distance (%) between the cumulative particle size distributions of DIA (CPA) and SLS (Mastersizer). Abbreviations: CPA = Computerized Particle Analyzer, DIA = Dynamic Image Analysis, SLS = Static Light Scattering.

It was evident that the D_{max} between the SLS and the sieving distributions was much larger compared to the DIA. The SLS showed a significantly higher D_{max} from the sieving distribution, indicating a greater deviation. In contrast, the DIA distributions were closer to the sieving distributions, suggesting a better agreement between these two methods.

However, D_{max} alone does not fully describe the overall distribution. Therefore, Figures 4.27 (nesting line) and 4.28 (shoreline) provide a visual interpretation of the full distribution for the three methods.

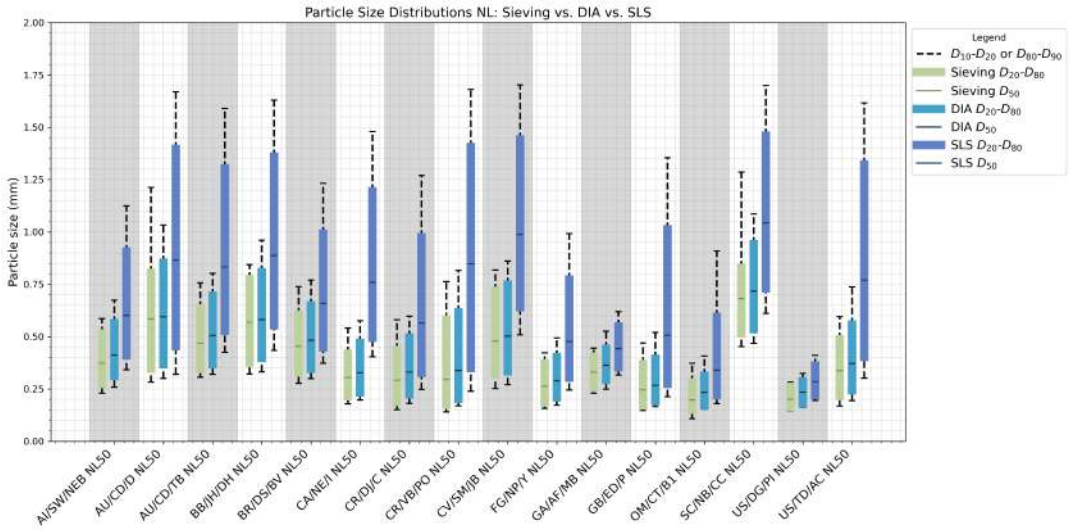

Figure 4.27: Comparison of particle size ranges at the nesting line using sieving, DIA (CPA), and SLS (Mastersizer). Abbreviations: CPA = Computerized Particle Analyzer, DIA = Dynamic Image Analysis, SLS = Static Light Scattering.

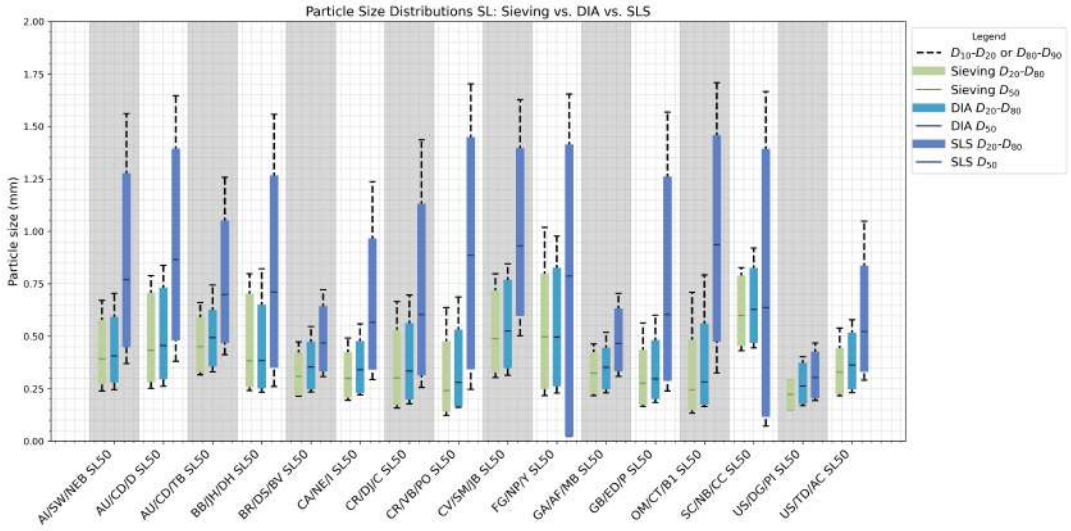

Figure 4.28: Comparison of particle size ranges at the shoreline using sieving, DIA (CPA), and SLS (Mastersizer). Abbreviations: CPA = Computerized Particle Analyzer, DIA = Dynamic Image Analysis, SLS = Static Light Scattering.

For both the nesting- and shoreline, the overall distribution of the DIA was closer to the sieving method than that of the SLS. The SLS distribution deviated substantially. Additionally, the median of the DIA was much closer to the sieving median than the SLS median, further supporting the higher accuracy of DIA in comparison to SLS.

Solid particle densities

The helium gas pycnometer analyzed seven samples from the nesting line. Therefore, the comparison between this method and the volume of water displacement method was based on these seven samples. Table 4.12 presents the solid particle densities obtained from both methods for the same beach.

Beach	Helium ρ_s (g/cm^3)	Vacuum ρ_s (g/cm^3)
AI/SW/NEB	2.96	3.03
AU/CD/D	2.77	2.66
BB/JH/DH	2.78	2.86
CR/DJ/C	2.93	2.94
GA/AF/MB	2.68	2.83
SC/NB/CC	2.79	2.88
US/TD/AC	2.71	2.75

Table 4.12: Solid particle density (ρ_s) differences of helium pycnometer and water displacement methods.

Applying the paired t-test, the analysis yields a p-value of 0.178, indicating that the difference between the helium and water displacement methods was not statistically significant. This means that there was not enough evidence to conclude that the two methods produce different results. The t-statistic was -1.525, suggesting that the values obtained from one method tend to be slightly lower than those from the other. However, this difference was not strong enough to be considered statistically significant. Figure 4.29 illustrates that the water displacement method generally produces higher density values than the helium gas pycnometer.

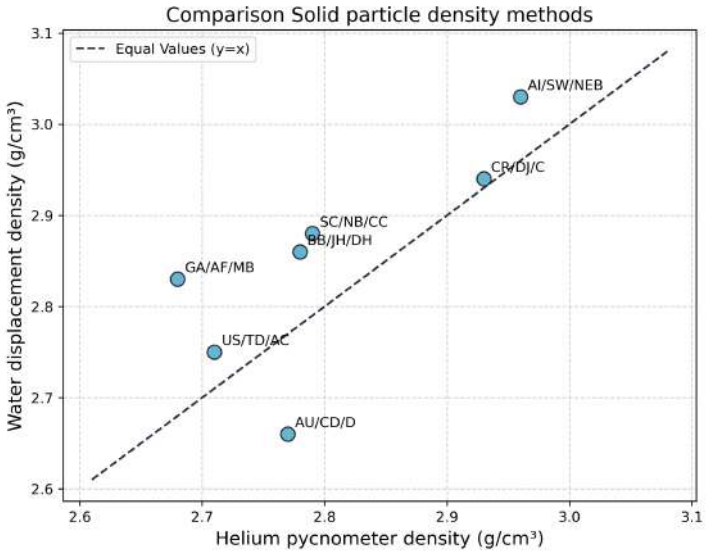

Figure 4.29: Scatterplot comparisons between helium pycnometer and water displacement method for solid particle density (ρ_s).

5

Discussion

This study analyzed key sediment characteristics (color, particle size, particle grading, particle shape, bulk density, solid particle density, angle of repose, thermal retention, and porosity) of sixteen sea turtle nesting beaches worldwide, with samples taken at both the nesting line and the shoreline.

Qualitative analysis classified all samples as well-sorted sand, and as a consequence the quantitative research primarily focused on sand-based methods. The results of the quantitative analyses confirmed that all samples, from both the nesting line and shoreline, consisted of well-sorted, sand-sized particles, predominantly medium sand. The particle shapes indicated moderate roundness and high circularity across all sea turtle nesting beaches. The minimum bulk densities of all samples fell within the typical range for surface mineral soils. However, the maximum bulk densities frequently exceeded this range. The solid particle density of all samples often exceeded 2.75 g/cm^3, suggesting a higher density than the average value for sand (quartz based). The angles of repose for both nesting line and shoreline samples were lower than the general angle of repose for sand, raising concerns about the reliability of this measurement. The thermal retention analysis of nesting line samples showed gradual cooling over time, with temperatures ranging from approximately 21–27°C after one hour. Lastly, the porosity of the sea turtle nesting beaches ranged from approximately 30% to 60%, aligning with typical values for sandy sediments.

No statistical difference were seen between most results of the key sediment characteristics of the nesting line and shoreline. There were only three exceptions, where the maximum distance of the cumulative particle size distributions was above 30%, indicating a slightly difference between these distributions of the nesting line and shoreline. Furthermore, no relationships were found between latitude and the key sediment characteristics. Additionally, observational analysis revealed no clear species-specific sediment preferences across the nesting sites.

PSDs were derived using dry sieving, DIA (CPA), and SLS (Mastersizer). Comparison of D_{max} values revealed that SLS produced greater D_{max} values than DIA, and overall, the SLS distributions were significantly larger than those obtained from DIA. Additionally, the median of the SLS derived PSDs deviated more from the median of the dry sieving results compared to DIA, suggesting greater varia-

tion in SLS measurements. Finally, there was no statistical significant difference between the helium pycnometer and the water displacement method to determine the solid particle density. However, there is a trend to larger solid particle densities by using the water displacement method.

5.1. Sediment characteristics

The literature on sediment characteristics of sea turtle nesting beaches is limited. Some studies have explored the particle size of these beaches, allowing for comparisons between the results of this study and broader trends observed in the literature.

All nesting beaches analyzed in this study consisted of sand-sized particles, aligning with findings from multiple previous studies (Cisneros et al. 2017, Siqueira-Silva et al. 2020, J. Mortimer 1990, Miller et al. 2003, Fadini et al. 2011, Campbell 2019). While it is widely recognized that sea turtles primarily nest in sandy environments, inconsistencies exist in the classification of sand types. This study found that the mean particle size of all sea turtle nesting beaches ranged from 0.195 to 0.651 mm at the nesting line, classifying most samples as medium sand. Additionally, no variation in sorting was found, with all samples classified as very well sorted.

Sediment composition plays a crucial role in sea turtle nesting site selection. For instance, Campbell examined the influence of physical beach characteristics (slope, beach length, sediment type, and anthropogenic impact) on DC turtles, nesting at Armila Beach, Guna Yala (Campbell 2019). The study found that 348 out of 354 nests were located in sandy areas, while only six were in locations containing some gravel. This is consistent with our findings, in which the median particle size of DC nesting beaches ranged from medium to coarse sand. Siqueira-Silve et al. found that nests of LO, CC and EI turtles in Una, Brazil, were composed of fine sand (Siqueira-Silva et al. 2020). However, Fadini et al. found that CC nests in Espírito Santo, Brazil, were primarily located in coarse or medium sand (Fadini et al. 2011). Similarly, Cisneros et al. analyzed sediment characteristics from dune restoration and beach nourishment projects in Palm Beach County, Florida, for CM, CC, and DC nesting beaches, finding that the native sediment consisted of moderately well-sorted medium sand. These findings are consistent with our study, which found that CC, LO and EI turtles preferred well-sorted medium sand (Cisneros et al. 2017). Mortimer concluded that CM turtle nesting beaches exhibited a wide range of sediment types, from moderately fine, well-sorted sand to very poorly sorted coarse sand (J. Mortimer 1990). However, in coarse sand, female sea turtles face difficulties in digging egg chambers, and hatching success is lower. Despite this variability, most of the major CM nesting beaches analyzed by Mortimer consisted of moderately sorted sand with mean particle sizes ranging from 0.2 to 1.0 mm (J. Mortimer 1990). Our study aligns with this particle size range but differs in terms of sorting. Additionally, Zhang et al. examined the microhabitat preferences of CM turtles nesting on North Island, Xisha Islands, to determine which environmental factors influenced nest site selection and hatching success (T. Zhang et al. 2025). They found that sand particle size affected CM turtle nest site selection, with a preference for coarse (0.425–1 mm) and medium (0.250–0.425 mm) sand. This study found that CM turtles nested in medium to coarse sand particles (mean diameter: 0.248–0.651 mm), resembling the findings of Zhang et al. (T. Zhang et al. 2025). Furthermore, Zhang et al. found that aborted nests contained more pebbles and coarser particles than successful nests (T. Zhang et al. 2025), which aligns with findings from Mortimer and Salleh et al. (J. Mortimer 1990 & Salleh et al. 2021). Mortimer also observed a correlation between CM nest numbers and mean particle diameter, suggesting that

CM turtles often create multiple trial nests in coarse sand before finally laying eggs (J. Mortimer 1990). Salleh et al. examined how environmental characteristics impact CM turtle nesting behavior in Malaysia (Salleh et al. 2021). Their study emphasized that sand particle size contributes to nest construction and gas exchange for embryonic development. However, the relative importance of particle size may vary depending on local environmental conditions (Salleh et al. 2021).

Thus, particle size is an important sediment characteristic influencing sea turtle nesting site selection. However, its impact may vary in combination with other sediment characteristics. Overall, it appears that sea turtle species may prefer nesting in moderately to very well-sorted sand, yet differences in sand classification among species are likely minor.

Mortimer categorized sand particle shape from 26 CM turtle nesting beaches worldwide using sphericity and roundness (J. Mortimer 1990). Sphericity was determined using Rittenhouse's chart, which classifies particles from elongated to spherical, while roundness was classified based on Krumbein's scale, ranging from least to most smooth. Their study found that particle shape varied between volcanic and biogenic sands, with similar sphericity values but rounder biogenic sands. Mortimer also noted that most CM turtle nesting beaches were characterized by high-sphericity particles (J. Mortimer 1990). In this study, particle shape was defined using circularity and roundness, which differ in definition from the parameters used by Mortimer (J. Mortimer 1990). The entire dataset in our study showed high circularity, indicating that particle circumferences closely resemble circles of equivalent area, meaning the edges of nesting beach sediments are relatively smooth. Roundness was moderate across all samples, suggesting a moderate resemblance to circular shapes. Due to differences in methodologies, direct comparison with Mortimer is not possible (J. Mortimer 1990). However, our study suggests that sand particles in sea turtle nesting beaches are relatively smooth and moderately rounded.

Bulk density can vary significantly depending on the degree of compaction. For this reason, this study determined both minimum (loose state) and maximum (compact state) bulk densities, representing extreme conditions. However, these measurements do not directly reflect the natural compaction state of sand in the nesting environment. Therefore, the mean bulk density of the samples in this study was used as a guidance. The typical bulk density of sand is approximately 1.65 g/cm^3 (Zeri et al. 2018). Zhang et al. reported that the bulk densities of successful nests ranged from 1.38$\pm$0.06 g/cm^3 (T. Zhang et al. 2025). In the present study, the average bulk density at the nesting line ranged from 1.37 to 1.82 g/cm^3 across all sea turtle species, indicating considerable variation in sand compaction across different nesting beaches globally. While the bulk densities reported by Zhang et al. fall within the range observed in this study, the majority of CM turtle nesting sites analyzed here had denser and more compacted sand (T. Zhang et al. 2025). Notably, four out of the eleven CM turtle nesting beaches examined in this study exceeded the typical bulk density of sand. However, Zhang et al. focused exclusively on sediment characteristics at the Xisha Islands (T. Zhang et al. 2025), whereas this study analyzed nesting beaches on a global scale. This broader geographic scope may explain the wider variation in bulk densities.

Therefore, this study suggests that sea turtles nest across a wide range of bulk densities. However, this study did not determine the bulk density of successful nests for each beach, meaning that no data were available to assess whether higher or lower bulk densities influence nest selection in sea turtles. Nevertheless, multiple studies have found that female sea turtles experience difficulty digging in rough and dry sand, and hatching success tends to be lower on beaches with high bulk density (T. Zhang

et al. 2025 & J. Mortimer 1990). These findings may indicate that high bulk density is not preferred by sea turtles and suggest that bulk density is a key factor in the nesting biology of sea turtles.

The particle density of successful nesting beaches reported by Zhang et al. was 2.35$\pm$0.09 g/cm^3 (T. Zhang et al. 2025), which was significantly lower than the solid particle densities observed in this study. The particle density of Zhang et al. was only based on the Xisha Islands, while the current study analyzed the particle density globally, leading to a wider range (T. Zhang et al. 2025). Particle density depends on the mineral composition of the sand sample. Quartz-based sand typically has a particle density of 2.65 g/cm^3 (Zeri et al. 2018). The samples of the current study often exceeded this value, indicating that the samples may contain minerals with higher densities. The presence of heavy minerals (e.g., magnetite) increases particle density, while the presence of feldspar or quartz results in lower particle densities. Furthermore, the presence of organic matter and calcium carbonate (e.g., from shell fragments) may also affect particle density.

The porosity in this study (40-58%) exhibited a broader range compared to the porosity of successful CM turtle nests reported by Zhang et al., which was 39.86$\pm$2.75% (T. Zhang et al. 2025). However, the majority of porosity values in this study fell within the typical range for sandy soils (30-50%) (Walters 2021).

Although sea turtles nest in a wide range of sand types, hatching success is influenced by the sediment characteristics of nesting beaches (J. Mortimer 1990, T. Zhang et al. 2025, Fadini et al. 2011 & Cisneros et al. 2017). However, there are contradictions regarding how these sediment characteristics impact hatching success, suggesting that variations in beach conditions may lead to different outcomes and that multiple sediment properties may play a role. Zhang et al. examined the effects of microhabitat ecological factors on hatching success and found that it was positively correlated with soil pore water content, particle density, porosity, humidity, and particle size ratio, while it was negatively correlated with soil bulk density (T. Zhang et al. 2025). Their study suggested that larger sand particles provide greater porosity, resulting in better ventilation. In contrast, Mortimer found that hatching success was highest on beaches with the lowest air-filled pore space (J. Mortimer 1990). This finding suggests that higher pore space in the sand could increase water loss from eggs, leading to greater embryo mortality due to desiccation. Their study also indicated that oxygen diffusion through the sand is not a limiting factor for sea turtle embryo development, as sea turtle eggshells have evolved to allow efficient gas exchange, even in low-oxygen and high-carbon dioxide conditions within the nest. The contradictory findings of Zhang et al. and Mortimer may be due to differences in environmental conditions. Zhang et al. examined a more humid location, where higher porosity may not cause egg drying, whereas Mortimer likely conducted research in drier conditions, where increased air-filled pore space could lead to higher water loss.

Mortimer also found that after hatchlings broke out of their eggs and attempted to climb to the surface, mortality was higher in nests with larger sand particles (J. Mortimer 1990). They suggested that coarse sand is unstable and prone to collapse (sand cave-ins), potentially trapping hatchlings inside the nest and making emergence more difficult. This study analyzed the angle of repose of sediment samples and found that it was significantly lower than the typical values reported for sand. A low angle of repose indicates that the sand spreads out easily and does not form a steep slope, making it more unstable. Salleh et al. stated that the angle of repose of coarse sand is generally greater than that of finer sand (Salleh et al. 2021), a trend confirmed in this study, where the correlation matrix of all analyzed

sediment characteristics (Figure 4.22) showed a positive correlation (0.61) between median particle size and angle of repose. Additionally, moisture content also influences the angle of repose, as wet sand tends to have a higher angle (Salleh et al. 2021). Since, no previous studies have specifically examined the angle of repose in relation to sea turtle nesting, the preference of sea turtles to this sediment characteristic remains unclear. Future research is needed to determine whether sand stability affects nesting site selection and hatching success.

Salleh et al. suggested that sand temperature is an important factor in sea turtle nest site selection (Salleh et al. 2021). However, the significance of sand temperature is not consistently supported in previous studies on sea turtles (Salleh et al. 2021). Nevertheless, it is well established that nest temperature plays a crucial role in sea turtle sex determination (Fadini et al. 2011). The pivotal temperature, which is the temperature that produces an equal sex ratio, has been established at 29.2°C (Fadini et al. 2011). Warmer temperatures result in a higher proportion of female hatchlings, while cooler temperatures produce more males (Patrício et al. 2021). Salleh et al. found that CM turtle nests in finer sand were hotter than those in coarser sand, which aligns with findings from CC turtle nests, where smaller sand particles were associated with higher thermal conductivity, leading to increased nest temperatures (Salleh et al. 2021). However, Fadini et al. reported that sea turtle nesting sites with coarse sand have higher temperatures (Fadini et al. 2011). Mineral composition also influence the temperature of sea turtle nesting sites. Sea turtle nest chambers in biogenic sediments (composed partially of mineral particles and organic material) are cooler than those in quartz-rich sediments, as biogenic sediments have lower thermal conductivity (Fadini et al. 2011). Additionally, darker sands tend to absorb more radiation and reach higher temperatures compared to lighter-colored sands. This phenomenon can be explained by Albedo, which describes the fraction of incident solar radiation reflected by a surface (Fadini et al. 2011). This study analyzed the temperature decrease of the sand samples of sea turtle nesting beaches. After 60 minutes, it was observed that samples with relatively high solid particle density (CR/VB/PO, CR/DJ/C, and AI/SW/NEB) retained higher temperatures. This trend was further confirmed by the correlation matrix (Figure 4.22), which showed a positive correlation between solid particle density and temperature.

Differences in solid particle density among the samples can be caused by variations in mineral composition and the presence of organic matter. Carbonate sands, which contain a higher proportion of organic material, tend to have greater porosity due to their naturally porous particles. This results in a unique thermal energy transfer mechanism (He et al. 2022). Because of their high porosity, carbonate sands cool more quickly than denser, mineral-rich sands, which have a greater capacity to retain heat (Suft et al. 2025). The correlation matrix also revealed a negative correlation between porosity and bulk density. This is expected, as more tightly packed particles result in lower porosity and higher bulk density. This difference is also reflected in the two methods used to measure bulk density: the free-fall method, which determines the minimum bulk density under higher porosity (loose state), and the Vibration Table method, which determines the maximum bulk density under lower porosity (compact state). Additionally, a positive correlation was found between particle circularity and bulk density, suggesting that smoother particle boundaries tend to pack more efficiently, leading to lower porosity. This finding aligns with the negative correlation observed between porosity and both circularity and roundness, indicating that smoother and more rounded particles contribute to higher bulk density and lower porosity. Zhang et al. conducted a correlation analysis of ecological factors, including particle

size ratio, bulk density, particle density, and porosity (T. Zhang et al. 2025). They found strong negative correlations between particle size and bulk density, as well as between porosity and bulk density. This finding is consistent with the negative correlations observed in the correlation matrix of this study, although Zhang et al. reported even stronger negative correlations (T. Zhang et al. 2025). Additionally, the positive correlation between porosity and solid particle density observed in this study aligns with the findings of Zhang et al.. However, while Zhang et al. reported a strong positive correlation between porosity and particle size ratio (T. Zhang et al. 2025), this study found no correlation between median particle size and porosity. This inconsistency may be due to differences in the measured parameters, as median particle size is not equivalent to particle size ratio, making direct comparisons challenging.

This study focused on the general differences in sediment characteristics between the nesting line and the shoreline, rather than the local variation per beach. This approach increased the sample size, as analyzing each beach individually would reduce statistical power, making it more difficult to detect significant differences. To investigate local variation between the two environments, future studies would need to include more transects per beach. The key sediment characteristics of the nesting line and shoreline were compared using various statistical tests. The D_{max} between PSDs from dry sieving was applied to assess differences between the two locations. In three beaches (BB/JH/DH, BR/DS/BV, and FG/NP/Y), the nesting line and shoreline showed a D_{max} greater than 30%, suggesting notable differences in PSD. Other sediment characteristics showed no statistical significant differences between the nesting- and shoreline, suggesting that sediment characteristics were largely consistent across the two locations. Based on the findings, this study suggests that large-scale research may initially focus on the nesting line, as no consistent general differences were observed between the two environments.

5.2. Dry sieving, CPA and Mastersizer

In this study, three different particle size analysis techniques were employed: dry sieving, DIA using CPA, and SLS using the Malvern Mastersizer 2000. Each of these approaches has unique benefits and drawbacks that affect the precision, accuracy, and usefulness of particle size measurements.

Sieving is a simple and cost-effective method that requires no calibration or software, but it is time-consuming compared to DIA and SLS. DIA has the advantage of measuring particle shape alongside particle size, while SLS is excellent at detecting very fine particles, including submicron sizes (Agusta and Putri 2023).

Zhang et al. suggested that dry sieving is the gold standard for particle size distributions in sand control applications (K. Zhang et al. 2015). This is consistent with the findings of Sanz, who also recommended sieving for sand-sized particles (Sanz 2018). Since qualitative analyses in this study confirmed that all sediment samples consisted of sand-based particles, the PSDs of DIA and SLS were compared against dry sieving as the reference method.

The results showed that DIA produced PSDs more consistent with sieving than SLS. Several differences between the three methods are evident from the tables and figures. First, the PSDs obtained from SLS deviated substantially, with the median particle size significantly differing from sieving, while DIA deviated only slightly. Furthermore, in this study, the D_{20}, D_{50} and D_{80} values obtained through sieving (Figures 4.27 & 4.28) were lower than those from DIA, suggesting that sieving tends to measure finer particle sizes. Finally, SLS reported a much larger overall particle size range compared to both sieving

and DIA. Since D_{20}, D_{50} and D_{80} values from SLS were consistently higher than those from sieving, it indicates that SLS tends to overestimate particle sizes across the entire distributions, particularly coarser fractions.

Although other significant factors may contribute, differences in measurement methods likely explain part of the observed inconsistencies:

- Sieving uses width-based classification (Ulusoy and Igathinathane 2015), meaning that particles orient themselves to their second-smallest dimension to fit through the sieve openings (K. Zhang et al. 2015). This means elongated particles can still pass through the sieve if their width is small enough, potentially underestimating particle size. PSDs from sieving are mass-based;
- DIA uses length-based classification, defining particle size as the diameter of a circle with the same area as the particle shadow (Ulusoy and Igathinathane 2015). PSDs from DIA are volume-based;
- SLS also uses length-based classification, but it assigns the equivalent diameter of a sphere with the same scattering properties as the particle (K. Zhang et al. 2015). PSDs from SLS are volume-based.

Since the PSDs of sieving are based on width, while those of DIA are based on volume, direct comparisons between their PSDs can be misleading (Ulusoy and Igathinathane 2015). Therefore, Ulusoy et al. applied length-transformation to sieving results, converting width-based data into length-based values to correct for differences in measurement approaches (Ulusoy and Igathinathane 2015). Their results confirmed that PSDs were better aligned after the transformation.

Zhang et al. demonstrated that when a sample contains elongated or irregularly shaped particles, SLS tends to overestimate particle sizes because it assigns an equivalent spherical diameter, which is larger than the true particle width (K. Zhang et al. 2015). Therefore, Zhang et al. suggested that (K. Zhang et al. 2015):

- For elongated particles, sieving will classify particles smaller than SLS;
- For spherical particles, sieving and SLS will produce more similar results.

Since this study found the particle shapes were classified as having moderate roundness and high circularity, it suggests that the particles are slightly irregular or elongated. This could support the observed differences in PSDs between sieving and SLS. Another potential reason for differences between dry sieving and SLS is sample size. Sieving requires a larger sample size, ensuring more representative PSD results. SLS uses only a small fraction of the sediment sample, meaning that if the subsample is not well-mixed, the PSD can differ significantly from sieving (K. Zhang et al. 2015). Additionally, particle aggregation during SLS measurements may cause clumped particles to be interpreted as a large single particle. This could be due to the fact that particles occasionally entered the SLS system in larger chunks, as the hose was sometimes blocked by coarse particles. The presence of air bubbles can further contribute to overestimating particle sizes

Sanz compared SLS with other PSD techniques and found that D_{90} values from SLS were consistently higher than sieving, which aligns with this study (Sanz 2018). Additionally, their research identified a shift toward coarser fractions and underestimation of fine particles. Therefore, she introduced a new protocol to improve PSD accuracy in laser diffraction, which could be useful for future work (Sanz 2018).

These findings emphasize the importance of carefully selecting a method based on sample properties and research objectives. Based on the results of this study, DIA most closely resembles sieving PSDs, and length transformation of sieving data could further improve alignment between the two. Sieving remains the most accurate method for sand-based particles, but since this study aims to analyze roughly 2000 samples, sieving is too time-consuming. Therefore, DIA seems to be a practical alternative for scaling up the analysis. While multiple DIA runs could improve accuracy, this would increase processing time.

5.3. Pycnometer and water displacement method

Accurate determination of solid particle density (ρ_s) is important because it could calculate heat capacity, PSD, and total porosity (Amoozegar et al. 2022). Various methods exist to measure ρ_s, each with advantages and limitations. This study compared two approaches:

1. Water displacement method;
2. Helium gas pycnometry.

The water displacement method determines ρ_s by measuring the volume of water displaced by a known mass of dry sediment. This technique is cost-effective, simple to perform, and does not require professional expertise. However, trapped air within the sample can influence results. In this study, a vacuum was used for 30 minutes to reduce air entrapment, but a longer duration might have further minimized trapped air. This water displacement method was developed based on professional insight rather than a standard protocol. However, Zhang et al. used a similar technique, with the difference that they stirred the sample to remove trapped air, whereas this study used a vacuum chamber (T. Zhang et al. 2025).

The helium gas pycnometer determines ρ_s by measuring solid volume via helium displacement, which penetrates even the finest pores. Amoozegar et al. compared ρ_s measurement measurements using helium, nitrogen, dry air, and water pycnometry, recommending helium as the most reliable method for both fine, medium and coarse soils (Amoozegar et al. 2022). Amoozegar et al. also found that water pycnometry tends to underestimate ρ_s due to air entrapment (Amoozegar et al. 2022). However, in this study, the water displacement method yielded higher ρ_s values than helium gas pycnometry. Despite both methods using water to penetrate pores, they are not identical approaches. Additionally, since helium penetrates finer pores than water, it may have measured a slightly larger volume, resulting in lower ρ_s values compared to water displacement.

The helium gas pycnometer is the more accurate method due to its ability to measure the true solid volume of sediment samples. However, it requires professional expertise and is more costly. Statistical tests showed no significant difference between the two methods, suggesting that the water displacement method is a valid alternative for determining ρ_s. However, this conclusion is based on only seven samples, meaning that further testing with a larger dataset is needed to confirm the reliability of water displacement method.

5.4. Limitations

While this study provides valuable insights into the sediment characteristics of sixteen sea turtle nesting beaches globally, certain limitations must be considered when interpreting the results. These limitations are caused by o.a. sample representativeness and measurement uncertainties

This study was limited to conducting experiences using methods available at TU Delft, Boskalis and Deltares. While numerous other techniques exist for analyzing sediment characteristics, this study was restricted to the methods provided by these three institutions. Furthermore, this study focused on the current status of the sediment without accounting for future changes due to climate change or human activities. In addition, the analyses were limited to the key sediment characteristics: particle size, particle grading, particle shape, bulk density, solid particle density, thermal retention, and porosity. However, sediment characteristics include a broader range of parameters that were not examined in this study. Many other factors besides sediment characteristics also influence the suitability of nesting conditions, including hydrodynamic, atmospheric, geophysical, and human pressures (Christiaanse et al. 2024, Campbell 2019, Siqueira-Silva et al. 2020 & T. Zhang et al. 2025). The influence of these factors was not included in this study.

Methodological consistency is a problem that goes beyond this particular study. Only a few studies have analyzed sediment characteristics of sea turtle nesting beaches, with particle size being the most commonly examined parameter. This study used dry sieving following BS1377-2:1990, whereas other studies, such as Cisneros et al., employed ASTM D422 (Cisneros et al. 2017). Differences in particle size determination methods raise questions about comparability between studies.

Sample representativeness

This study analyzed 32 sediment samples from sixteen sea turtle nesting beaches worldwide. However, a sample size of sixteen beaches may be insufficient to draw definitive conclusions regarding sea turtles preferred sediment characteristics. Given the potential diversity in sediment characteristic across different geographical regions, a larger dataset would provide a more comprehensive understanding of how key sediment characteristics may influence nesting site selection. The limited number of sediment samples also affects the ability to establish definitive correlations between key sediment characteristics. Furthermore, no significant differences could be confirmed between the nesting line and shoreline sediments, nor determine whether latitude variations affect sediment properties. The findings only suggest that there is no consistent general difference between the nesting- and shoreline. A larger dataset would be necessary to validate these findings with higher confidence. Additionally, increasing the number of nesting beaches studied would enhance knowledge of sediment preferences for different sea turtle species. While this study aimed to identify species-specific preferences, the limited number of beaches per species restricted definitive conclusions, leading to the conclusion that there is no preferred sediment characteristics per specie. Notably, no literature was found on the ND turtles, highlighting the need for further research.

The sediment samples were collected from the top layer of the nesting beaches. However, sediment characteristics can vary with depth, meaning that the results may not fully represent conditions across the entire nest site. Deeper layers may exhibit different PSDs and compaction levels, which could influence nest site selection and hatching success. Some previous studies have accounted for sediment depth during sampling (Fadini et al. 2011 & T. Zhang et al. 2025). However, since sea turtles interact

primarily with the top layer of sediment, this study focused on surface characteristics. Nevertheless, while no significant difference was found between nesting line and shoreline sediments, deeper layers may exhibit more stable sediment properties due to reduced exposure to environmental fluctuations.

Measurement uncertainties

This study employed various methods to analyze sediment characteristics, each with its own limitations. The major limitations are outlined below:

- Dry sieving;
  - Ineffective for very fine particles (silt and clay fractions). However, qualitative analysis suggests that only a small fraction of fine particles was present;
  - Irregular or elongated particles may pass through smaller sieve openings, leading to an underestimation of particle size compared to DIA and SLS;
  - Sufficient shaking time is required for particles to orient properly during sieving;
  - Sieves at TU Delft sometimes retained stuck particles, resulting in slightly higher recorded weights when summing mass per sieve compared to the initial sample weight;
  - Sieving provides discrete size classes, whereas DIA and SLS could generate continuous PSD curves with higher resolution;
- DIA:
  - Sensitive to optical conditions, such as overlapping particles, which may lead to incorrect size estimation;
  - Particle orientation affects measurements. For instance, flat, elongated particles may be recorded inconsistently depending on how they pass through the camera;
  - Not yet universally standardized, unlike dry sieving;
  - Particle shape parameters are not universally defined, making comparisons across methods difficult. However, if all samples are analyzed using HAVER CPA 2-1, they remain comparable within this dataset;
- SLS:
  - Overestimates coarse particles due to the assumption of an equivalent spherical diameter, which does not account for irregular or elongated particle shapes;
  - Large particles occasionally clogged the pumping tubes, potentially affecting results;
  - Results depend on the RI and absorption coefficient; incorrect values may lead to misinterpretation of PSD results. Sample color could affects light scattering (absorption), potentially introducing additional uncertainty;
  - Air bubbles can be misidentified as large particles, leading to overestimation of coarse fractions and underestimation of fine particles hidden behind them;
- Water displacement method:
  - Used only a 10 mL measuring cylinder, making it difficult to detect minor volume changes accurately;

  - Prone to human error in reading water levels due to the small scale of measurement;
  - Developed based on expert knowledge, but not standardized by any universal protocol;
  - Producing more accurate results requires a larger measuring cylinder, but this leads to greater sample loss;
  - Showed notable variations in solid particle density at some nesting beaches (e.g., BB/JH/DH and OM/CT/B1) between nesting line and shoreline. While statistical analysis suggests no significant difference, the presence of outliers raises questions about the reliability of the water displacement method.
- Helium gas displacement pycnometer:
  - Requires professional expertise, making it cost-intensive;
- Image-Based Angle of Repose Analysis:
  - Developed based on expert knowledge, but not standardized by any universal protocol;
  - Human error in funnel lifting rate affects how sand flows freely;
  - Angle determination may vary due to human error, particularly in defining measurement points within ImageJ software;
- Thermal Retention Analysis
  - Variability in sediment quantity across samples, despite using the same insulated cup;
  - Sediment composition differences (particle size, porosity, mineralogy) influence heat retention, making direct comparisons difficult;
  - Ambient temperature variations during cooling may introduce inconsistencies in final stabilization temperature;

To improve the comparability between sieving and DIA results, samples could be analyzed multiple times using DIA to obtain more accurate results. Additionally, converting sieving data to length-based PSDs or transforming DIA data to width-based PSDs could help reduce variations between the PSDs. Furthermore, PSDs obtained from SLS could be more comparable if the protocol described by Sanz is followed (Sanz 2018).

The angle of repose measured in this study was significantly lower than the typical values reported for sand. This could be due to complete drying of the sand in the oven, which removed all moisture. Moisture increases cohesion between sand particles, resulting in a higher angle of repose, whereas completely dry sand has minimal cohesion, leading to a much lower angle. Consequently, the true angle of repose in natural conditions is likely higher than what was observed in this study.

The thermal retention analysis in this study is highly limited. While it is well known that sand temperature plays a crucial role in influencing sea turtle sex ratios, this study does not provide insights into thermal conductivity or heat retention in relation to sea turtle nesting beach conditions.

5.5. Coastal management

Analyzing sediment characteristics of the nesting beaches of sea turtles may offer valuable information to develop natural-based coastal protections that support ecological conservation goals. Hard engi-

neering constructions, such as breakwaters and groins, have played an important role in traditional coastal defense (Toimil et al. 2019 & Van Der Meulen et al. 2022). Although these techniques offered safety, they had some significant long-term disadvantages, particularly in dynamic coastal environments where they harmed ecosystems and interfered with natural processes, leading to the loss of biodiversity (Van Der Meulen et al. 2022). These issues encouraged the collaboration between engineers and ecologists to explore more sustainable, nature-based alternatives to reduce flood risk and counteract erosion. Nature-based solutions aim to harness the force of nature for the benefit of society by implying local natural elements and processes within coastal ecosystems (Van Der Meulen et al. 2022).

The effectiveness of a nature-based solution depends on local conditions, which is why a wide range of adapted approaches have been developed to suit different coastal environments (Van Der Meulen et al. 2022). One example is mangrove restoration. The '*Building with Nature Indonesia*' project, for instance, uses semi-permeable dams to trap sediment and enable the regrowth of mangrove forests (Van Der Meulen et al. 2022). Mangroves themselves also contribute to shoreline protection by reducing wave energy (Jordan and Fröhle 2022). In addition, native grass species are used to stabilize sand dunes and promote nature dune formation (Van Der Meulen et al. 2022 & Jordan and Fröhle 2022). Other natural systems such as salt marshes, seagrass beds, and coral/shellfish reefs also help reduce wave energy, thereby decreasing coastline erosion (Van Der Meulen et al. 2022 & Jordan and Fröhle 2022). Finally, sand nourishment is commonly applied along sandy coasts to counteract erosion and maintain beach profiles (Van Der Meulen et al. 2022 & Jordan and Fröhle 2022). A well-known example is the Sand Engine in the Netherlands, a mega-nourishment project where a large volume of sand was placed in one location and allowed to spread naturally along the Dutch coastline over time.

Among the many factor influencing the effectiveness of nature-based solutions, sediment composition plays an important role, especially in nourishment projects. Wijsman et al. investigated the long-term ecological effects of shoreface nourishment, focusing on macrobenthic communities and sediment composition (Jordan and Fröhle 2023). They found that four years after nourishment, the sediment at the nourished site had become significantly coarser while nearby reference areas, where no nourishment took place, retained their native sediment. Furthermore, the macrobenthic community did not recover at the nourishment location, In fact, both specie diversity and density continued to decline in the four years (Jordan and Fröhle 2023). This highlights the sensitivity of macrobenthos to sediment composition and underscores the importance of using sand with particle sizes that closely match the native beach (Jordan and Fröhle 2023). Similarly, Saengsupavanich et al. emphasizes the importance of sediment characteristics in successful nourishment projects (Saengsupavanich et al. 2023). They argue that using local sand sources with sediment characteristics, including particle size, composition and color, that closely resemble the native beach is crucial for successful nourishment (Saengsupavanich et al. 2023). Many nourishment failures are due to nourishment sediments being finer than native sediments (Saengsupavanich et al. 2023). Unfortunately, it is difficult to find a source with sufficient sand quantities for beach nourishment. While using finer sediment may result in quick loss, coarser sediment, can lead to the formation of steeper beach profiles and alter the beach ecosystem, although they are more stable (Climate Adapt 2023).

In summary, the effectiveness of nature-based coastal solutions depends on the careful selection and management of sediment. Choosing sediments that closely resemble the native sediments may en-

hance ecological compatibility and may improve the resilience of coastal ecosystems. Therefore, analyzing the sediment characteristics of sea turtle nesting beaches becomes particularly valuable for informing coastal management strategies that aim to protect both biodiversity and shoreline stability.

6

Conclusion

6.1. Findings

Based on data from sixteen sea turtle nesting beaches, it can be hypothesized that sea turtles prefer nesting sites with well-sorted, sand-sized particles (predominantly medium sand). These sites may also be characterized by particles with moderate roundness and high circularity. The wide variety in average bulk density suggests diverse nesting beach conditions, with some sites exhibit denser, more compacted sands. Similarly, substantial variation in solid particle density across beaches may indicate that sea turtles do not have a specific preference for this sediment characteristic when selecting nesting sites. The wide variation in solid particle density suggests that sea turtles nest both in quartz-rich sand and in sands composed of heavier minerals. The porosity values measured across sites fall within the typical range expected for sandy sediments. In contrast, results for angle of repose and thermal retention did not provide valuable insights regarding sea turtle nesting preferences. These findings serve as hypotheses for global patterns in key sediment characteristics across sixteen globally important sea turtle nesting beaches. However, further research is needed to test these hypotheses across a broader range of sites.

Findings from this study suggest a strong positive correlation between particle circularity and average bulk density, implying that smoother particle boundaries tend to pack more efficiently, leading also to lower porosity. Additional strong positive correlations were observed between solid particle density and porosity, the median particle size and angle of repose and solid particle density and temperature. Moderate negative correlations were revealed between porosity and bulk density, circularity and roundness and between particle size and bulk density.

No general differences in key sediment characteristics between nesting line and shoreline were identified along the 50% transect in this study. Based on the findings, this study suggests that large-scale research may initially focus on the nesting line, as no consistent general differences were observed between the two environments. Furthermore, this study did not reveal any relationships between latitude and the examined sediment characteristics. It is also hypothesized that sea turtle per species do not exhibit clear preferences for specific key sediment characteristics. However, these hypotheses should

be confirmed through future research involving a large number of sampling sites.

The most reliable method to analyze particle size is dry sieving. However, when scaling up the amount of samples, dry sieving is too time consuming. This research demonstrated that DIA seems to be a good alternative for dry sieving. PSDs of DIA slightly differ from the distributions of sieving, particular overestimating the coarse fraction. However, when scaling up to approximately 2000 samples, DIA is considered the more feasible method, as suggested by the findings of this study. Additionally, the most reliable method to analyze solid particle density is using a helium gas pycnometer. However, this method ask professional expertise. The volume of water displacement method is a good alternative method. However, the reliability of this method is questioned because only a few samples were tested to validate this.

Expanding knowledge of sediment characteristics on sea turtle nesting beaches contributes to the development of nature-based solutions in coastal management. Further research is essential to enhance these solutions, ensuring the protection of the nesting beaches. Due to the limited samples and study sites, this research can only propose hypotheses rather than draw definitive conclusions. Therefore, future research should include a broader range of sites.

6.2. Implications for practice

Based on the findings of this pilot study, which analyzed key sediment characteristics at sixteen globally significant sea turtle nesting beaches along the 50% transect, a design plan has been made which outlines the next phase: a large-scale, global analysis of 209 sea turtle nesting beaches. The pilot study provided valuable insights into key sediment characteristics - including color, particle size, particle grading, particle shape, bulk density, solid particle density, angle of repose, thermal retention, and porosity - as well as methods for analyzing these characteristics efficiently. This design plan will continue to focus on these characteristics. The main objective of the extended study will be the development of a comprehensive, globally representative understanding of the key sediment characteristics relevant to sea turtle nesting. By broadening the geographic scope of the samples, this study will aim to identify global patterns, explore potential species-specific preferences and contribute critical data that can inform the development of nature-based coastal solutions.

In the proposed study 209 sediment samples will be analyzed: one sample from each 209 nesting beaches, taken at the nesting line at the 50% transect. By adding all beaches in this expanded analysis, the study will strengthen the global trends across different regions and nesting environments. The methodology of the future study is based on the results and evaluation conducted during the pilot study. A combination of qualitative and quantitative analyzes will be used to examine each sediment sample. The following sediment characteristics were selected for their significance in the context of sea turtle nesting beaches and because of the effectiveness and feasibility of their methods:

- **Color**: An important sediment characteristic for both ecological assessment and potential nature-based coastal solutions. Color will be assessed using the Munsell Color chart.
- **Particle size and grading**: These are really critical factors influencing nesting behavior, egg survival and hatching success, as well as broader coastal processes. For large-scale research, the pilot study recommended DIA, which also provides particle shape measurements.
- **Bulk density**: This can be measured using free-fall & Vibration Table methods to determine

minimum and maximum bulk density values, which can be used to determine the porosity. The bulk density values represent the extremes of compaction within the sediment samples.

- **Solid particle density**: The helium gas pycnometer is the preferred method due to its accuracy. However, this device available at Deltares is outdated and requires professional expertise to operate. As alternative, the water displacement method could be used, but it still requires further refinements to ensure reliability.
- **Porosity**: This will be calculated using values from bulk density and solid particle density measurements.

The other key sediment characteristics may be important for sea turtle nesting, but the methods used in this pilot study were not sufficient to analyze them effectively. Therefore, alternative methods should be explored to analyze these characteristics. Additional recommendations for future studies can be found in Section 6.3. The primary outcome of this study will be the first comprehensive global dataset of sediment characteristics at sea turtle nesting beaches. This dataset will be a valuable resource for researchers, ecologists and coastal engineers. In addition, the knowledge gathered from this study may contribute to the design of nature-based solutions, such as beach nourishment to protect nesting sites for sea turtles.

6.3. Implications for future research

Several recommendations can be made to enhance future research, improve methodological techniques, and refine analytical approaches.

The most important recommendation is to scale up research to include more beaches and test the key sediment characteristics introduced in this pilot study. At least one sample (preferred from 50% transect) at the nesting line of the 209 beaches should be tested to ensure a more comprehensive understanding of global variations in sediment characteristics and their influence on sea turtle nesting preferences. A larger dataset would improve the reliability of findings and support the development of more effective conservation and coastal management strategies. It would also enhance our understanding of whether certain sea turtle species exhibit specific nesting preferences. A proposed design to support this recommendation is provided in Subsection 6.2.

Since sediment characteristics between the nesting line and shoreline showed did not show general statistically significant differences along the 50% transect, future research may prioritize sampling at the nesting line. This approach will optimize time and resources while maintaining relevant data collection. However, as this conclusion is based on only sixteen nesting beaches, further studies should examine whether this pattern holds across a broader range of sites. While such research is valuable, it is not a priority at this stage.

Sediment samples were collected from different transects at each nesting beach. Therefore, future studies could investigate variations between transects within individual beaches, starting, for example, with a comparison between the 10% and 90% transects.

While this study focused on key sediment characteristics — including particle size, grading, shape, bulk density, solid particle density, angle of repose, thermal retention, and porosity — further research on mineral composition and organic matter could provide valuable insights into the interrelationships

between sediment properties and sea turtle nesting preferences.

Although dry sieving remains the most reliable method for analyzing particle size, DIA is a viable alternative for handling large datasets. Future studies should refine DIA calibration to minimize overestimation of the coarse fraction. The accuracy of DIA for large-scale applications could be further improved by comparative research between DIA and sieving across different sediment samples. Additionally, a universal standard protocol should be developed for sediment analysis using DIA.

This study did not provide strong insights into thermal retention and angle of repose at sea turtle nesting beaches. Developing improved methodologies for investigating these key sediment characteristics would be beneficial.

The helium gas pycnometer is the most accurate method for measuring solid particle density but requires specialized expertise. Therefore, the water displacement method should be further validated with a larger sample size to assess its reliability. If this method proves insufficiently accurate, alternative techniques for analyzing solid particle densities should be considered.

Finally, this study generated microscope images using a LEICA digital microscope. Buscombe 2019 introduced SediNet, a deep learning model designed to analyze sediment particle size and shape from optical images, offering both qualitative and quantitative assessments of sediment characteristics. Unfortunately, this deep learning model could not be used in this study due to issues related to updated software packages. However, improving this model and applying it to sediment analysis would be highly beneficial, especially given the availability of high-quality optical images produced in this study.

References

Abu-Hamdeh, N. H. (2003). Thermal properties of soils as affected by density and water content. *Biosystems Engineering*, *86*, 97–102. https://doi.org/10.1016/s1537-5110(03)00112-0

Agusta, V. C., & Putri, M. R. (2023). Grain size trend analysis for sediment characteristic of cirebon waters. *IOP Conference Series: Earth and Environmental Science*, *1163*, 1639–1644. https://doi.org/10.1088/1755-1315/1163/1/012016

Al-Hashemi, H. M. B., & Al-Amoudi, O. S. B. (2018). A review on the angle of repose of granular materials. *Powder Technology*, *330*, 397–417. https://doi.org/10.1016/j.powtec.2018.02.003

Ali, W., Enthoven, D., Kirichek, A., Helmons, R., & Chassagne, C. (2022). Can flocculation reduce the dispersion of deep sea sediment plumes? *TU Delft*.

Amoozegar, A., Heitman, J. L., & Kranz, C. N. (2022). Comparison of soil particle density determined by a gas pycnometer using helium, nitrogen, and air. *Soil Science Society Of America Journal*, *87*, 1–12. https://doi.org/10.1016/j.fuproc.2015.11.007

Barbados.org. (n.d.). *Barbados coastal features*. Retrieved February 24, 2024, from https://barbados.org/barbados-beaches-coastal.htm

Beggs, J. A., Horrocks, J. A., & Krueger, B. H. (2007). Increase in hawksbill sea turtle eretmochelys imbricata nesting in barbados, west indies. *Endangered Species Research*, *3*, 159–168.

Bensharada, M., Telford, R., Stern, B., & Gaffney, V. (2021). Loss on ignition vs. thermogravimetric analysis: A comparative study to determine organic matter and carbonate content in sediments. *Journal Of Paleolimnology*, *67*, 191–197. https://doi.org/10.1007/s10933-021-00209-6

Bosboom, J., & Stive, M. (2023). *Coastal dynamics*. TU Delft Open. https://doi.org/10.5074/T.2021.001

Boskalis Environmental. (n.d.[a]). *Bepaling van de minimale en maximale dichtheid van zand (grond)*.

Boskalis Environmental. (n.d.[b]). *Bepaling van het gehalte aan carbonaat in grond door de volumetrische methode*.

Boskalis Environmental. (n.d.[c]). *Gehalte aan organische stof van grond*.

Boskalis Environmental. (n.d.[d]). *Massaverlies bij zoutzuurbehandeling van grond*.

Buscombe, D. (2019). Sedinet: A configurable deep learning model for mixed qualitative and quantitative optical granulometry. *Soil Science Society Of America Journal*, *43*, 638–651. https://doi.org/10.1002/esp.4760

Campbell, S. (2019). Beach composition preferences for nesting populations of leatherback sea turtles (dermochelys coriacea), armila beach, guna yala comarca. *Independent Study Project (ISP) Collection*, *3112*.

Carter, M. R., & Gregorich, E. G. (2008). *Soil sampling and methods of analysis*. Canadian Society of Soil Science.

Catry, P., Barbosa, C., Indjai, B., Almeida, A., Godley, B. J., & Vié, J. (2002). First census of the green turtle at poilão, bijagós archipelago, guinea-bissau: The most important nesting colony on the atlantic coast of africa. *Oryx*, *36*. https://doi.org/10.1017/s0030605302000765

Chevallier, D., Girondot, M., Péron, C., Martin, J., Bonola, M., Chevalier, J., & Anthony, E. J. (2023). Beach erosion aggravates the drastic decline in marine turtle populations in french guiana. *Regional Environmental Change*, *23*. https://doi.org/10.1007/s10113-023-02105-3

Christiaanse, J. C., Antolínez, J. A. Á., Luijendijk, A., Athanasiou, P., Duarte, C. M., & Aarninkhof, S. (2024). Distribution of global sea turtle nesting explained from regional-scale coastal characteristics. *Scientific Reports*, *14*. https://doi.org/10.1038/s41598-023-50239-5

Chu, J., Varaksin, S., Klotz, U., & Mengé, P. (2009). Construction processes. *International Conference on Soil Mechanics and Geotechnical Engineering*. https://doi.org/10.3233/978-1-60750-031-5-3006

Cisneros, J. A., Briggs, T. R., & Martin, K. (2017). Placed sediment characteristics compared to sea turtle nesting and hatching patterns: A case study from palm beach county, fl. *Shore Beach*, *85*, 35–40.

Clark, P., Shakun, J., Marcott, S., Mix, A., Eby, M., Kulp, S., Levermann, A., Milne, G., Pfister, P., Santer, B., Schrag, D., Solomon, S., Stocker, T., Strauss, B., Weaver, A., Winkelmann, R., Archer, D., Bard, E., Goldner, A., … Plattner, G. (2016). Consequences of twenty-first-century policy for multi-millennial climate and sea-level change. *Nature Climate Change*, *6*, 360–369. https://doi.org/10.1038/nclimate2923

Climate Adapt. (2023). *Beach and shoreface nourishment*. Retrieved March 29, 2025, from https://climate-adapt.eea.europa.eu/en/metadata/adaptation-options/beach-and-shoreface-nourishment

Clyde, W. (2019). *What is a computerized particle analyzer?* Retrieved May 27, 2024, from https://blog.wstyler.com/cpa/what-is-a-computerized-particle-analyzer

Coffey Testing. (2024). *Permeability testing - coffey testing*. Retrieved September 26, 2024, from https://coffeytesting.com.au/soil-permeability-testing/#:~:text=The%20Triaxial%20permeability%20method%20is,to%20measure%20the%20volume%20change.

Ehrhart, L., Redfoot, W., Bagley, D., & Mansfield, K. (2021). Long-term trends in loggerhead (caretta caretta) nesting and reproductive success at an important western atlantic rookery. *Chelonian Conservation And Biology*, *13*, 173–181. https://doi.org/10.2744/ccb-1100.1

Eijkelkamp Soil Water. (n.d.). *Sand ruler / zandliniaal*. Retrieved October 21, 2024, from https://www.royaleijkelkamp.com/media/4ecokegd/manual-08-04-04-sand-ruler.pdf

Encyclopedia Britannica. (n.d.). *Bioclast*. Retrieved May 23, 2024, from https://www.britannica.com/science/bioclast

Fadini, L. S., Silva, A. G., & Ferreira-Júnior, P. D. (2011). Sedimentary characteristics and their effects on hatching success and incubation duration of caretta caretta (testudines: Cheloniidae) in espirito santo, brazil. *Zoologia (Curitiba)*, *28*, 312–320. https://doi.org/10.1590/S1984-46702011000300005

Flint, L. E., & Flint, A. L. (2002). Porosity. *Methods of soil analysis*, 241–254. https://doi.org/10.2136/sssabookser5.4.c11

Fossette, S., Kelle, L., Girondot, M., Goverse, E., Hilterman, M. L., Verhage, B., De Thoisy, B., & Georges, J. (2008). The world's largest leatherback rookeries: A review of conservation-oriented research in french guiana/suriname and gabon. *Journal Of Experimental Marine Biology And Ecology*, *356*, 69–82. https://doi.org/10.1016/j.jembe.2007.12.024

Fossette, S., Loewenthal, G., Peel, L., Vitenbergs, A., Hamel, M., Douglas, C., Tucker, A., Mayer, F., & Whiting, S. (2021). Using aerial photogrammetry to assess stock-wide marine turtle nesting

distribution, abundance and cumulative exposure to industrial activity. *Remote Sens*, *13*, 1116. https://doi.org/10.3390/rs13061116

Fuentes, M. M. P. B., Limpus, C. J., Hamann, M., & Dawson, J. (2010). Potential impacts of projected sea-level rise on sea turtle rookeries. *Aquatic conservation: marine and freshwater ecosystems*, *20*, 132–139. https://doi.org/10.1002/aqc.1088

Girard, A., Godgenger, M. C., Gibudi, A., Fretey, J., Billes, A., Roumet, D., Bal, G., Bréhéret, N., Bitsindou, A., Van Leeuwe, H., Verhage, B., Ricois, S., P., B. J., Carvalho, J., Lima, H., Neto, E., Angoni, H., Ayissi, I., Bebeya, C., … Girondot, M. (2016). Marine turtles nesting activity assessment and trend along the central african atlantic coast for the period of 1999-2008. *International Journal Of Marine Science And Ocean Technology*, *3*.

Godley, B. J., Broderick, A. C., & Hays, G. C. (2001). Nesting of green turtles (chelonia mydas) at ascension island, south atlantic. *Biological Conservation*, *92*, 151–158.

Hall, J., Dawson, R., Sayers, P., Rosu, C., Chatterton, J., & Deakin, R. (2003). A methodology for national-scale flood risk assessment. *Proceedings of the Institution of Civil Engineers. Water, maritime and energy*, 235–248.

Hanson, H., Brampton, A., Capobianco, M., Dette, H., Hamm, L., Laustrup, C., Lechuga, A., & Spanhoff, R. (2002). Beach nourishment projects, practices and objectives—a european overview. *Coastal Engineering*, *47*, 81–111. https://doi.org/10.1016/S0378-3839(02)00122-9

Haver and Boecker. (n.d.). *Digital. time-saving. noise- and dust-free. how you can increase efficiency in your lab.* Retrieved November 6, 2024, from https://www.abmbv.nl/media/files/haver_cpa_21_brochure_en.pdf

He, H., He, Y., Cai, G., Wang, Y., & Zhang, G. (2022). Influence of particle size and packing on the thermal conductivity of carbonate sand. *Granular Matter*, *24*. https://doi.org/10.1007/s10035-022-01277-9

Humboldt Mfg. Co. (n.d.). *Permeability testing of soil*. Retrieved September 26, 2024, from https://www.humboldtmfg.com/permeability.html#:~:text=The%20soil%20sample%20is%20first,reached%20a%20previously%20determined%20level.

Iskander, M., & Li, L. (2024). *Dynamic image analysis of granular materials*. Springer, Cham. https://doi.org/10.1007/978-3-031-47534-4_3

IUCN. (2020). Global standard for nature-based solutions. *A user-friendly framework for the verification, design and scaling up of NbS.*, *'First edition.'* https://doi.org/10.2305/IUCN.CH.2020.08.en

IUCN Red List Of Threatened Species. (n.d.). *The iucn red list of threatened species*. Retrieved May 13, 2024, from https://www.iucnredlist.org/

Jordan, P., & Fröhle, P. (2022). Bridging the gap between coastal engineering and nature conservation? *Journal of Coastal Conservation*, *26*. https://doi.org/10.1007/s11852-021-00848-x

Jordan, P., & Fröhle, P. (2023). Changed sediment composition prevents recovery of macrobenthic community four years after a shoreface nourishment at the holland coast. *Estuarine Coastal And Shelf Science*, *293*. https://doi.org/10.1016/j.ecss.2023.108521

Kalore, S. A., & Babu, G. S. (2023). Significance of cu and cc in evaluating internal stability with application to design of subbase gradation in pavements. *Transportation Geotechnics*, *40*. https://doi.org/10.1016/j.trgeo.2023.100972

Kikukawa, A., Kamezaki, N., & Ota, H. (1999). Factors affecting nesting beach selection by loggerhead turtles (caretta caretta): A multiple regression approach. *Journal of Zoology*, *249*, 447–454.

Kraus, N. (1996). History and heritage of coastal engineering. *American Society of Civil Engineering*. https://doi.org/10.1061/9780784401965

Labmate. (n.d.). *Computerised particle analysis (cpa) for fine sample materials*. Retrieved November 6, 2024, from https://www.labmate-online.com/news/laboratory-products/3/haver-and-boecker/computerised-particle-analysis-cpa-for-fine-sample-materials/16962

Libretexts. (n.d.). *3.6: Mineral formation*. Retrieved September 21, 2024, from https://geo.libretexts.org/Courses/Lumen_Learning/Book%3A_Earth_Science_(Lumen)/03%3A_Minerals/3.06%3A_Mineral_Formation#:~:text=Minerals%20can%20form%20from%20volcanic,fluid%2C%20to%20list%20a%20few.

Łukowiak, M., Cramer, K., Madzia, D., Hynes, M., Norris, R., & O'Dea, A. (2018). Historical change in a caribbean reef sponge community and long-term loss of sponge predators. *Marine Ecology Progress Series*, *601*, 127–137. https://doi.org/10.3354/meps12694

Malvern Panalytical. (n.d.). *Laser diffraction particle size analysis*. Retrieved September 23, 2024, from https://www.malvernpanalytical.com/en/products/technology/light-scattering/laser-diffraction

Mancino, C., Hochscheid, S., & Maiorano, L. (2023). Increase of nesting habitat suitability for green turtles in a warming mediterranean sea. *Scientific Reports*, *13*. https://doi.org/10.1038/s41598-023-46958-4

Marco, A., Abella, E., Liria□Loza, A., Martins, S., López, O., Jiménez□Bordón, S., Medina, M., Oujo, C., Gaona, P., Godley, B. J., & López□Jurado, L. F. (2012). Abundance and exploitation of loggerhead turtles nesting in boa vista island, cape verde: The only substantial rookery in the eastern atlantic. *Animal Conservation*, *15*. https://doi.org/10.1111/j.1469-1795.2012.00547.x

Marcovaldi, M. A., Lopez, G. G., Soares, L. S., Santos, A. J., Bellini, C., & Barata, P. C. (2007). Fifteen years of hawksbill sea turtle (eretmochelys imbricata) nesting in northern brazil. *Chelonian Conservation And Biology*, *6*, 223. https://doi.org/10.2744/1071-8443(2007)6

McGehee, M. A. (1990). Effects of moisture on eggs and hatchlings of loggerhead sea turtles (caretta caretta). *Herpetologica*, 251–258.

Microtrac. (n.d.[a]). *Belpycno I - dichtheidsmeting - gas adsorptie meting*. Retrieved September 25, 2024, from https://www.microtrac.nl/nl/producten/gas-adsorptie-meting/density-measurement/belpycno-I/#:~:text=Gas%20pycnometer%20BELPYCNO%20L&text=De%20pycnometer%20vervangt%20de%20klassieke,poreuze%20materialen%20exact%20worden%20bepaald.

Microtrac. (n.d.[b]). *Dynamic image analysis (dia)*. Retrieved November 6, 2024, from https://www.microtrac.com/products/particle-size-shape-analysis/dynamic-image-analysis/#:~:text=In%20Dynamic%20Image%20Analysis%2C%20a,motion%20during%20the%20image%20acquisition.

Miller, J. D., Limpus, C. J., & Godfrey, M. H. (2003). Nest site selection, oviposition, eggs, development, hatching, and emergence of loggerhead turtles. *Loggerhead sea turtles*, *8*, 125–143.

Mortimer, J. A., Guzman, N. E. A. N., & Hays, G. C. (2020). Estimates of marineturtle nesting populations in the south-west indian ocean indicate the importance of the chagos archipelago. *Oryx*, *54*, 332–343. https://doi.org/10.1017/S0030605319001108

Mortimer, J. (1990). The influence of beach sand characteristics on the nesting behavior and clutch survival of green turtles (chelonia mydas). *Copeia*, *3*, 802–817.

Mrosovsky, N., Ryan, G. D., & James, M. C. (2009). Leatherback turtles: The menace of plastic. *Marine Pollution Bulletin*, *58*, 287–289. https://doi.org/10.1016/j.marpolbul.2008.10.018

Muis, S., Aerts, J. C. J. H., Antolínez, J. A. Á., Dullaart, J. C., Duong, T. M., Erikson, L., Haarsma, R. J., Apecechea, M. I., Mengel, M., Bars, D. L., O'Neill, A., Ranasinghe, R., Roberts, M. J., Verlaan, M., Ward, P. J., & Yan, K. (2023). Global projections of storm surges using high□resolution cmip6 climate models. *Earth's Future*, *11*. https://doi.org/10.1029/2023ef003479

Munsell Color Company. (2017). *How to read a munsell color chart*. Retrieved October 21, 2024, from https://munsell.com/about-munsell-color/how-color-notation-works/how-to-read-color-chart/

Nakashima, H., Shioji, Y., Kobayashi, T., Aoki, S., Shimizu, H., Miyasaka, J., & Ohdoi, K. (2010). Determining the angle of repose of sand under low-gravity conditions using discrete element method. *Journal Of Terramechanics*, *48*, 17–26.

National Geographic. (n.d.[a]). *Green sea turtle*. Retrieved May 13, 2024, from https://www.nationalgeographic.com/animals/reptiles/facts/green-sea-turtle

National Geographic. (n.d.[b]). *Hawksbill turtle*. Retrieved May 13, 2024, from https://www.nationalgeographic.com/animals/reptiles/facts/hawksbill-sea-turtle

National Geographic. (n.d.[c]). *Leatherback sea turtle*. Retrieved May 13, 2024, from https://www.nationalgeographic.com/animals/reptiles/facts/leatherback-sea-turtle

National Geographic. (n.d.[d]). *Loggerhead sea turtle*. Retrieved May 13, 2024, from https://www.nationalgeographic.com/animals/reptiles/facts/loggerhead-sea-turtle

National Geographic. (n.d.[e]). *Olive ridley sea turtle*. Retrieved May 13, 2024, from https://www.nationalgeographic.com/animals/reptiles/facts/olive-ridley-sea-turtle

Nerem, R. S., Beckley, B. D., Fasullo, J. T., Hamlington, B. D., Masters, D., & Mitchum, G. T. (2018). Climate-change–driven accelerated sea-level rise detected in the altimeter era. *Proceedings Of The National Academy Of Sciences*, *115*. https://doi.org/10.1073/pnas.1717312115

Nicholls, R., Brown, S., Goodwin, P., Wahl, T., Lowe, J., Solan, M., Godbold, J., Haigh, I., Lincke, D., Hinkel, J., Wolff, C., & Merkens, J. (2018). Stabilization of global temperature at 1.5°c and 2.0°c: Implications for coastal areas. *Royal Society*. https://doi.org/10.1098/rsta.2016.0448

Nicholls, R., Townend, I., Bardbury, A., Ramsbottom, D., & Day, S. (2013). Planning for long-term coastal change: Experiences from england and wales. *Ocean Engineering*, *71*, 3–16. https://doi.org/10.1016/j.oceaneng.2013.01.025

Oceana. (n.d.[a]). *Flatback turtle*. Retrieved May 13, 2024, from https://oceana.org/marine-life/flatback-turtle/

Oceana. (n.d.[b]). *Kemp's ridley turtle*. Retrieved May 13, 2024, from https://oceana.org/marine-life/kemps-ridley-turtle/

Oceana. (2010). *Why healthy oceans need sea turtles*. Retrieved April 30, 2024, from https://oceana.org/reports/why-healthy-oceans-need-sea-turtles/

Odong, J. (2008). Evaluation of empirical formulae for determination of hydraulic conductivity based on grain-size analysis. *The Journal of American Science*, *4*, 1623–1629.

OLADIPO, V. O., ADEDOYIN, A. D., & ATAT, J. G. (2018). Geostatistical investigation of grain size and heavy minerals of stream sediments from agunjin area, kwara state. *World Journal of Applied Science and Technology*, *10*, 249–257.

Patrício, A. R., Hawkes, L. A., Monsinjon, J. R., Godley, B. J., & Fuentes, M. M. P. B. (2021). Climate change and marine turtles: Recent advances and future directions. *Endangered Species Research*, *44*, 363–395. https://doi.org/10.3354/esr01110

Powers, M. C. (1953). A new roundness scale for sedimentary particles. *journal of sedimentary petrology*, *23*, 117–119.

Preene groundwater consulting. (2014). *Assessing hydraulic conductivity of soils from particle size data*. Retrieved September 26, 2024, from https://www.preene.com/blog/2014/08/assessing-hydraulic-conductivity-of-soils-from-particle-size-data

Pritchard, A., Sanchez, C., Bunbury, N., Burt, A., Currie, J., Doak, N., Fleischer-Dogley, F., Metcalfe, K., Mortimer, J., Richards, H., Van de Crommenacker, J., & Godley, B. (2021). Green turtle population recovery at aldabra atoll continues after 50 yr of protection. *Endangered Species Research*, *47*, 205–215. https://doi.org/10.3354/esr01174

Reinhold, L., & Whiting, A. (2014). High-density loggerhead sea turtle nesting on dirk hartog island, western australia. *Marine Turtle Newsletter*, *141*, 7–10.

Rojas-Cañizales, D., Mejías-Balsalobre, C., Espinoza-Rodríguez, N., Bézy, V. S., Naranjo, I., Arauz, R., & Valverde, R. A. (2022). Corozalito: A nascent arribada nesting beach in costa rica. *Marine Biology*, *169*. https://doi.org/10.1007/s00227-022-04039-6

Saengsupavanich, C., Pranzini, E., Ariffin, E. H., & Yun, L. S. (2023). Jeopardizing the environment with beach nourishment. *The Science Of The Total Environment*, *868*. https://doi.org/10.1016/j.scitotenv.2023.161485

Salleh, S. M., Nishizawa, N., Sah, S. A. M., Chowdhury, A. J. K., & Rusli, M. U. (2021). Sand particle size influences nest site selection of green turtles (chelonia mydas) differently in east and west peninsular malaysia. *Herpetological Conservation and Biology*, *16*, 671–680.

Santos, C. F., Ribeiro, I. C. A., Pelegrino, M. H. P., Carneiro, J. P., & Silva, B. M. (2022). A simple gravimetric methodology to determine soil particle density. *Communications in Soil Science And Plant Analysis*, *53*, 1623–1629. https://doi.org/10.1080/00103624.2022.2063310

Sanz, M. I. (2018). *Flocculation and consolidation of cohesive sediments under the influence of coagulant and flocculant* [Master's thesis, Delft University of Technology]. https://doi.org/https://doi.org/10.4233/uuid:6e96db66-1df0-4ed1-b343-92939d58d864

Shaver, D. J., Rubio, C., Walker, J. S., George, J., Amos, A. F., Reich, K., Jones, C., & Shearer, T. (2016). Kemp's ridley sea turtle (lepidochelys kempii) nesting on the texas coast: Geographic, temporal, and demographic trends through 2014. *Gulf Of Mexico Science*, *33*. https://doi.org/10.18785/goms.3302.04

Siqueira-Silva, I. S., Arantes, M. O., Hackradt, C. W., & Schiavetti, A. (2020). Environmental and anthropogenic factors affecting nesting site selection by sea turtles. *Environmental Research*, *162*. https://doi.org/10.1016/j.marenvres.2020.105090

Slott, J. M., Murray, A. B., Ashton, A. D., & Crowley, T. J. (2006). Coastline responses to changing storm patterns. *Geophysical Research Letters*, *33*. https://doi.org/10.1029/2006GL027445

Suft, O., Hagenauer, H., & Bertermann, D. (2025). Relationship between thermal conductivity, mineral composition and major element composition in rocks from central and south germany. *Geosciences*, *15*. https://doi.org/10.3390/geosciences15010019

Sweijen, T., Hassanizadeh, S. M., Aslannejad, H., & Leszczynski, S. (2019). The effect of particle shape on porosity of swelling granular materials: Discrete element method and the multi-sphere approximation. *Powder Technology*, *360*, 1295–1304. https://doi.org/10.1016/j.powtec.2019.09.036

The Australian Museum. (n.d.). *Mineral properties*. Retrieved September 21, 2024, from https://australian.museum/learn/minerals/properties/

Toimil, A., Losada, I. J., Nicholls, R. J., Dalrymple, R. A., & Stive, M. J. F. (2019). Addressing the challenges of climate change risks and adaptation in coastal areas: A review. *Coastal Enginering*. https://doi.org/10.1016/j.coastaleng.2019.103611

TU Delft. (n.d.). *Soil-water mixture and its phases - dredge pumps and slurry transport*. Retrieved October 21, 2024, from https://ocw.tudelft.nl/course-readings/soil-water-mixture-and-its-phases/

Ulusoy, U., & Igathinathane, C. (2015). Particle size distribution modeling of milled coals by dynamic image analysis and mechanical sieving. *Fuel Processing Technology*, *143*, 100–109. https://doi.org/10.1016/j.fuproc.2015.11.007

Univerzita Karlova. (n.d.). *Pycnometer density and porosimetry*.

U.S National Park Service. (n.d.). *Sediment sorting*. Retrieved November 6, 2024, from https://www.nps.gov/teachers/classrooms/sediment-sorting.htm

Valverde, R. A., Orrego, C. M., Tordoir, M. T., Gómez, F. M., Solís, D. S., Hernández, R. A., Gómez, G. B., Brenes, L. S., Baltodano, J. P., Fonseca, L. G., & Spotila, J. R. (2012). Olive ridley mass nesting ecology and egg harvest at ostional beach, costa rica. *Chelonian Conservation and Biology*, *11*. https://doi.org/10.2744/ccb-0959.1

Van Der Meulen, F., IJff, S., & Van Zetten, R. (2022). Nature□based solutions for coastal adaptation management, concepts and scope, an overview. *Nordic Journal Of Botany*, *1*. https://doi.org/10.1111/njb.03290

Vitousek, S., Barnard, P. L., Fletcher, C. H., Frazer, N., Erikson, L., & Storlazzi, C. D. (2017). Doubling of coastal flooding frequency within decades due to sea-level rise. *Scientific Reports*, *7*. https://doi.org/10.1038/s41598-017-01362-7

Vousdoukas, M. I., Ranasinghe, R., Mentaschi, L., Plomaritis, T. A., Athanasiou, P., Luijendijk, A., & Feyen, L. (2020). Sandy coastlines under threat of erosion. *Nature Climate Change*, *10*, 260–263. https://doi.org/10.1038/s41558-020-0697-0

Walters, R. (2021). Soil particle and bulk density technical note 2. *NCSU Department of Biological and Agricultural Engineering*.

Webb, P. [P.]. (2020). *Introduction to oceanography*. Rebus Community.

Webb, P. [P.A.]. (2001). Volume and density determinations for particle technologists. *Micromeritics Instrument Corp*.

Wentworth, C. K. (1922). A scale of grade and class terms for clastic sediments. *The Journal of Geology*, *30*, 377–392. https://doi.org/https://www.jstor.org/stable/30063207

Willson, A., Witherington, B., Baldwin, R., Tiwari, M., Sariri, T. A., Kiyumi, A. A., Harthi, S. A., Willson, M. S., Bulushi, A. A., Farsi, G. A., Humaidy, J. A., Araimi, J. A., Daar, L. A., Schroeder, B., Ross, J. P., & Possardt, E. (2020). Evaluating the long-term trend and management of a globally important loggerhead population nesting on masirah island, sultanate of oman. *Frontiers in Marine Science*, *7*. https://doi.org/10.3389/fmars.2020.00666

Wood, D. W., & Bjorndal, K. A. (2000). Relation of temperature, moisture, salinity, and slope to nest site selection in loggerhead sea turtles. *Copeia*, *1*, 119–128.

WWF. (2025). *Sea turtle: Green turtle*. https://www.worldwildlife.org/species/green-turtle#:~:text=Why%20They%20Matter&text=Green%20turtles%20graze%20on%20seagrasses,lawn%20to%20keep%20it%20healthy).

Zeri, M., Alvalá, R. C. S., Carneiro, R., Cunha-Zeri, G., Costa, J. M., Spatafora, L. R., Urbano, D., Vall-Llossera, M., & Marengo, J. (2018). Tools for communicating agricultural drought over the brazilian semiarid using the soil moisture index. *Water*, *10*. https://doi.org/10.3390/w10101421

Zhang, K., Chanpura, R. A., Mondal, S., Wu, C., Sharma, M. M., Ayoub, J. A., & Parlar, M. (2015). Particle-size-distribution measurement techniques and their relevance or irrelevance to wire-wrap-standalone-screen selection for gradual-formation-failure conditions. *SPE Drilling Completion*, *30*. https://doi.org/10.2118/168152-PA

Zhang, T., An, X., Zhang, C., Liu, Y., Li, Y., Yu, Y., Wang, J., Lin, L., & Shi, H. (2025). Nest site selection by green sea turtles (chelonia mydas) and implications for conservation on qilianyu, xisha islands, south china sea. *Ecology And Evolution*, *15*. https://doi.org/10.1002/ece3.70841

A

Sediment sample locations

All samples were provided by the University of Exeter in the United Kingdom. The locations of each sample are shown in Figure A.1.

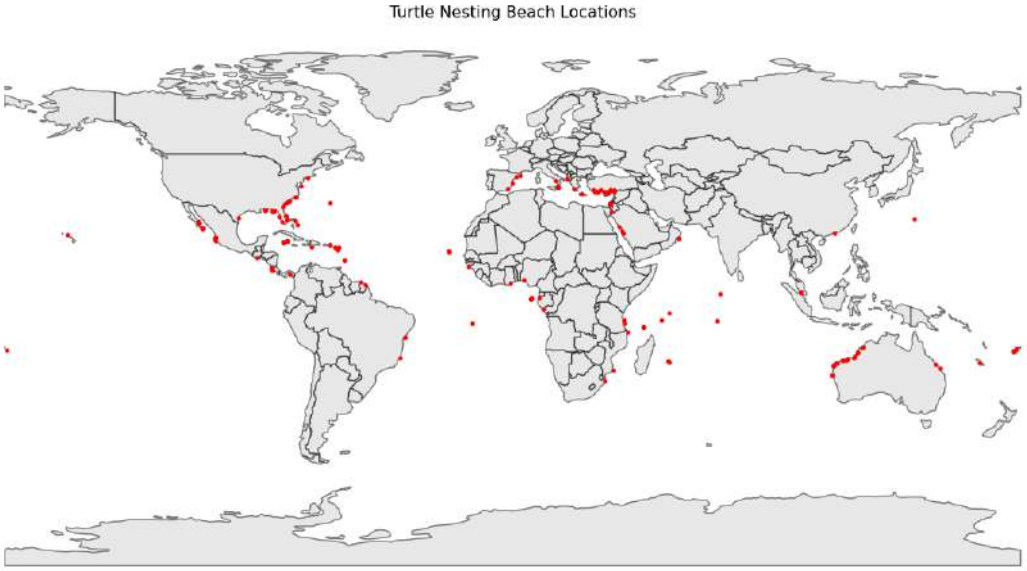

Figure A.1: Locations of the sea turtle nesting beach samples provided by the University of Exeter.

Table A.1 provides a summary of the sixteen selected beaches, highlighting their detailed information on each nesting site.

Sample	Coordinates	Beach type	Key Features / Notes	Source
AI/SW/NEB	7°92' S;14°34' W	Volcanic island	Isolated mid-Atlantic peak; 32 beaches and coves.	Godley et al. 2001
AU/CD/D	20°46' S;117°08' E	Sandy beaches		Fossette, Loewenthal, et al. 2021
AU/CD/TB	25°50' S;112°99' E	Rocky shores		Reinhold and Whiting 2014
BB/JH/DH	13°08' N;59°61' W	Coral-based beaches	Calm, low wave energy; narrow, sloping beach. Windward coast of island has wide, high-energy beaches.	Barbados.org. n.d. & Beggs et al. 2007
BR/DS/BV	12°88' S;38°27' W	Sandy beach	Rocks and coral reefs located close to shore.	Marcovaldi et al. 2007
CA/NE/I	7°40' S;72°47' E	Coral atoll	Main Chagos atoll.	J. A. Mortimer et al. 2020
CR/DJ/C	9°85' N;85°38' E	Sandy beach	7 km protected beach with estuary.	Valverde et al. 2012
CR/VB/PO	9°99' N;85°70' E	Sandy with rocky ends	768 m long beach with rocky outcrops.	Rojas-Cañizales et al. 2022
CV/SM/JB	16°03' N;22°72' W	White sandy beach	High-energy shore; no offshore islands or reefs.	Marco et al. 2012
FG/NP/Y	5°74' N;53°94' W	Long sandy beaches	Mangroves and coastal forest with extensive mudflats.	Fossette, Kelle, et al. 2008
GA/AF/MB	3°45' S;10°66' W	Long sandy beach	Major DC nesting area; Few rocky areas.	Girard et al. 2016
GB/ED/P	10°87' N;15°73' E	Sandy beaches	Major CC turtle nesting area; Rocky subtidal zone.	Catry et al. 2002
OM/CT/B1	20°65' N;58°91' E	Sandy beach		Willson et al. 2020
SC/NB/CC	9°43' S;46°52' E	Coral atoll	Largest raised coral atoll worldwide; 68 turtle nesting beaches.	Pritchard et al. 2021
US/DG/PI	28°04' N;80°55' E	Sandy beach	Protected area with high energy beaches; Largest CC nesting site in Western Hemisphere.	Ehrhart et al. 2021
US/TD/AC	27°42' N;97°30' E	Sandy beach	East side is the Gulf coast; West side boarder high salinity Laguna Madre composed of extensive mudflats.	Shaver et al. 2016

Table A.1: Overview of the sixteen sea turtle nesting sites sampled in this study, including sample codes, geographic coordinates, beach types, key geographical and ecological features, and literature sources.

B

Qualitative analysis

B.1. Macroscopic images nesting Line

AI/SW/NEB NL50 – North East Bay – Ascension Island

Sediment Characteristic	
Color	10YR 5/3
Particle grade	Well sorted
Particle shape	0.49 – 0.70 Low sphericity angular
Particle size (D_{50})	355 – 500 µm

(a) AI/SW/NEB

AU/CD/D NL50 – Australia – Delambre Island

Sediment Characteristic	
Color	10YR 8/3
Particle grade	Well sorted
Particle shape	0.35 – 0.49 Low sphericity angular
Particle size (D_{50})	500 – 710 µm

(b) AU/CD/D

AU/CD/TB NL50 – Australia – Dirk Hartog Island

Sediment Characteristic	
Color	10YR 7/2
Particle grade	Well sorted
Particle shape	0.35 – 0.49 Low sphericity angular
Particle size (D_{50})	500 – 710 µm

(c) AU/CD/TB

BB/JH/DH NL50 – Barbados – Needhams

Sediment Characteristic	
Color	10YR 8/2
Particle grade	Well sorted
Particle shape	0.35 – 0.49 High sphericity angular
Particle size (D_{50})	355 – 500 µm

(d) BB/JH/DH

BR/DS/BV NL50 - Brazil - Busca Vida

Sediment Characteristic	
Color	10YR 7/4
Particle grade	Well sorted
Particle shape	0.17-0.25 High sphericity angular
Particle size (D_{50})	250-355 µm

(e) BR/DS/BV

CA/NE/I NL50 – Chagos – Diego Garcia

Sediment Characteristic	
Color	10YR 7/1
Particle grade	Well sorted
Particle shape	0.35 - 0.49 High sphericity angular
Particle size (D_{50})	250 - 355 µm

(f) CA/NE/I

CR/DJ/C NL50 – Costa Rica – Corozalito

Sediment Characteristic	
Color	2.5YR 5/2
Particle grade	Well sorted
Particle shape	0.49 - 0.70 Low sphericity angular
Particle size (D_{50})	355 - 500 µm

(g) CR/DJ/C

CR/VB/PO NL50 – Costa Rica – Ostional

Sediment Characteristic	
Color	10YR 4/1
Particle grade	Well sorted
Particle shape	0.35 - 0.49 Low sphericity angular
Particle size (D_{50})	355 - 500 µm

(h) CR/VB/PO

CV/SM/JB NL50 – Cabo Verde – Joao Barrosa

Sediment Characteristic	
Color	2.5YR 8/4
Particle grade	Well sorted
Particle shape	0.17 - 0.25 High sphericity angular
Particle size (D_{50})	250 - 355 µm

(i) CV/SM/JB

FG/NP/Y NL50 – French Guiana – Awala-Yalimapo

Sediment Characteristic	
Color	10YR 6/4
Particle grade	Well sorted
Particle shape	0.17-0.25 High sphericity angular
Particle size (D_{50})	250-355 µm

(j) FG/NP/Y

GA/AF/MB NL50 - Gabon - Mayumba

Sediment Characteristic	
Color	10YR 8/3
Particle grade	Well sorted
Particle shape	0.35-0.49 High sphericity angular
Particle size (D_{50})	180-250 µm

(k) GA/AF/MB

GB/ED/P NL50 – Guinea-Bissau – Poilao Island

Sediment Characteristic	
Color	10YR 6/3
Particle grade	Well sorted
Particle shape	0.25 - 0.35 High sphericity angular
Particle size (D_{50})	250-355 µm

(l) GB/ED/P

OM/CT/B1 NL50 – Oman – Masirah Island

Sediment Characteristic	
Color	2.5YR 7/1
Particle grade	Well sorted
Particle shape	0.49 - 0.70 Low sphericity angular
Particle size (D_{50})	250 - 355 µm

(m) OM/CT/B1

SC/NB/CC NL50 – Seychelles – Aldabra Atoll

Sediment Characteristic	
Color	7.5YR 9.5/2
Particle grade	Well sorted
Particle shape	0.49 - 0.70 Low sphericity angular
Particle size (D_{50})	500 – 710 µm

(n) SC/NB/CC

US/TD/AC NL50 – US – Archie Carr

Sediment Characteristic	
Color	2.5YR 7/1
Particle grade	Well sorted
Particle shape	0.17 - 0.25 High sphericity angular
Particle size (D_{50})	250 - 355 µm

(o) US/DG/PI

US/DG/PI NL50 – US – Padre Island

Sediment Characteristic	
Color	2.5YR 7/2
Particle grade	Well sorted
Particle shape	0.35 - 0.49 High sphericity angular
Particle size (D_{50})	180 - 250 µm

(p) US/TD/AC

Figure B.1: Macroscopic images of the sixteen sea turtle nesting lines (qualitative analyses).

B.2. Macroscopic images shoreline

AI/SW/NEB SL50 – North East Bay – Ascension Island

Sediment Characteristic	
Color	10YR 5/3
Particle grade	Well sorted
Particle shape	0.49 - 0.70 Low sphericity angular
Particle size (D_{50})	500 - 710 µm

(a) AI/SW/NEB

AU/CD/D SL50 – Australia – Delambre Island

Sediment Characteristic	
Color	10YR 8/3
Particle grade	Well sorted
Particle shape	0.35 - 0.49 Low sphericity angular
Particle size (D_{50})	500 – 710 µm

(b) AU/CD/D

AU/CD/TB SL50 – Australia – Dirk Hartog Island

Sediment Characteristic	
Color	10YR 7/2
Particle grade	Well sorted
Particle shape	0.35 - 0.49 Low sphericity angular
Particle size (D_{50})	500 - 710 µm

(c) AU/CD/TB

BB/JH/DH SL50 – Barbados – Needhams

Sediment Characteristic	
Color	10YR 8/2
Particle grade	Well sorted
Particle shape	0.35 - 0.49 High sphericity angular
Particle size (D_{50})	250 - 355 µm

(d) BB/JH/DH

BR/DS/BV SL50 - Brazil - Busca Vida

Sediment Characteristic	
Color	10YR 7/4
Particle grade	Well sorted
Particle shape	0.17-0.25 High sphericity angular
Particle size (D_{50})	250-355 µm

(e) BR/DS/BV

CA/NE/I SL50 – Chagos – Diego Garcia

Sediment Characteristic	
Color	10YR 9.5/1
Particle grade	Well sorted
Particle shape	0.49 - 0.70 Low sphericity angular
Particle size (D_{50})	180 – 250 µm

(f) CA/NE/I

CR/DJ/C SL50 – Costa Rica – Corozalito

Sediment Characteristic	
Color	2.5YR 5/2
Particle grade	Well sorted
Particle shape	0.49 - 0.70 Low sphericity angular
Particle size (D_{50})	355 - 500 µm

(g) CR/DJ/C

CR/VB/PO SL50 – Costa Rica – Ostional

Sediment Characteristic	
Color	10YR 4/1
Particle grade	Well sorted
Particle shape	0.35 - 0.49 Low sphericity angular
Particle size (D_{50})	355 - 500 µm

(h) CR/VB/PO

CV/SM/JB SL50 – Cabo Verde – Joao Barrosa

Sediment Characteristic	
Color	2.5YR 8/4
Particle grade	Well sorted
Particle shape	0.17 - 0.25 High sphericity angular
Particle size (D_{50})	250 - 355 µm

(i) CV/SM/JB

FG/NP/Y SL50 – French Guiana – Awala-Yalimapo

Sediment Characteristic	
Color	10YR 6/4
Particle grade	Well sorted
Particle shape	0.17-0.25 High sphericity angular
Particle size (D_{50})	500-710 µm

(j) FG/NP/Y

GA/AF/MB SL50 - Gabon - Mayumba

Sediment Characteristic	
Color	10YR 8/3
Particle grade	Well sorted
Particle shape	0.35-0.49 High sphericity angular
Particle size (D_{50})	180-250 µm

(k) GA/AF/MB

GB/ED/P SL50 – Guinea-Bissau – Poilao Island

Sediment Characteristic	
Color	10YR 6/3
Particle grade	Well sorted
Particle shape	0.25 – 0.35 High sphericity angular
Particle size (D_{50})	355-500 µm

(l) GB/ED/P

OM/CT/B1 SL50 – Oman – Masirah Island

Sediment Characteristic	
Color	2.5YR 7/1
Particle grade	Well sorted
Particle shape	0.49 – 0.70 Low sphericity angular
Particle size (D_{50})	250 – 355 µm

(m) OM/CT/B1

SC/NB/CC SL50 – Seychelles – Aldabra Atoll

Sediment Characteristic	
Color	7.5YR 9.5/2
Particle grade	Well sorted
Particle shape	0.49 – 0.70 Low sphericity angular
Particle size (D_{50})	500 – 710 µm

(n) SC/NB/CC

US/TD/AC SL50 – US – Archie Carr

Sediment Characteristic	
Color	2.5YR 7/1
Particle grade	Well sorted
Particle shape	0.17 – 0.25 High sphericity angular
Particle size (D_{50})	250 – 355 µm

(o) US/DG/PI

US/DG/PI SL50 – US – Padre Island

Sediment Characteristic	
Color	2.5YR 7/2
Particle grade	Well sorted
Particle shape	0.35 – 0.49 High sphericity angular
Particle size (D_{50})	180 – 250 µm

(p) US/TD/AC

Figure B.2: Macroscopic images of the sixteen sea turtle shoreline (qualitative analyses).

C

LEICA digital miscroscope images

C.1. Microscopic images nesting Line

(a) AI/SW/NEB

(b) AU/CD/D

(c) AU/CD/TB

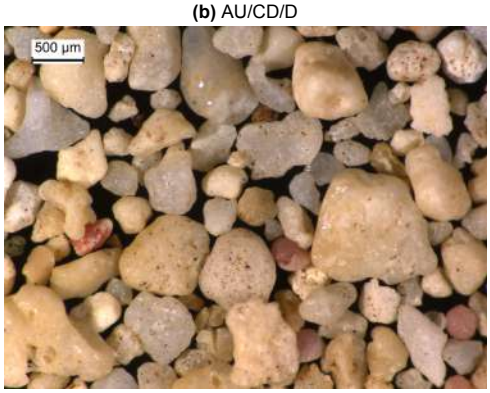

(d) BB/JH/DH

(e) BR/DS/BV

(f) CA/NE/I

(g) CR/DJ/C

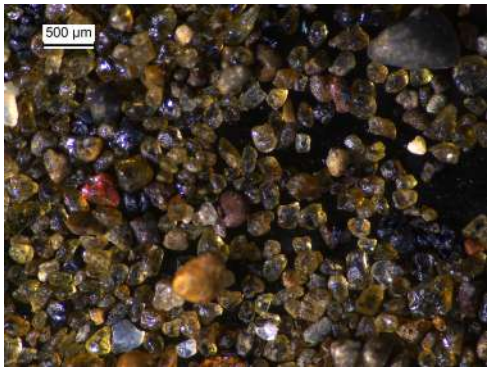

(h) CR/VB/PO

(i) CV/SM/JB

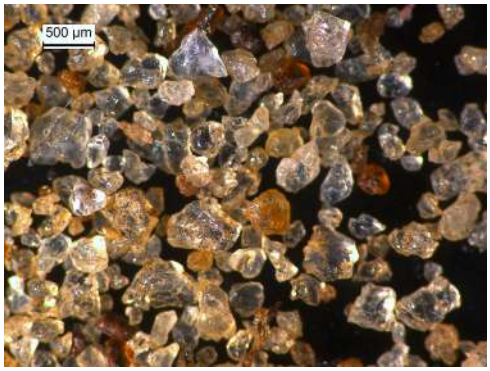

(j) FG/NP/Y

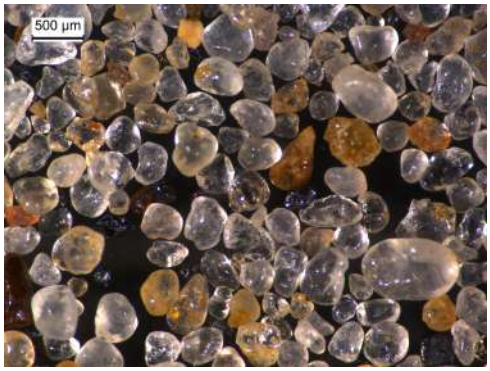

(k) GA/AF/MB

(l) GB/ED/P

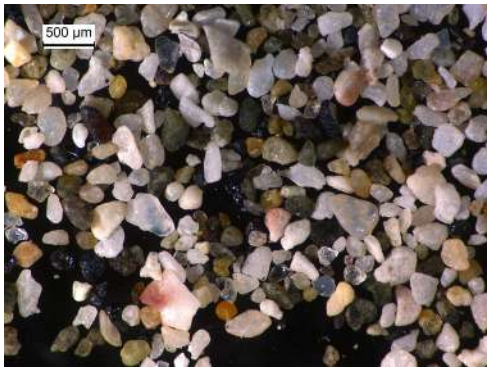

(m) OM/CT/B1

(n) SC/NB/CC

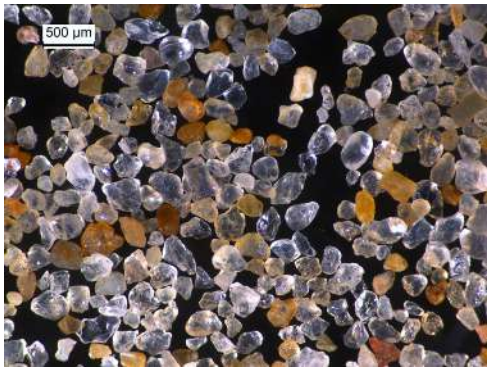

(o) US/DG/PI

(p) US/TD/AC

Figure C.1: LEICA Microscope images of the sixteen sea turtle nesting lines (zoom 4).

C.2. Microscopic images shoreline

(a) AI/SW/NEB

(b) AU/CD/D

(c) AU/CD/TB

(d) BB/JH/DH

(e) BR/DS/BV

(f) CA/NE/I

(g) CR/DJ/C

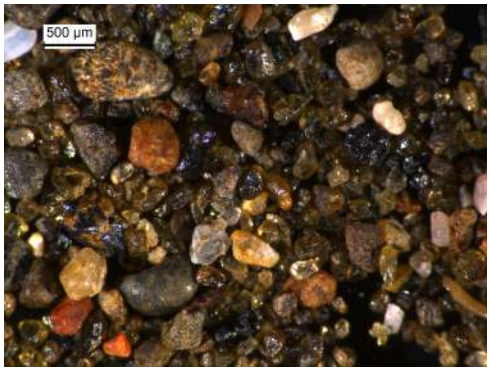

(h) CR/VB/PO

(i) CV/SM/JB

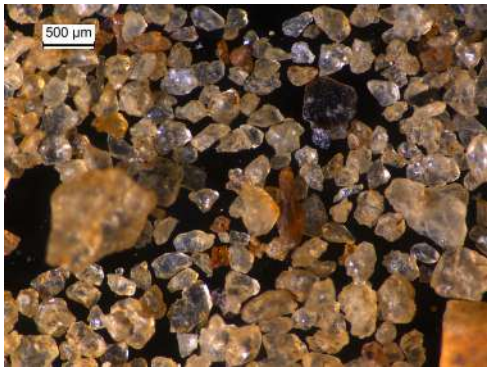

(j) FG/NP/Y

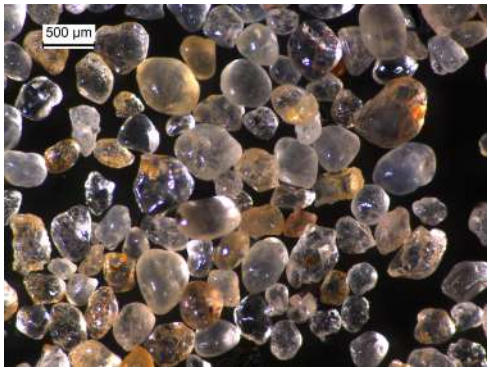

(k) GA/AF/MB

(l) GB/ED/P

(m) OM/CT/B1

(n) SC/NB/CC

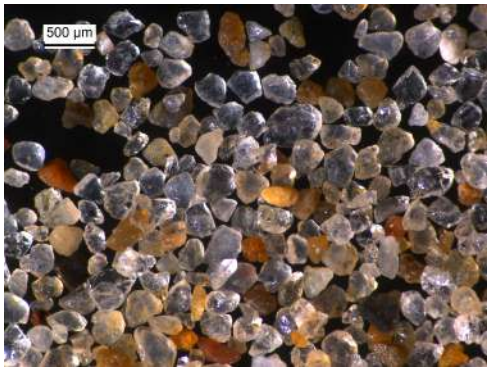

(o) US/DG/PI

(p) US/TD/AC

Figure C.2: LEICA Microscope images of the sixteen sea turtle strand lines (zoom 4).

D

Additional results

D.1. Dry sieving

The statistical particle size distribution parameters from dry sieving were calculated using the Method of Moments by Folk and Ward to provide a more comprehensive statistical description. Table D.1 presents the results for the nesting line and Table D.2 shows the results for the shoreline.

Sample code	M	D_{mean} (mm)	SD	S_r	Characterization S_r	S_k	K	Characterization K
AI/SW/NEB NL50	1.441	0.368	-0.272	-0.545	Very well sorted	-0.003	1.101	Mesokurtic
AU/CD/D NL50	0.898	0.537	-0.345	-0.759	Very well sorted	-0.096	1.085	Mesokurtic
AU/CD/TB NL50	1.099	0.467	-0.263	-0.512	Very well sorted	0.008	0.945	Mesokurtic
BB/JH/DH NL50	0.893	0.539	-0.297	-0.578	Very well sorted	-0.139	0.877	Platykurtic
BR/DS/BV NL50	1.152	0.450	-0.267	-0.537	Very well sorted	-0.035	0.990	Mesokurtic
CA/NE/I NL50	1.728	0.302	-0.295	-0.596	Very well sorted	0.015	1.023	Mesokurtic
CR/DJ/C NL50	1.790	0.289	-0.377	-0.806	Very well sorted	-0.044	1.209	Leptokurtic
CR/VB/PO NL50	1.677	0.313	-0.498	-0.996	Very well sorted	0.071	0.936	Mesokurtic
CV/SM/JB NL50	1.081	0.473	-0.331	-0.657	Very well sorted	-0.030	0.910	Mesokurtic
FG/NP/Y NL50	1.953	0.258	-0.294	-0.635	Very well sorted	-0.045	1.169	Leptokurtic
GA/AF/MB NL50	1.650	0.319	-0.192	-0.385	Very well sorted	-0.037	0.945	Mesokurtic
GB/ED/P NL50	2.011	0.248	-0.321	-0.719	Very well sorted	0.038	1.235	Leptokurtic
OM/CT/B1 NL50	2.356	0.195	-0.293	-0.712	Very well sorted	0.024	1.568	Very leptokurtic
SC/NB/CC NL50	0.620	0.651	-0.202	-0.498	Very well sorted	0.043	1.427	Leptokurtic
US/DG/PI NL50	2.312	0.201	-0.192	-0.441	Very well sorted	-0.113	1.212	Leptokurtic
US/TD/AC NL50	1.627	0.324	-0.355	-0.742	Very well sorted	-0.089	1.193	Leptokurtic

Table D.1: The statistical particle size distribution parameters for the sixteen sea turtle nesting line samples were determined using the dry sieving method (OLADIPO et al. 2018). Abbreviations: M = Graphic mean, D_{mean} = Mean particle size diameter, SD = Standard deviation, S_r = Sorting, S_k = Skewness, K = Kurtosis, mm = Millimeter.

Sample code	M	D_{mean} (mm)	SD	S_r	Characterization S_r	S_k	K	Characterization K
AI/SW/NEB SL50	1.353	0.392	-0.281	-0.560	Very well sorted	0.049	1.021	Mesokurtic
AU/CD/D SL50	1.175	0.443	-0.339	-0.627	Very well sorted	0.041	0.799	Platykurtic
AU/CD/TB SL50	1.176	0.443	-0.205	-0.406	Very well sorted	0.045	0.907	Mesokurtic
BB/JH/DH SL50	1.278	0.412	-0.368	-0.667	Very well sorted	0.237	0.746	Platykurtic
BR/DS/BV SL50	1.707	0.306	-0.218	-0.462	Very well sorted	0.015	1.032	Mesokurtic
CA/NE/I SL50	1.737	0.300	-0.236	-0.501	Very well sorted	0.042	1.030	Mesokurtic
CR/DJ/C SL50	1.694	0.309	-0.413	-0.826	Very well sorted	0.032	1.027	Mesokurtic
CR/VB/PO SL50	1.917	0.265	-0.440	-0.914	Very well sorted	0.174	1.048	Mesokurtic
CV/SM/JB SL50	1.044	0.485	-0.290	-0.556	Very well sorted	-0.029	0.875	Platykurtic
FG/NP/Y SL50	1.124	0.459	-0.430	-0.876	Very well sorted	-0.066	0.929	Platykurtic
GA/AF/MB SL50	1.676	0.313	-0.211	-0.444	Very well sorted	-0.090	1.031	Mesokurtic
GB/ED/P SL50	1.824	0.282	-0.336	-0.666	Very well sorted	0.162	1.003	Mesokurtic
OM/CT/B1 SL50	1.864	0.275	-0.450	-0.939	Very well sorted	0.217	1.160	Leptokurtic
SC/NB/CC SL50	0.745	0.596	-0.198	-0.408	Very well sorted	-0.013	0.972	Mesokurtic
US/DG/PI SL50	2.216	0.215	-0.200	-0.447	Very well sorted	-0.245	1.152	Leptokurtic
US/TD/AC SL50	1.620	0.325	-0.249	-0.511	Very well sorted	0.015	1.054	Mesokurtic

Table D.2: The statistical particle size distribution parameters for the sixteen sea turtle shoreline samples were determined using the dry sieving method (OLADIPO et al. 2018). Abbreviations: M = Graphic mean, D_{mean} = Mean particle size diameter, SD = Standard deviation, S_r = Sorting, S_k = Skewness, K = Kurtosis, mm = Millimeter.

D.2. DIA by CPA

The statistical particle size distribution parameters from DIA were calculated using the Method of Moments by Folk and Ward to provide a more comprehensive statistical description. Table D.3 presents the results for the nesting line and Table D.4 shows the results for the shoreline.

Sample code	M	D_{mean} (mm)	SD	S_r	Characterization S_r	S_k	K	Characterization K
AI/SW/NEB NL50	1.275	0.413	-0.245	-0.516	Very well sorted	0.037	1.031	Mesokurtic
AU/CD/D NL50	0.817	0.568	-0.361	-0.690	Very well sorted	-0.147	0.881	Platykurtic
AU/CD/TB NL50	1.002	0.499	-0.270	-0.516	Very well sorted	0.013	0.929	Mesokurtic
BB/JH/DH NL50	0.831	0.562	-0.297	-0.579	Very well sorted	-0.076	0.933	Mesokurtic
BR/DS/BV NL50	1.079	0.473	-0.271	-0.537	Very well sorted	-0.058	1.011	Mesokurtic
CA/NE/I NL50	1.599	0.330	-0.299	-0.615	Very well sorted	0.076	1.087	Mesokurtic
CR/DJ/C NL50	1.595	0.331	-0.334	-0.679	Very well sorted	0.050	1.046	Mesokurtic
CR/VB/PO NL50	1.515	0.350	-0.469	-0.890	Very well sorted	0.150	0.867	Platykurtic
CV/SM/JB NL50	1.018	0.494	-0.333	-0.662	Very well sorted	-0.026	0.935	Mesokurtic
FG/NP/Y NL50	1.813	0.285	-0.278	-0.565	Very well sorted	0.010	1.014	Mesokurtic
GA/AF/MB NL50	1.483	0.358	-0.196	-0.398	Very well sorted	-0.008	1.227	Leptokurtic
GB/ED/P NL50	1.892	0.269	-0.304	-0.624	Very well sorted	0.169	1.056	Mesokurtic
OM/CT/B1 NL50	2.087	0.235	-0.270	-0.623	Very well sorted	0.074	1.381	Leptokurtic
SC/NB/CC NL50	0.505	0.704	-0.244	-0.459	Very well sorted	-0.009	0.948	Mesokurtic
US/DG/PI NL50	2.143	0.226	-0.194	-0.389	Very well sorted	-0.041	0.958	Mesokurtic
US/TD/AC NL50	1.460	0.363	-0.351	-0.735	Very well sorted	0.034	1.095	Mesokurtic

Table D.3: The statistical particle size distribution parameters for the sixteen sea turtle nesting line samples were determined using Dynamic Image Analysis by a Computerized Particle Analyzer (OLADIPO et al. 2018). Abbreviations: M = Graphic mean, D_{mean} = Mean particle size diameter, SD = Standard deviation, S_r = Sorting, S_k = Skewness, K = Kurtosis, mm = Millimeter.

Sample code	M	D_{mean} (mm)	SD	S_r	Characterization S_r	S_k	K	Characterization K
AI/SW/NEB SL50	1.307	0.404	-0.278	-0.562	Very well sorted	0.029	1.001	Mesokurtic
AU/CD/D SL50	1.103	0.465	-0.335	-0.660	Very well sorted	0.092	0.925	Mesokurtic
AU/CD/TB SL50	1.054	0.482	-0.223	-0.435	Very well sorted	-0.001	1.023	Mesokurtic
BB/JH/DH SL50	1.302	0.406	-0.365	-0.698	Very well sorted	0.228	0.946	Mesokurtic
BR/DS/BV SL50	1.522	0.348	-0.237	-0.456	Very well sorted	0.028	1.036	Mesokurtic
CA/NE/I SL50	1.564	0.338	-0.265	-0.530	Very well sorted	0.063	1.047	Mesokurtic
CR/DJ/C SL50	1.567	0.338	-0.381	-0.741	Very well sorted	0.075	0.917	Mesokurtic
CR/VB/PO SL50	1.739	0.300	-0.422	-0.798	Very well sorted	0.228	0.862	Platykurtic
CV/SM/JB SL50	0.953	0.516	-0.298	-0.593	Very well sorted	-0.001	0.965	Mesokurtic
FG/NP/Y SL50	1.077	0.474	-0.432	-0.805	Very well sorted	-0.078	0.793	Platykurtic
GA/AF/MB SL50	1.554	0.340	-0.219	-0.437	Very well sorted	-0.066	1.113	Mesokurtic
GB/ED/P SL50	1.663	0.316	-0.323	-0.663	Very well sorted	0.218	1.098	Mesokurtic
OM/CT/B1 SL50	1.671	0.314	-0.443	-0.867	Very well sorted	0.321	1.030	Mesokurtic
SC/NB/CC SL50	0.687	0.621	-0.207	-0.415	Very well sorted	0.032	0.923	Mesokurtic
US/DG/PI SL50	1.944	0.260	-0.250	-0.478	Very well sorted	0.011	0.998	Mesokurtic
US/TD/AC SL50	1.475	0.360	-0.266	-0.525	Very well sorted	0.078	1.047	Mesokurtic

Table D.4: The statistical particle size distribution parameters for the sixteen sea turtle shoreline samples were determined using Dynamic Image Analysis by a Computerized Particle Analyzer (OLADIPO et al. 2018). Abbreviations: M = Graphic mean, D_{mean} = Mean particle size diameter, SD = Standard deviation, S_r = Sorting, S_k = Skewness, K = Kurtosis, mm = Millimeter.

D.3. SLS by MasterSizer2000

The statistical particle size distribution parameters from SLS were calculated using the Method of Moments by Folk and Ward to provide a more comprehensive statistical description. Table D.5 presents the results for the nesting line and Table D.6 shows the results for the shoreline.

Sample code	M	D_{mean} (mm)	SD	S_r	Characterization S_r	S_k	K	Characterization K
AI/SW/NEB NL50	0.721	0.607	-0.336	-0.667	Very well sorted	0.054	0.978	Mesokurtic
AU/CD/D NL50	0.316	0.803	-0.474	-0.926	Very well sorted	-0.208	0.933	Mesokurtic
AU/CD/TB NL50	0.271	0.829	-0.380	-0.733	Very well sorted	-0.025	0.901	Mesokurtic
BB/JH/DH NL50	0.208	0.866	-0.379	-0.735	Very well sorted	-0.083	0.923	Mesokurtic
BR/DS/BV NL50	0.587	0.666	-0.337	-0.666	Very well sorted	0.049	0.968	Mesokurtic
CA/NE/I NL50	0.386	0.765	-0.372	-0.722	Very well sorted	0.026	0.924	Mesokurtic
CR/DJ/C NL50	0.829	0.563	-0.465	-0.911	Very well sorted	-0.008	0.949	Mesokurtic
CR/VB/PO NL50	0.460	0.727	-0.579	-1.084	Very well sorted	-0.296	0.839	Platykurtic
CV/SM/JB NL50	0.054	0.963	-0.345	-0.672	Very well sorted	-0.101	0.932	Mesokurtic
FG/NP/Y NL50	1.052	0.482	-0.395	-0.780	Very well sorted	0.047	0.962	Mesokurtic
GA/AF/MB NL50	1.181	0.441	-0.191	-0.380	Very well sorted	-0.001	0.992	Mesokurtic
GB/ED/P NL50	0.939	0.522	-0.543	-1.028	Very well sorted	0.060	0.852	Platykurtic
OM/CT/B1 NL50	1.471	0.361	-0.434	-0.891	Very well sorted	0.207	1.094	Mesokurtic
SC/NB/CC NL50	-0.046	1.032	-0.295	-0.570	Very well sorted	-0.049	0.915	Mesokurtic
US/DG/PI NL50	1.817	0.284	-0.210	-0.417	Very well sorted	-0.005	0.965	Mesokurtic
US/TD/AC NL50	0.445	0.735	-0.493	-0.934	Very well sorted	-0.118	0.848	Mesokurtic

Table D.5: The statistical particle size distribution parameters for the sixteen sea turtle nesting line samples were determined using Statistic Light Scattering by the MasterSizer2000 (OLADIPO et al. 2018). Abbreviations: M = Graphic mean, D_{mean} = Mean particle size diameter, SD = Standard deviation, S_r = Sorting, S_k = Skewness, K = Kurtosis, mm = Millimeter.

Sample code	M	D_{mean} (mm)	SD	S_r	Characterization S_r	S_k	K	Characterization K
AI/SW/NEB SL50	0.385	0.766	-0.417	-0.800	Very well sorted	-0.021	0.890	Platykurtic
AU/CD/D SL50	0.268	0.830	-0.425	-0.815	Very well sorted	-0.120	0.894	Platykurtic
AU/CD/TB SL50	0.502	0.706	-0.316	-0.623	Very well sorted	0.056	0.961	Mesokurtic
BB/JH/DH SL50	0.555	0.681	-0.511	-1.024	Very well sorted	-0.150	0.971	Mesokurtic
BR/DS/BV SL50	1.092	0.469	-0.244	-0.479	Very well sorted	0.021	0.957	Mesokurtic
CA/NE/I SL50	0.782	0.582	-0.410	-0.801	Very well sorted	0.083	0.940	Mesokurtic
CR/DJ/C SL50	0.721	0.607	-0.503	-0.958	Very well sorted	0.006	0.871	Platykurtic
CR/VB/PO SL50	0.418	0.749	-0.573	-1.072	Very well sorted	-0.321	0.849	Platykurtic
CV/SM/JB SL50	0.123	0.918	-0.338	-0.655	Very well sorted	-0.051	0.916	Mesokurtic
FG/NP/Y SL50	1.533	0.346	-1.348	-2.565	Very well sorted	-0.675	0.705	Platykurtic
GA/AF/MB SL50	1.106	0.465	-0.233	-0.459	Very well sorted	0.004	0.958	Mesokurtic
GB/ED/P SL50	0.710	0.611	-0.569	-1.050	Very well sorted	0.014	0.766	Platykurtic
OM/CT/B1 SL50	0.236	0.849	-0.462	-0.914	Very well sorted	-0.270	1.000	Mesokurtic
SC/NB/CC SL50	1.093	0.469	-0.938	-1.742	Very well sorted	-0.382	0.757	Platykurtic
US/DG/PI SL50	1.725	0.302	-0.250	-0.493	Very well sorted	-0.016	0.959	Mesokurtic
US/TD/AC SL50	0.907	0.533	-0.361	-0.716	Very well sorted	0.085	0.980	Mesokurtic

Table D.6: Statistical particle size distribution parameters of the sixteen sea turtle strand line samples were determined using Statistic Light Scattering by the MasterSizer2000 (OLADIPO et al. 2018). Abbreviations: M = Graphic mean, D_{mean} = Mean particle size diameter, SD = Standard deviation, S_r = Sorting, S_k = Skewness, K = Kurtosis, mm = Millimeter.

D.4. Scatterplots of sediment characteristics between NL and SL

This section of the appendix includes the complete set of scatterplots comparing additional key sediment characteristics at the nesting line and shoreline for each sampled beach. These plots show a more complete overview of the data.

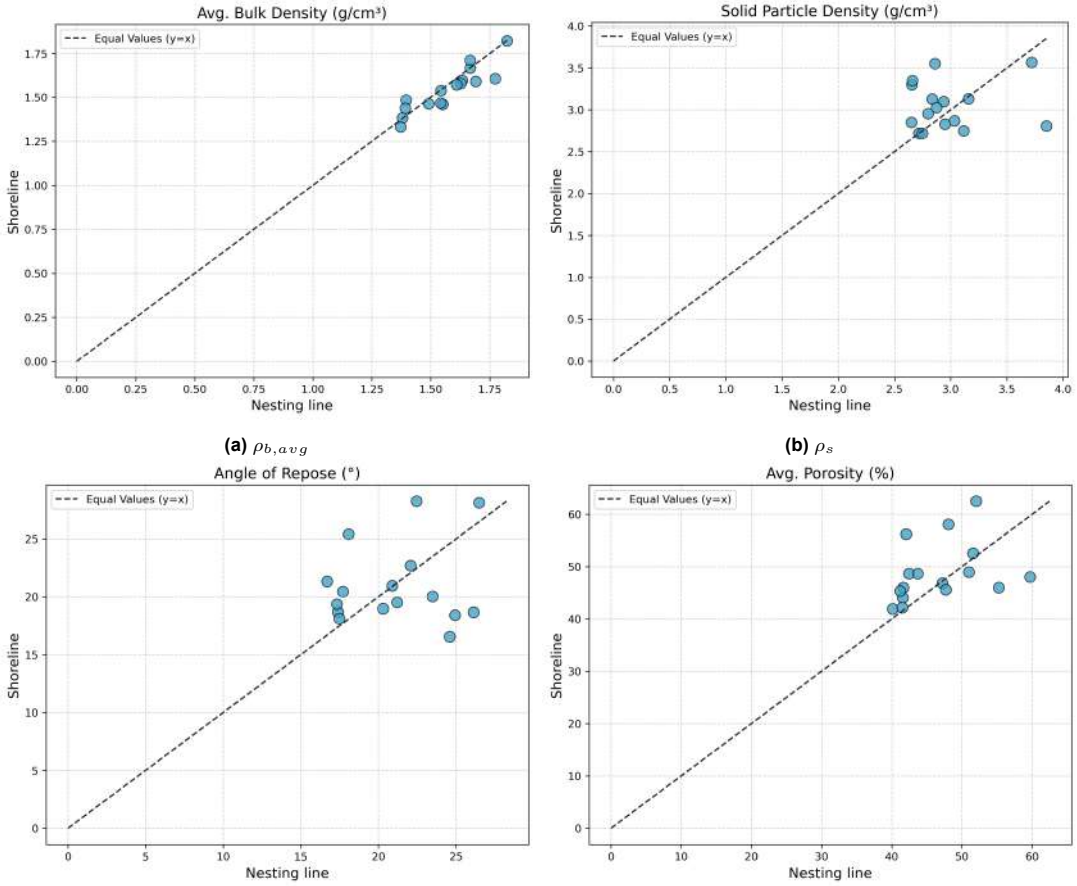

(a) $\rho_{b,avg}$

(b) ρ_s

(c) Angle of repose

(d) Porosity

Figure D.1: Scatterplot comparisons between nesting line and shoreline for average bulk density ($\rho_{b,avg}$), solid particle density (ρ_s), angle of repose and porosity. The x-axis displayed the value of a given key sediment characteristic at the nesting line, while the y-axis showed the same key characteristic at the shoreline. A dashed line was included as a reference line indicating equal values between the two locations.

D.5. Boxplots of sediment characteristics between NL and SL

This section of the appendix includes the complete set of boxplots comparing additional key sediment characteristics at the nesting line and shoreline for each sampled beach. These plots show a more complete overview of the data.

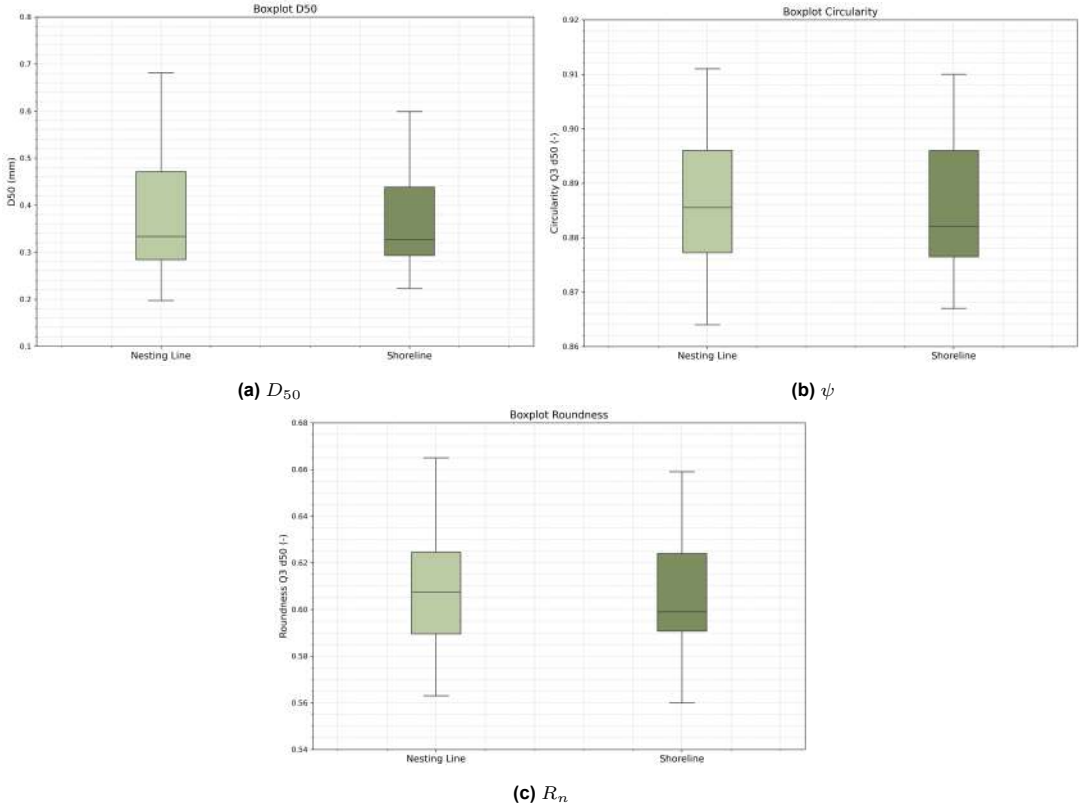

(a) D_{50} **(b)** ψ

(c) R_n

Figure D.2: Boxplot comparisons between nesting line and shoreline for median particle diameter (D_{50}), circularity (ψ) and roundness (R_n).

D.6. Relationships between latitude and sediment characteristics

This section of the appendix presents additional scatterplots exploring the relationships between the remaining key sediment characteristics and latitude at the nesting line. These plots provide a more comprehensive overview of the data and support further visual interpretation of potential geographic patterns.

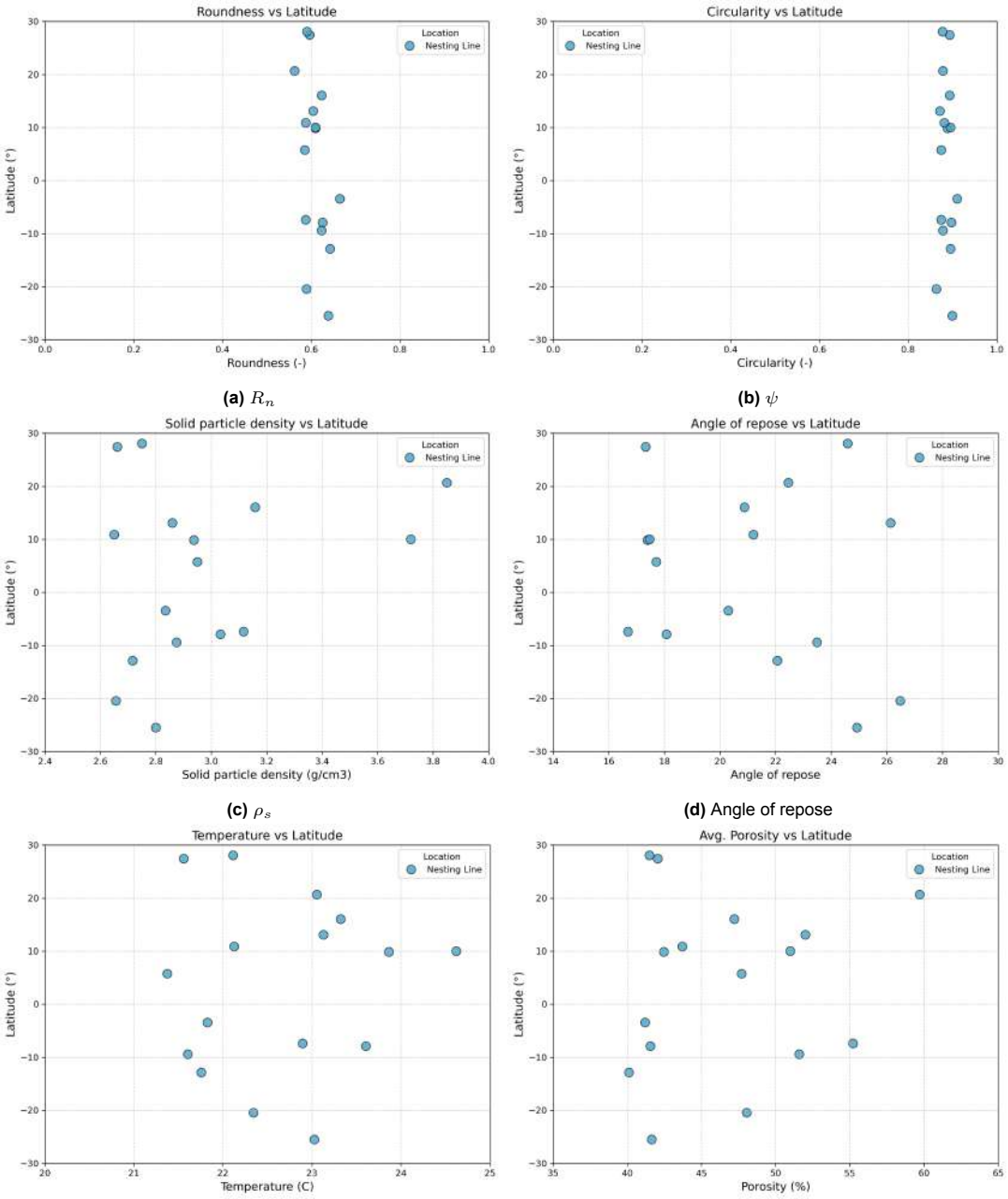

(a) R_n

(b) ψ

(c) ρ_s

(d) Angle of repose

(e) Thermal retention after 60 min.

(f) Avg. porosity

Figure D.3: Distribution of roundness (R_n), circularity (ψ), solid particle density (ρ_s), angle of repose, thermal retention after 60 minutes and average porosity across latitude at the nesting line.

D.7. Sediment characteristics by sea turtle pecies

This section of the appendix presents the remaining key sediment characteristics at the nesting line grouped by sea turtle species, allowing for visual comparison of sediment properties across different species.

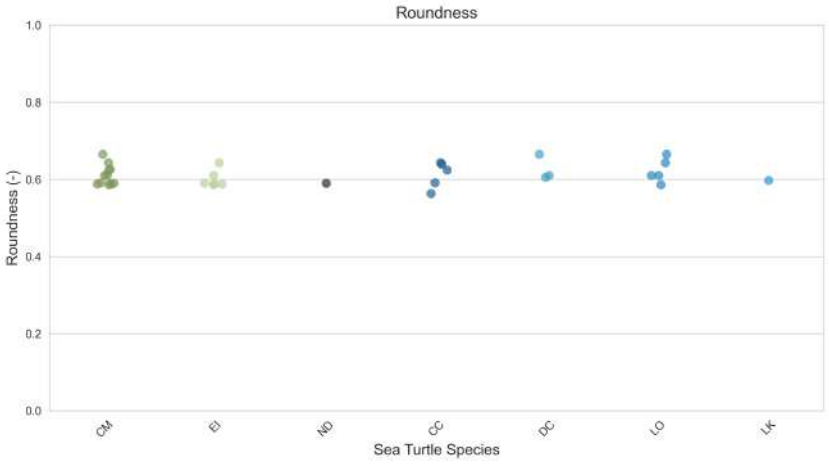

(a) R_n

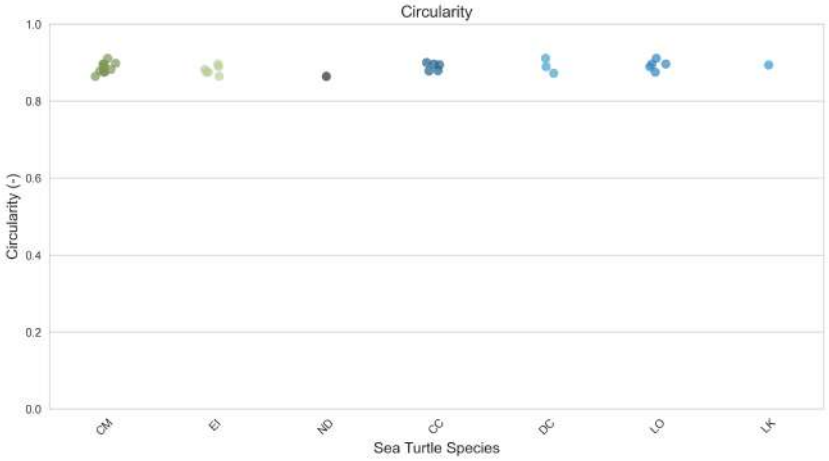

(b) ψ

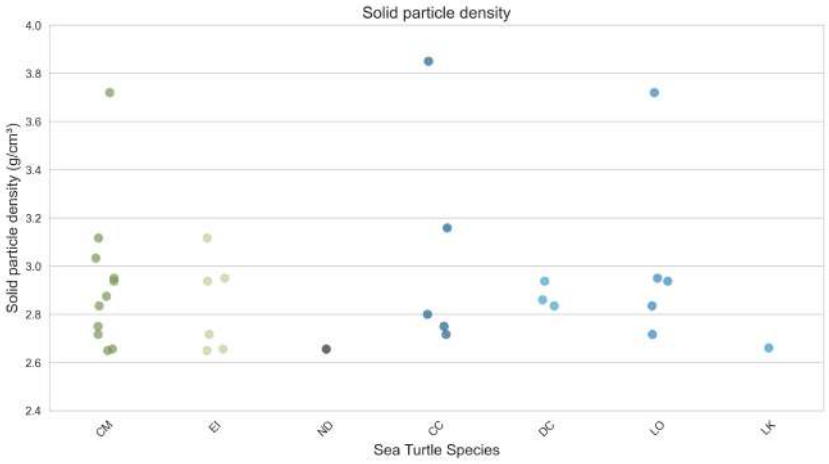

(c) ρ_s

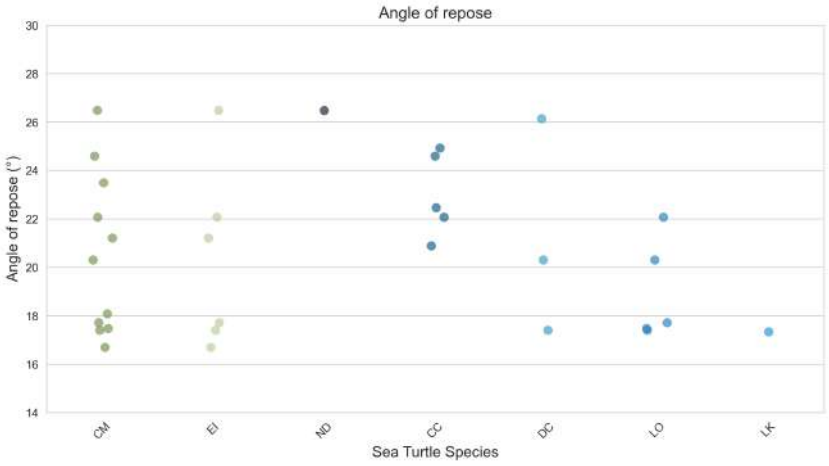

(d) Angle of repose

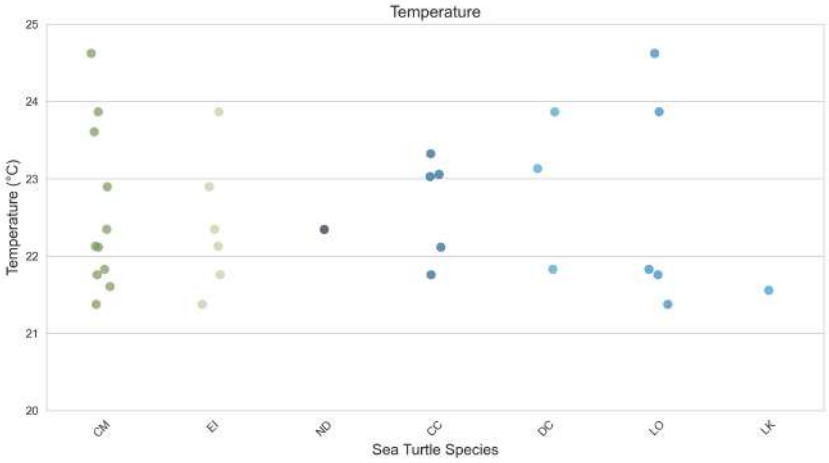

(e) Thermal retention after 60 min.

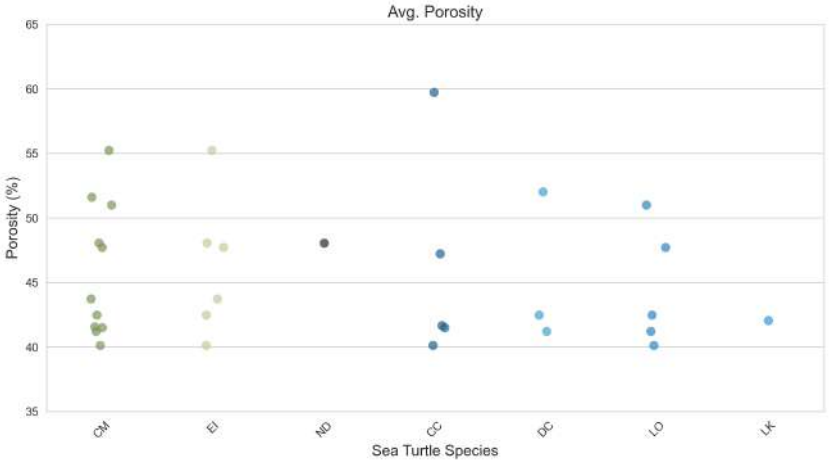

(f) Porosity

Figure D.4: Scatterplots of roundness (R_n), circularity (ψ), solid particle density (ρ_s), angle of repose, thermal retention after 60 minutes and average porosity per sea turtle species at the nesting line. The x-axis displayed the sea turtle species, while the y-axis showed the value of a given key sediment characteristic at the nesting line.